

THE ROLE OF THE CGAS-STING PATHWAY IN DNA VACCINATION AND
AUTOIMMUNE DISEASE

APPROVED BY SUPERVISORY COMMITTEE

Zhijian 'James' Chen, Ph.D.

Lora Hooper, Ph.D.

Edward Wakeland, Ph.D.

Andrew Zinn, M.D., Ph.D.

DEDICATION

I would like to thank my mentor, Dr. James Chen, for giving me the opportunity to work in his lab. I would also like to thank my mentor and my graduate thesis committee for providing scientific advice and guidance during my graduate training. I would like to thank all of my fellow lab members and colleagues for providing helpful discussions and advice regarding experiments and other scientific matters. I would like to thank the people who collaborated with me on my projects for their assistance and help. Lastly, I would like to thank my family and my girlfriend for their continued support and love over the years.

THE ROLE OF THE CGAS-STING PATHWAY IN DNA VACCINATION AND
AUTOIMMUNE DISEASE

by

PHILIP R. CHENG

DISSERTATION

Presented to the Faculty of the Graduate School of Biomedical Sciences

The University of Texas Southwestern Medical Center at Dallas

In Partial Fulfillment of the Requirements

For the Degree of

DOCTOR OF PHILOSOPHY

The University of Texas Southwestern Medical Center at Dallas

Dallas, Texas

May, 2019

Copyright

by

Philip R. Cheng, 2019

All Rights Reserved

THE ROLE OF THE CGAS-STING PATHWAY IN DNA VACCINATION AND
AUTOIMMUNE DISEASE

Publication No. 1

Philip R. Cheng, M.D., Ph.D.

The University of Texas Southwestern Medical Center at Dallas, 2019

Supervising Professor: Zhijian 'James' Chen, Ph.D.

The innate immune system recognizes certain molecular patterns expressed by pathogens via pattern recognition receptors (PRR). As a PRR, cyclic GMP-AMP synthase (cGAS) functions as a cytosolic DNA sensor. Stimulator of Interferon Genes (STING) functions as the downstream adaptor protein. Activation of the cGAS-STING pathway results in proinflammatory cytokine production. Here I show that the cGAS-STING pathway plays dual roles in mediating DNA adjuvant activity and the use of 2'3'-cyclic GMP-AMP

(cGAMP) as a vaccine adjuvant in mice, in addition to promoting autoantibody production and autoimmune inflammatory cell accumulation in lupus-prone mice.

It is unclear which DNA sensor is responsible for mediating the adjuvant effects of plasmid DNA during the course of DNA vaccination. I show that the cGAS-STING pathway is required for generation of antigen-specific immune responses following DNA-adjuvanted vaccination. Mice vaccinated with influenza antigens co-administered with 2'3'-cGAMP develop robust neutralizing antibody titers, enhanced antigen-specific CD8⁺ T-cell responses, and are protected against lethal influenza virus challenge. The efficacy of 2'3'-cGAMP as a vaccine adjuvant can be enhanced by liposome-assisted delivery, the use of non-hydrolyzable analogs, or co-administration with CpG-C DNA.

Systemic lupus erythematosus (SLE) is a chronic autoimmune disease. The exact etiology of SLE is unclear, but work utilizing mouse models of SLE have shown that the PRRs of the innate immune system contribute to disease pathogenesis. My results show that in C57BL/6J-*Fas*^{lpr}/*Fas*^{lpr} mice, genetic ablation of cGAS or STING significantly decreases antinuclear autoantibody titers as well as a number of autoimmune inflammatory cell populations. These results are dependent on the genetic background of the mice, as genetic ablation of cGAS or STING in B6.MRL/Mp-*Fas*^{lpr}/*Fas*^{lpr} mice or B6.*Sle1*-*Fas*^{lpr}/*Fas*^{lpr} mice does not recapitulate the phenotype of *cGAS*^{-/-} or *STING* *gt/gt*.C57BL/6J-*Fas*^{lpr}/*Fas*^{lpr} mice.

My results provide more insight into the innate immune mechanisms involved in DNA vaccination and show that 2'3'-cGAMP promotes the enhanced development of protective immune responses, thereby demonstrating the potential utility of 2'3'-cGAMP as a molecular adjuvant for vaccines. Furthermore, my results demonstrate that the cGAS-STING

pathway contributes to autoimmune disease development in C57BL/6J-*Fas^{lpr}*/*Fas^{lpr}* mice and implicates cGAS or STING as potential therapeutic targets for the treatment of SLE.

TABLE OF CONTENTS

CHAPTER ONE: Introduction	1
CHAPTER TWO: The cGAS-STING pathway mediates DNA adjuvant activity and use of 2'3'-cGAMP as a vaccine adjuvant	37
Results	37
Conclusions and Discussions	46
Materials and Methods	54
CHAPTER THREE: The cGAS-STING pathway promotes autoantibody production and autoimmune inflammatory cell accumulation in C57BL/6J- <i>Fas</i> ^{lpr} / <i>Fas</i> ^{lpr} mice	69
Results	69
Conclusions and Discussions	82
Materials and Methods	96
CHAPTER FOUR: Miscellaneous experiments investigating the adjuvant effects of ultra-pH sensitive nanoparticles loaded with 2'3'-cGAMP and investigating the potential role cGAS-STING pathway signaling may play in the immune response to influenza infection in vivo	111
Results	111
Conclusions and Discussions	115
Materials and Methods	120
REFERENCES	126

PRIOR PUBLICATIONS

Su MA, Davini D, **Cheng P**, et al. Defective Autoimmune Regulator-Dependent Central Tolerance to Myelin Protein Zero Is Linked to Autoimmune Peripheral Neuropathy. *J Immunol.* 2012; PubMed PMID: 22490868

Gris P., **Cheng P.**, Pierson J., Maixner W., Diatchenko L. *Molecular assays for characterization of alternatively spliced isoforms of the mu opioid receptor (MOR).* *Methods Mol Biol.* 2010;617:421-35. PubMed PMID: 20336438.

Gris P., Gauthier J., **Cheng P.**, Gibson D.G., Gris D., Laur O., Pierson J., Wentworth S., Nackley A.G., Maixner W., Diatchenko L. The novel alternatively spliced isoform of mu-opioid receptor: functional antagonism. *Molecular Pain* 2010, 6:33. PubMed PMID: 20525224

LIST OF FIGURES

FIGURE ONE.....	59
FIGURE TWO.....	60
FIGURE THREE.....	61
FIGURE FOUR.....	62
FIGURE FIVE.....	63
FIGURE SIX.....	64
FIGURE SEVEN.....	65
FIGURE EIGHT.....	66
FIGURE NINE.....	67
FIGURE TEN.....	68
FIGURE ELEVEN.....	102
FIGURE TWELVE.....	103
FIGURE THIRTEEN.....	104
FIGURE FOURTEEN.....	105
FIGURE FIFTEEN.....	106
FIGURE SIXTEEN.....	107
FIGURE SEVENTEEN.....	108
FIGURE EIGHTEEN.....	109
FIGURE NINETEEN.....	110
FIGURE TWENTY.....	123

FIGURE TWENTYONE	124
FIGURE TWENTYTWO	125

LIST OF DEFINITIONS

PRR – pattern recognition receptor

cGAS – cyclic GMP-AMP synthase

STING – stimulator of interferon genes

cGAMP – cyclic GMP-AMP

SLE – systemic lupus erythematosus

PAMP – pathogen-associated molecular pattern

Type-I IFN – type-I interferon

IFNAR – interferon- α/β receptor

JAK – Janus kinase

STAT – signal transducer activator of transcription

ISGF3 – IFN-stimulated gene factor 3

IRF – IFN-regulatory factor

ISG – interferon-stimulated gene

APC – antigen-presenting cell

MHC – major histocompatibility complex

CTL – cytotoxic T lymphocyte

TCR – T-cell receptor

DC – dendritic cell

TLR – Toll-like receptor

LPS – lipopolysaccharide

CpG – cytosine-guanosine motif

MyD88 – myeloid differentiation primary response protein 88

TIR – Toll/interleukin-1 receptor

TRIF – TIR domain-containing adaptor protein inducing interferon beta

AP-1 – activating protein-1

NF- κ B – nuclear factor kappa-light-chain-enhancer of activated B cells

pDC – plasmacytoid dendritic cell

Mab21 – male abnormal 21

ATP – adenosine triphosphate

GTP – guanosine triphosphate

TBK1 – TANK-binding kinase 1

IKK – I κ B kinase

HSV – herpes simplex virus

HIV – human immunodeficiency virus

DAMP – damage-associated molecular pattern

NLRP – nucleotide-binding oligomerization domain, leucine rich repeat and pyrin domain

CARD – caspase recruitment domain

NLRC – nucleotide-binding oligomerization domain, leucine rich repeat and CARD domain

AIM2 – absent in melanoma 2

ASC – apoptosis-associated speck-like protein containing a CARD

DAI – DNA-dependent activator of IRFs

MEF – mouse embryonic fibroblast

DDX41 – DEAD-box helicase 41

IFI16 – interferon-gamma inducible protein 16

KSHV – Kaposi sarcoma-associated herpes virus

HFF – human foreskin fibroblast

Alum – aluminum salt

HA – hemagglutinin

NP – nucleoprotein

RNP – ribonucleoprotein

ANA – antinuclear antibody

Syk – spleen tyrosine kinase

EBV – Epstein-Barr virus

Lpr – lymphoproliferation

TREX1 – three prime repair exonuclease 1

AGS – Aicardi-Goutieres syndrome

cGAS KO – cGAS knockout

STING gt/gt – STING goldenticket

RT-PCR – reverse transcription-polymerase chain reaction

H1N1 PR8 – influenza A/PR/8/34 virus

OVA – ovalbumin

MLD₅₀ – median lethal dose

ENPP1 – ecto-nucleotide pyrophosphatase/phosphodiesterase 1

Invivo – invivofectamine

ODN – oligodeoxynucleotides

MAVS - mitochondrial antiviral-signaling protein

CHAPTER ONE

Introduction

Innate and Adaptive Immunity and Immunopathology

Innate and Adaptive Immunity

To defend against the constant threat of invading pathogens, our bodies utilize a powerful defense system capable of discriminating between self and infectious non-self (Medzhitov and Janeway 2002). This defense system takes the form of an integrated immune response, traditionally split into two distinct branches: innate and adaptive immunity. The innate and adaptive immune systems coordinate responses to pathogenic threats such as bacteria, viruses, fungi, and parasites emanating from the environment, protecting us from infectious disease (Janeway CA Jr 2001).

Innate immunity serves as the body's first line of defense against intruding pathogens. Innate immunity is characterized as being a non-specific (antigen-independent) defensive response. For this reason, the innate immune response has no capacity for immunologic memory, meaning it is unable to "memorize" and therefore recognize a specific pathogen should the body be exposed to that pathogen again in a subsequent infection (Warrington, Watson et al. 2011). One of the hallmarks of the innate immune response is speed, as the host innate immune system is capable of reacting to an invading pathogen within minutes to hours of exposure (Turvey and Broide 2010). The recognition of pathogens by the innate immune system is accomplished through the use of a limited repertoire of germline-encoded pattern recognition receptors (PRRs), which recognize certain structural components of microorganisms termed pathogen-associated molecular patterns (PAMPs). The detection of

PAMPs by the PRRs of the innate immune system triggers inflammatory cytokine production, leading to the induction of inflammatory and anti-pathogen responses (Medzhitov and Janeway 2000). Production of type-I interferon (Type-I IFN) cytokines is a key component of the anti-viral response (Murira and Lamarre 2016). Type-I IFN (IFN- α/β) acts in both autocrine and paracrine fashions, binding to the interferon- α/β receptor (IFNAR) found on the surface of cells. Activation of IFNAR by type-I IFN leads to the downstream activation of the Janus kinase (JAK)-signal transducer activator of transcription (STAT) signaling pathway. Phosphorylation of STAT1 and STAT2 facilitates the formation and activation of the transcription factor IFN-stimulated gene factor 3 (ISGF3). ISGF3 is a complex of STAT1, STAT2, and IFN-regulatory factor 9 (IRF9) (Platanias 2005). ISGF3 induces the transcription of a diverse array of genes known as interferon-stimulated genes (ISGs), which are involved in the anti-viral response through various mechanisms such as inducing apoptosis of virally-infected cells, restricting viral replication in infected cells, and conferring resistance to viral infection on uninfected cells (Perdiguero and Esteban 2009). In addition to establishing an anti-viral state within cells, type-I IFN is also known to have wide-ranging effects on the function and regulation of cells within the innate and adaptive immune systems (Trinchieri 2010).

A number of different cell types are involved in the innate immune response against infection. Phagocytic cells (macrophages and neutrophils) function to engulf microbes. Macrophages, which are derived from monocytes, are also capable of producing a number of cytokines and chemokines that enhance the immune response to infection. Macrophages also act as antigen-presenting cells (APCs) (Dempsey, Vaidya et al. 2003; Janeway and

Medzhitov 2002; Warrington, Watson et al. 2011). Neutrophils contain an impressive arsenal of anti-microbial weaponry within cytosolic granules. When released, these granules expel a combination of proteolytic enzymes and anti-microbial proteins/metabolites (Dempsey, Vaidya et al. 2003). Natural killer (NK) cells function by seeking out and destroying virally-infected or cancerous cells through the use of a complex system of activating/inhibitory receptors and major histocompatibility complex (MHC) class I interactions. NK cells can induce target cell death through the use of the cytotoxic perforin-granzyme system or Fas ligand/receptor interactions (Dempsey, Vaidya et al. 2003; Janeway and Medzhitov 2002; Medzhitov and Janeway 2002). Other cells of the innate immune system include eosinophils and basophils, which are enigmatic cells thought to play a role in controlling parasite infections. Mast cells, eosinophils, and basophils are also implicated in allergic reactions (Warrington, Watson et al. 2011).

A separate and important component of the innate immune response is the complement system. The complement system is comprised of a number of proteins found in the blood. When activated, these proteins form a signaling cascade that results in fixation of certain complement components to cell membranes. These complexes of complement proteins can induce lysis of the target cell or act as opsonins, facilitating phagocytosis of the target cell. The complement system plays a vital role in the clearance of microbes during infection (Dempsey, Vaidya et al. 2003; Frank 2010).

Adaptive immunity, present only in vertebrates and cartilaginous fish, is an antigen-specific immune response characterized by the capacity for immunologic memory. The ability to “memorize” exposure to specific pathogens allows the adaptive immune system to

mount a rapid and targeted protective response upon repeat exposure to that pathogen (Dempsey, Vaidya et al. 2003; Warrington, Watson et al. 2011). Unlike the innate immune system, the antigen-specific receptors used by the adaptive immune system to detect threats to the host rely on receptor gene rearrangement in order to create a vast and extremely diverse repertoire of receptors that allow the cells of the adaptive immune system to recognize virtually any antigen (Turvey and Broide 2010). However, this means that there is a lag time between initial exposure to pathogen and the development of a protective, antigen-specific, adaptive immune response. Each cell of the adaptive immune system expresses its own unique receptor, and after initial encounter and recognition of pathogenic antigen, must undergo clonal expansion in order to produce enough quantities of antigen-specific cells capable of clearing the pathogen or threat. This initial clonal expansion process can take up to five days (Janeway and Medzhitov 2002; Turvey and Broide 2010).

The adaptive immune system is comprised of T-cells and B-cells, which mediate the cellular and humoral adaptive immune responses, respectively. B-cells and the plasma cells they differentiate into, function in the humoral adaptive immune response through the production of antibodies (Warrington, Watson et al. 2011). Antigen-specific antibodies bind to their cognate antigen, whether it is on the surface of a pathogen or cell or even a soluble toxin, and flag the antigen for destruction. Antibodies can directly neutralize soluble toxins, trigger complement activation, and promote phagocytosis of antigen by acting as an opsonin (Schroeder and Cavacini 2010). Two main types of T-cells, CD4⁺ T helper (Th) cells and CD8⁺ cytotoxic T lymphocytes (CTL), comprise the cellular adaptive immune response (Janeway CA Jr 2001). CD8⁺ T-cells primarily kill pathogen-infected host cells or cancer

cells through the use of the cytotoxic perforin-granzyme system and granulysin. Perforin and granzyme are proteins that function cooperatively to lyse the target cell, and granulysin is a protein that can induce apoptosis of the target cell. CD8⁺ T-cells recognize target cells through the interaction of their antigen-specific T-cell receptor (TCR) with peptide-bound MHC class I molecules (Bonilla and Oettgen 2010; Warrington, Watson et al. 2011). CD4⁺ T-cells, which have no cytotoxic or phagocytic capabilities, cannot clear infected or cancerous cells from the body directly. However, CD4⁺ T-cells play an important role in facilitating and mediating the overall immune response by directing other immune cells to perform these tasks. In addition, CD4⁺ T-cells provide help to B-cells in the form of stimulating class switching of antibodies. CD4⁺ T-cells are activated upon recognition of antigen bound to MHC class II molecules by their antigen-specific TCR (Bonilla and Oettgen 2010; Iwasaki and Medzhitov 2015; Warrington, Watson et al. 2011). There are two main subtypes of CD4⁺ T-cells, Th1 and Th2, which are distinctly characterized by their cytokine expression profile, cell surface markers, and transcription factors required to induce their differentiation. The transcription factor T-bet drives the differentiation of naïve CD4⁺ T-cells into a Th1 phenotype. Th1 cells are distinguished by their production of interferon- γ (IFN- γ), a cytokine that activates the anti-microbial activity of macrophages and stimulates CD8⁺ T-cell activity. The transcription factor GATA3 drives the differentiation of naïve CD4⁺ T-cells into a Th2 phenotype, and Th2 cells are characterized by their production of interleukin-4 (IL-4), IL-5, and IL-13. These cytokines promote the activation and recruitment of IgE-producing B-cells, eosinophils, and basophils (Warrington, Watson et al. 2011; Zhu, Yamane et al. 2010). Th1 and Th2-associated cytokines can induce class switching of B-cell

antibodies to specific isotypes. In the mouse, a Th1 response promotes IgG2a/2b and IgG3 antibody production, whereas a Th2 response promotes IgG1 antibody production (Germann, Bongartz et al. 1995; Stevens, Bossie et al. 1988). Most activated T-cells and B-cells will die upon resolution of infection. However, a few will remain as long-living memory T- or B-cells. These memory cells can be distinguished by their cell surface markers. For example, effector memory T-cells are CD62L⁻CD44^{hi}, compared to naïve T-cells which are CD62L⁺CD44^{lo} (Dillon, Sprecher et al. 2004).

The innate immune system plays a critical role in the subsequent activation of the adaptive immune response. Linking these two components of the immune response is the responsibility of APCs. Macrophages and dendritic cells (DCs) are the professional APCs of the body. Located in the body at sites of interaction with the environment, these APCs sample the extracellular environment through macropinocytosis. Foreign and native proteins that are taken up from cell debris or microbes are degraded into peptides, which are subsequently loaded onto MHC molecules for presentation to T-cells (Dempsey, Vaidya et al. 2003; Iwasaki and Medzhitov 2015). In addition to presenting antigen to T-cells, APCs also express a number of co-stimulatory molecules on their cell surface, and the binding of these co-stimulatory molecules to their corresponding co-receptor on the T-cell is required for activation of the T-cell. Innate immune activation of APCs causes their upregulation of co-stimulatory molecules CD80 and CD86, which bind to CD28 on the T-cell. This interaction constitutes the second signal required for T-cell activation following the TCR-MHC molecule interaction. Inflammatory cytokines produced by the APC following innate immune activation constitutes the third signal needed for T-cell activation and differentiation

(Dempsey, Vaidya et al. 2003; Janeway and Medzhitov 2002; Medzhitov and Janeway 2000). These cytokines produced by APCs can influence T-cell differentiation. Exposure of a naïve CD4⁺ T-cell to APC generated IL-12, IL-6, and IL-1 β promotes differentiation into a Th1 effector cell, while IL-4 exposure promotes differentiation into a Th2 effector cell (Iwasaki and Medzhitov 2015; Zhu, Yamane et al. 2010).

Immunopathology

Although the immune system is critical for host defense against infection and cancer, a malfunctioning immune system can cause disease on its own. A growing body of work has implicated both the innate and adaptive immune responses as important regulators of inflammatory disease. These inflammatory disorders can be generally grouped into two main categories, hypersensitivity reactions caused by an overactive immune response and autoimmune disease stemming from an inappropriate reaction to self (Warrington, Watson et al. 2011).

Hypersensitivity reactions occur when a healthy immune system produces an undesirable response. There are four main types of hypersensitivity reactions: Type I (immediate or anaphylactic hypersensitivity), Type II (cytotoxic or antibody-dependent hypersensitivity), Type III (immune complex hypersensitivity), and Type IV (cell-mediated or delayed type hypersensitivity) (Levinson 2016). Type I hypersensitivity reactions encompass allergic reactions, whereby the immune response triggers allergic symptoms upon re-exposure to a particular antigen (allergen). Often the allergen is an innocuous substance that provokes an abnormally strong immune response. Unlike the normal immune response to antigen, a type I hypersensitivity reaction is mediated by IgE antibody. The primary

cellular mediators of type I hypersensitivity reactions are mast cells and basophils, with secondary amplification of the reaction occurring through neutrophil and eosinophil activity. IgE antibodies directed against an allergen can bind to IgE Fc-receptors on the surface of mast cells and basophils, and subsequent re-exposure to allergen causes cross-linking of cell-bound IgE, triggering cell degranulation and release of pharmacologically active substances that induce the traditional symptoms of allergies. An example of type I hypersensitivity is allergic rhinitis (Larche, Akdis et al. 2006; Warrington, Watson et al. 2011). Type II hypersensitivity reactions are mediated by IgG and IgM antibodies which recognize and bind to self-antigens on the surface of cells in the body, leading to the formation of antibody complexes capable of activating the complement system. This, in turn, induces opsonization and cell lysis, leading to cell death. Exogenous chemicals such as drugs can also attach to cell membranes and trigger a type II hypersensitivity response. An example of type II hypersensitivity is Goodpasture's syndrome (Janeway CA Jr 2001; Levinson 2016). Type III hypersensitivity reactions are mediated by the formation of soluble immune complexes containing IgG or IgM antibody bound to soluble antigen. These immune complexes deposit in tissues and trigger complement activation. The subsequent inflammation leads to neutrophil influx and results in tissue damage. An example of type III hypersensitivity is systemic lupus erythematosus (SLE) (Eggleton 2001). Type IV hypersensitivity reactions are antibody-independent, with tissue damage occurring through the recruitment of overstimulated T-cells and macrophages to the target area containing antigen. Th1 cells produce cytokines in response to antigen exposure, activating macrophages and assisting the CD8⁺ CTL response. Macrophages and CTLs are responsible for the bulk of the tissue

damage that occurs during type IV hypersensitivity reactions. An example of type IV hypersensitivity is contact dermatitis (Levinson 2016; Warrington, Watson et al. 2011).

Autoimmune disease occurs when the immune system experiences some form of dysregulation, which disrupts normal immune homeostasis and allows for the abnormal generation of self-reactive T-cells and antibodies (Warrington, Watson et al. 2011). As lymphocytes contain a diverse array of antigen-specific receptors created through the random process of receptor gene rearrangement, some of the T- and B-cell receptors generated through this process will invariably recognize self-antigens. The normal immune system therefore utilizes elaborate mechanisms of central and peripheral tolerance to find and eliminate or neutralize self-reactive lymphocytes (Bonilla and Oettgen 2010; Mueller 2010). Central to the development of autoimmune disease is a loss of tolerance to self, which may be caused by genetic or environmental factors. How these genetic and environmental risk factors contribute to the breakdown of normal immune tolerance mechanisms and subsequently give rise to autoreactive lymphocytes and autoimmune disease is a question under active investigation. Although numerous discoveries have helped to shed light on this question, much still remains unknown or unclear.

Sensing of PAMPs by Toll-like Receptors

The Toll-like receptors (TLRs) were the first class of PRRs to be discovered, and consequently are the best characterized. Unsurprisingly, TLRs are expressed in the cells of the innate immune system, particularly in APCs like dendritic cells and macrophages. However, some TLRs are also expressed by non-immune cells like fibroblasts and epithelial cells (Kawasaki and Kawai 2014). In humans, there are 10 distinct TLRs whereas the mouse

contains 12 distinct TLRs. TLR1–9 are conserved between humans and mice (Takeda and Akira 2005). These conserved TLRs can be divided into two subgroups based on their cellular localization. TLRs localized on the cell surface include TLR1, TLR2, TLR4, TLR5, and TLR6. TLRs localized intracellularly in endosomes include TLR3, TLR7, TLR8, and TLR9 (Kawai and Akira 2011). Each TLR recognizes a specific PAMP found on or in microbes. TLR2 works in conjunction with TLR1 or TLR6 to recognize distinct forms of microbial-derived lipoproteins, lipopeptides, peptidoglycan, lipotechoic acid, and zymosan. TLR4 recognizes lipopolysaccharide (LPS) found in the outer membrane of Gram-negative bacteria while TLR5 recognizes flagellin found in bacterial flagella. In the endosome, TLR3 recognizes viral double-stranded RNA (dsRNA) while TLR7 and TLR8 both recognize viral single-stranded RNA (ssRNA). TLR9 recognizes unmethylated cytosine-guanosine (CpG)-motif containing DNA derived from bacteria or viruses in the endosome (Kawai and Akira 2011; Takeda and Akira 2005).

After recognition of a PAMP, TLRs initiate a signaling cascade to induce activation of the innate immune response. Individual TLRs will recruit either a single member or specific combination of TIR domain-containing adaptor proteins (MyD88, TRIF, TRAM, or TIRAP) in a differential manner (Kawasaki and Kawai 2014). With the exception of TLR3, MyD88 is utilized by all TLRs. TLR3 signals through a TRIF-dependent signaling cascade (Takeda and Akira 2005). Engagement of Myd88 by a TLR results in further downstream signals which culminate in the activation of AP-1 and NF- κ B transcription factors. In certain cell types like plasmacytoid dendritic cells (pDCs), MyD88 signaling will also activate the IRF7 transcription factor. Downstream signaling events following engagement of TRIF by a

TLR culminates in the activation of NF- κ B and IRF3 transcription factors (Akira and Takeda 2004; Kawasaki and Kawai 2014). The transcription factors IRF3 and IRF7 translocate to the nucleus and initiate transcription of type-I IFN genes. NF- κ B translocates to the nucleus and initiates transcription of a number of proinflammatory cytokines (Takeda and Akira 2005).

As both Myd88 and TRIF activation can induce type-I IFN and inflammatory cytokine production, TLR signaling pathways serve to activate the innate immune response.

Cytosolic DNA Sensing Pathways

The cGAS-STING Pathway

In eukaryotes, DNA carries the genetic information required for life. This DNA is localized to specific membrane-bound compartments in the cell such as the nucleus and mitochondria. The cytoplasm is therefore free of DNA under normal conditions. However, DNA can enter the cytoplasm via microbial infection of the cell or from cellular damage which causes DNA leakage from the mitochondria or nucleus into the cytoplasm. Under these abnormal conditions, DNA becomes a danger signal (O'Neill 2013). Although TLR9 is capable of sensing double-stranded DNA (dsDNA), it faces the lumen of the endosome, making cytosolic detection of dsDNA by TLR9 highly improbable. In addition, many cell types that do not express TLR9 can still mount innate immune responses to exogenous DNA when it is delivered into the cytosol (Ishii, Coban et al. 2005; Stetson and Medzhitov 2006). Recent work has established cGAS as an essential, non-redundant, cytosolic DNA sensor (Sun, Wu et al. 2012). Both cGAS and its downstream adaptor protein STING are widely expressed in cells throughout the body (Zhong, Yang et al. 2008).

The cytosolic DNA sensor cGAS is a member of the nucleotidyltransferase (NTase) family of enzymes. Analysis of the structural domains of cGAS by sequence alignment revealed a highly conserved NTase motif which partially overlaps with a C-terminal male abnormal 21 (Mab21) domain. The N-terminus of cGAS contains an unstructured region (Sun, Wu et al. 2012). Crystal structures of cGAS alone or in complex with dsDNA show that upon binding to dsDNA, the NTase catalytic pocket undergoes a large conformational change which repositions catalytic residues to allow ATP and GTP to bind (Civril, Deimling et al. 2013; Gao, Ascano et al. 2013; Kranzusch, Lee et al. 2013). Subsequently, cGAS catalyzes the formation of cyclic GMP-AMP (2'3'-cGAMP) from GTP and ATP. Interestingly, 2'3'-cGAMP contains mixed phosphodiester linkages, with one phosphodiester bond formed between the 2'-hydroxyl of GMP and the 5'-phosphate of AMP and the other phosphodiester bond formed between the 3'-hydroxyl of AMP and the 5'-phosphate of GMP (Gao, Ascano et al. 2013; Wu, Sun et al. 2012). The binding of dsDNA to cGAS is mediated through hydrogen bonds and electrostatic interactions formed between the negatively charged sugar-phosphate backbone of DNA and the positively charged surfaces of cGAS (Gao, Ascano et al. 2013). This allows cGAS to recognize and bind dsDNA in a sequence-independent manner (Sun, Wu et al. 2012). Further structural and biochemical analyses demonstrated that active cGAS forms a dimer and binds to dsDNA in a 2:2 ratio. Mutations to either the dimerization interface or DNA binding domains of cGAS abolish 2'3'-cGAMP production and type-I IFN induction (Li, Shu et al. 2013; Zhang, Wu et al. 2014).

Upon binding to dsDNA, cGAS catalyzes the formation of 2'3'-cGAMP, which acts as a cyclic dinucleotide second messenger molecule that further binds and activates the

endoplasmic reticulum membrane protein STING (Zhang, Shi et al. 2013). STING was originally identified as a signaling adaptor protein in the cytosolic DNA sensing pathway. STING is required for type-I IFN induction in response to cytoplasmic dsDNA, as STING-deficient cells are incapable of producing type-I IFN when transfected with DNA (Ishikawa and Barber 2008; Ishikawa, Ma et al. 2009). In addition to its role in the cytosolic DNA sensing pathway, STING has been shown to bind bacterial cyclic dinucleotides like 3'5'-cyclic diguanylate (c-di-GMP) and 3'5'-cyclic diadenylate (c-di-AMP) (Burdette, Monroe et al. 2011; Jin, Hill et al. 2011). However, 2'3'-cGAMP binds with much higher affinity to STING than bacterially derived cyclic dinucleotides. For example, 2'3'-cGAMP binds to STING with a K_d of ~ 4 nM while c-di-GMP binds to STING with a K_d of $4.9 \mu\text{M}$ (Wu and Chen 2014). Upon binding to 2'3'-cGAMP, STING undergoes a large conformational change, with the two STING proteins that comprise the dimeric STING complex undergoing an approximately 20 \AA inward rotation, resulting in the formation of a β -sheet lid that covers the 2'3'-cGAMP binding site (Gao, Ascano et al. 2013; Zhang, Shi et al. 2013). Concurrently, STING re-localizes from the endoplasmic reticulum to the Golgi complex. This conformational and locational change likely frees the C-terminal tail of STING, which is required for the further downstream recruitment and activation of TANK-binding kinase 1 (TBK1) and I κ B kinase (IKK) (Tanaka and Chen 2012; Wu and Chen 2014). Activation of TBK1 and IKK culminates in translocation of transcription factors IRF3 and NF- κ B into the nucleus, resulting in the production of type-I IFN and other proinflammatory cytokines (Ishikawa and Barber 2008; Wu and Chen 2014). The end result is initiation of the host innate immune response.

The cGAS-STING pathway has been shown to be essential in host defense against numerous microbes. Studies utilizing *cGAS*^{-/-} and *STING*^{-/-} mice infected with the DNA virus herpes simplex virus 1 (HSV1) demonstrated that lack of cGAS or STING severely attenuated type-I IFN production following viral infection when compared to wild-type controls. Both *cGAS*^{-/-} and *STING*^{-/-} mice showed increased susceptibility to HSV1 infection, with higher mortality seen after infection in mice lacking cGAS or STING compared to wild-type controls. In addition, HSV1 titers in brain tissue harvested from infected *cGAS*^{-/-} and *STING*^{-/-} mice were significantly elevated compared to wild-type controls (Ishikawa, Ma et al. 2009; Li, Wu et al. 2013). Recent work has demonstrated that the cGAS-STING pathway can sense infection of cells by retroviruses like human immunodeficiency virus (HIV). Knockdown of cGAS or STING expression in THP1 cells resulted in abrogation of IFN- β production following infection with a modified HIV-1 virus capable of infecting multiple cell types (HIV-GFP). HIV-GFP infection of THP-1 cells resulted in measurable 2'3'-cGAMP production, which lead to STING activation and type-I IFN production in wild-type cells. Interestingly, the use of HIV reverse transcriptase inhibitors eliminated HIV-mediated type-I IFN production in cells, suggesting that reverse-transcribed viral DNA is responsible for stimulating cGAS activity (Cai, Chiu et al. 2014; Gao, Wu et al. 2013). Indeed, a separate independent study demonstrated that HIV cDNA is recognized by cGAS in infected DCs, with the subsequent innate immune activation causing DC maturation which facilitates activation of T-cells (Lahaye, Satoh et al. 2013). In addition to HSV1 and HIV, numerous studies have shown that cytosolic sensing of microbial DNA by the cGAS-STING pathway and the subsequent production of type-I IFN and inflammatory cytokines that results is

critical in controlling infections by *Mycobacterium tuberculosis*, vaccinia virus, human cytomegalovirus, hepatitis B virus, *Neisseria gonorrhoeae*, and other pathogens (Andrade, Agarwal et al. 2016; Collins, Cai et al. 2015; He, Hao et al. 2016; Li, Wu et al. 2013; Paijo, Doring et al. 2016; Watson, Bell et al. 2015).

AIM2 Inflammasome Pathway

The cGAS-STING pathway has a broad tissue distribution, meaning the presence of cytosolic DNA in cells of various lineages will trigger type-I IFN and inflammatory cytokine production. However, in addition to producing type-I IFN and inflammatory cytokines, myeloid lineage cells like macrophages will activate the inflammasome in response to cytosolic DNA (Wu and Chen 2014). This indicates the presence of an additional cytosolic DNA sensing pathway in myeloid cells.

The inflammasome is a multiprotein complex responsible for mediating the inflammatory immune response to pathogens and other danger signals. This is accomplished through the activation of caspase-1 by the inflammasome (Guo, Callaway et al. 2015). Caspase-1, a proteolytic enzyme, cleaves inactive pro-IL-1 β and pro-IL-18. This cleavage results in release of mature, active IL-1 β and IL-18 cytokines (Broz and Dixit 2016). IL-1 β is an important mediator of inflammation, acting as a pyrogen while stimulating T-cell and macrophage activity (Dinarello 2009). IL-18 induces IFN- γ production by T-cells and NK cells while promoting the development of Th1 cells, events that are critical in the development of the cellular adaptive immune response to infection (Janeway CA Jr 2001). Activated caspase-1 can also trigger an inflammatory form of cell death known as pyroptosis (Guo, Callaway et al. 2015). There are numerous sensors that can activate the inflammasome

in response to various PAMPs and damage-associated molecular patterns (DAMPs). The composition of the inflammasome complex is dependent on the sensor that activates it. For example, NLRP1 acts as a sensor capable of recognizing anthrax lethal toxin, triggering assembly of the NLRP1 inflammasome. NLRP3 is a sensor that detects a variety of PAMPs from viruses like influenza virus, bacteria like *Neisseria gonorrhoeae*, and bacterial toxins like nigericin. In addition, NLRP3 recognizes DAMPs such as low intracellular potassium levels, reactive oxygen species, and extracellular ATP. NLRP3 activates the NLRP3 inflammasome. NLRC4 senses the presence of bacterial flagellin, triggering assembly of the NLRC4 inflammasome (Broz and Dixit 2016; Guo, Callaway et al. 2015; Latz, Xiao et al. 2013).

Absent in melanoma 2 (AIM2) functions as the cytosolic dsDNA sensor for the inflammasome pathway (Hornung, Ablasser et al. 2009). AIM2 is an interferon-inducible member of the PYHIN protein family, containing an N-terminal pyrin domain and C-terminal HIN-200 domain. The HIN-200 domain can bind to oligonucleotides and oligosaccharides. AIM2 therefore recognizes and binds to cytoplasmic dsDNA through its HIN-200 domain (Ratsimandresy, Dorfleutner et al. 2013). Binding to dsDNA allows AIM2 to associate with its downstream adaptor protein, apoptosis-associated speck-like protein containing a CARD (ASC). This association is mediated by pyrin domain interactions between AIM2 and ASC (Wu and Chen 2014). The CARD domain of ASC recruits and activates caspase-1 through CARD-CARD interactions, which is facilitated by the formation of prion-like filaments by ASC (Cai, Chen et al. 2014). AIM2 binding to ASC also triggers the assembly of the ASC pyroptosome, which induces pyroptosis in a caspase-1 dependent

fashion (Fernandes-Alnemri, Yu et al. 2009). The AIM2 inflammasome pathway plays an important role in host defense against certain pathogens, as *AIM2*^{-/-} mice are more susceptible to lethal infection by *Francisella tularensis* than wild-type mice. In addition, AIM2 has been shown to activate the inflammasome in response to infection of myeloid cells by DNA viruses such as vaccinia virus and mouse cytomegalovirus. In the case of mouse cytomegalovirus infection, production of IL-18 and NK cell-derived IFN- γ is dependent on AIM2 in vivo (Rathinam, Jiang et al. 2010).

Other Putative Cytosolic DNA Sensors

Prior to the discovery of cGAS, a number of proteins were considered possible cytosolic DNA sensor candidates. DNA-dependent activator of IRFs (DAI) is a putative cytosolic DNA sensor that contains Z-DNA binding domains and a D3 B-DNA binding domain. Knockdown of DAI in L929 cells inhibited type-I IFN induction in response to DNA (Takaoka, Wang et al. 2007). However, mouse embryonic fibroblasts (MEFs) from *DAI*^{-/-} mice displayed no deficiency in type-I IFN production following DNA stimulation. In addition, *DAI*^{-/-} mice demonstrated a normal type-I IFN response and adaptive immune response to DNA vaccination in vivo, suggesting DAI is not an essential or non-redundant sensor for cytosolic DNA (Ishii, Kawagoe et al. 2008).

DEAD-box helicase 41 (DDX41) is a putative cytosolic DNA sensor that binds DNA through a DEADc domain. In an RNAi screen utilizing THP-1 cells and D2SC/1 cells, DDX41 was identified as being required for the induction of type-I IFN by cytosolic DNA. Knockdown of DDX41 in DCs blocked the induction of type-I IFN and inflammatory cytokine production in response to cytosolic DNA stimulation and HSV1 infection. DDX41

was also shown to co-localize with STING in the cytoplasm (Zhang, Yuan et al. 2011). However, other groups demonstrated that RNAi-mediated knockdown of DDX41 did not affect type-I IFN production induced by DNA stimulation or DNA virus infection (Abe, Harashima et al. 2013; Lam, Stein et al. 2014; Sun, Wu et al. 2012). Further studies will be needed to clarify the role of DDX41 in cytosolic DNA sensing.

Interferon-gamma inducible protein 16 (IFI16) is another putative cytosolic DNA sensor. IFI16 contains two HIN-200 DNA binding domains, and was initially discovered in THP-1 cells using a dsDNA affinity pull-down experiment, which showed that IFI16 could directly bind to both viral and transfected DNA in cytoplasmic extracts. IFI16 is predominantly located in the nucleus, with a small fraction of the protein present in the cytoplasm. Knockdown of IFI16 resulted in the partial inhibition of IFN- β production following DNA transfection or HSV1 infection of cells. In the cytoplasm, IFI16 bound to viral DNA appears capable of activating STING (Unterholzner, Keating et al. 2010). In the nucleus, IFI16 has been shown to mediate sensing of HSV1 or Kaposi sarcoma-associated herpes virus (KSHV) DNA following viral infection of the cell (Kerur, Veetil et al. 2011; Orzalli, DeLuca et al. 2012). However, using IFI16 knockdown, some groups were unable to demonstrate any defect in cellular type-I IFN production in response to cytoplasmic DNA stimulation (Abe, Harashima et al. 2013; Sun, Wu et al. 2012). More recent work has demonstrated that there appears to be crosstalk between IFI16 and cGAS following viral infection or DNA transfection of cells. In the nucleus of human foreskin fibroblasts (HFFs), cGAS regulates IFI16 protein stability and siRNA depletion studies indicate that both cGAS and IFI16 are required for type-I IFN production by HFFs following HSV1 infection (Orzalli,

Broekema et al. 2015). In human macrophages, knockdown of IFI16 results in impaired cGAMP production following DNA stimulation (Jonsson, Laustsen et al. 2017). Due to conflicting results, further investigation will be required to clarify the role of IFI16 in cytoplasmic DNA sensing. Further work will also be needed to elucidate the mechanisms of cGAS-STING pathway and IFI16 crosstalk.

Vaccination Strategies

The development and use of vaccines to prevent and eradicate communicable disease is one of the great successes in the history of medical science. Current vaccine formulations center on the use of live attenuated/inactivated pathogen or protein subunit vaccines (Gurunathan 2000). Live attenuated pathogen vaccines are capable of stimulating both protective cellular and humoral immune responses, but there are safety concerns associated with production of the vaccine and use of the vaccine in immunocompromised individuals. Inactivated pathogen vaccines similarly have safety concerns associated with their production. Protein subunit vaccines, on the other hand, are generally considered safe but require the use of an adjuvant to elicit an immune response against the protective antigen. Typical adjuvants like aluminum salt (alum) used in these traditional vaccine formulations are capable of stimulating a protective humoral immune response but fail to elicit a significant Th1 CD4⁺/CD8⁺ T-cell response, resulting in suboptimal vaccine immunogenicity and protection (Comoy EE 1997; Cunningham, Serre et al. 2004; Gurunathan 2000; Jankovic D 1997; Sokolovska, Hem et al. 2007). DNA vaccination, though still experimental, is capable of inducing both humoral and cellular immune responses against the plasmid-encoded protective antigen (Wang, Epstein et al. 2001; Yang 2004). It is known that DNA

vaccines contain two components necessary for their optimal immunogenicity. The first component is the protective antigen encoded by the plasmid, which when expressed in vivo, is presented by the transfected cell via MHC-I and MHC-II dependent antigen-processing pathways to the immune system. The second component is the DNA adjuvant element contributed by the plasmid DNA itself, which triggers innate immune activation and subsequently leads to antigen-specific T- and B-cell responses (Gurunathan 2000; Kutzler and Weiner 2008). It is unclear which DNA sensor is responsible for detecting the plasmid DNA adjuvant component of DNA vaccines. Since plasmid DNA backbones contain unmethylated CpG motifs, these were previously considered to be the primary adjuvant component of plasmid DNA, stimulating the immune response to DNA vaccination via a TLR9-dependent mechanism. However, mice lacking TLR9 or MyD88 mount similar immune responses to DNA vaccination as wild-type mice, suggesting that sensing of the plasmid DNA adjuvant component of DNA vaccines is TLR9-independent (Babiuk, Mookherjee et al. 2004; Spies, Hochrein et al. 2003). More recent work has implicated the importance of DNA sensing outside of the endosomal TLR9. Cytosolic double-stranded DNA strongly stimulates production of type-I IFN and other proinflammatory cytokines through the cGAS-STING pathway (Andrade, Agarwal et al. 2016; Gao, Wu et al. 2013; Li, Wu et al. 2013; Paijo, Doring et al. 2016; Peihong Dai 2014; Reinert, Lopusna et al. 2016; Sun, Wu et al. 2012; Wu, Sun et al. 2012). STING activates TBK1, resulting in the phosphorylation and translocation of IRF3 into the nucleus and the subsequent induction of type-I IFN production. Both STING and TBK1 are required for the immune response to DNA vaccination (Ishii, Kawagoe et al. 2008; Ishikawa, Ma et al. 2009). Whether cGAS is

the upstream sensor responsible for recognizing the plasmid DNA component of a DNA vaccine and mediating its adjuvant effects is still unclear.

Influenza Virus

Influenza Virus Biology

Influenza viruses are members of the Orthomyxoviridae family of viruses and are enveloped, negative-strand RNA viruses (Fields, Knipe et al. 2007). The segmented genome of influenza viruses consists of seven to eight gene segments, with each gene segment encoding at least one viral protein. Within the family of influenza viruses, one genus contains influenza A and B viruses while a separate genus contains influenza C viruses (Taubenberger and Morens 2008). These three influenza virus types exhibit differences in host range and pathogenicity. Both influenza B and C viruses mainly infect humans. Influenza B viruses have also been isolated from seals while influenza C viruses have been isolated from pigs and dogs. In comparison, influenza A viruses infect a wide variety of animals, including birds and mammals. Of the three influenza virus types, only influenza A viruses pose a significant risk of zoonotic infection, host switching, and generation of pandemic viral strains (Taubenberger and Kash 2010).

The influenza A virus genome contains eight single-stranded RNA segments (Taubenberger and Kash 2010). The proteins encoded by these gene segments include hemagglutinin (HA), neuraminidase (NA), matrix 2 (M2), nuclear export protein (NEP, also named NS2), non-structural protein 1 (NS1), matrix 1 (M1), nucleoprotein (NP), polymerase basic protein 2 (PB2), polymerase basic protein 1 (PB1), and polymerase acidic protein (PA). In addition, a novel protein encoded by the PB1 gene segment, N40, was recently identified.

However, the function of N40 protein is still unclear (Medina and Garcia-Sastre 2011).

Inside the virus capsid, the viral gene segments form individual ribonucleoprotein (RNP) complexes with NP. These viral RNP complexes are bound to the viral RNA-dependent RNA polymerase complex, which consists of PB1, PB2, and PA (Medina and Garcia-Sastre 2011).

Influenza A viruses are subtyped according to the antigenic properties of their surface HA and NA glycoproteins (Taubenberger and Morens 2008). The specific HA subtype of an influenza A virus determines its host tropism, as HA mediates binding of influenza virus to host cell receptors containing α -2,6-linked or α -2,3-linked sialic acid moieties (Bouvier and Palese 2008). Upon binding to a host cell, influenza virus enters the cell via receptor-mediated endocytosis (Grove and Marsh 2011). Cleavage of HA by host cell proteases exposes an HA fusion peptide that mediates fusion of the viral envelope with the endosomal membrane, allowing the viral genome RNP complexes to enter the cytoplasm. This fusion process is a pH-dependent step that is facilitated by acidification of the endosome, which concurrently triggers opening of viral M2 ion channels located on the virion surface.

Activation of M2 ion channels results in acidification of the interior of the virion, which is required for the proper unpacking of viral genome RNP complexes. Viral genome RNP complexes translocate to the nucleus of the host cell, where viral genome transcription and replication occurs (Bouvier and Palese 2008; Medina and Garcia-Sastre 2011). NS1 viral protein aids the viral genome replication process by enhancing viral mRNA translation, inhibiting host mRNA processing, and antagonizing host type-I interferon production (Hale, Randall et al. 2008). Newly synthesized viral RNPs are subsequently exported to the cytoplasm for packaging into progeny virion, a process mediated by M1 and NEP viral

proteins. After M1-assisted formation of new virus particles, viral progeny exit the host cell via budding. Release of budding virions from the host cell membrane is facilitated by NA, which cleaves sialic acid-containing host cell receptors at the cell surface (Bouvier and Palese 2008; Taubenberger and Kash 2010).

The influenza A virus RNA polymerase complex is incapable of proofreading, resulting in the introduction of numerous point mutations within the viral genome during replication (Fields, Knipe et al. 2007). As a result, mutations to the antigenic portions of surface proteins HA and NA produce selective advantages for newly formed virions by allowing them to escape pre-existing immune responses. This process of antigenic drift driven by mutations allows influenza A virus to constantly adapt and respond to strong immunologic pressures (Taubenberger and Kash 2010). It is also known that infection of a cell with two different strains of influenza A virus can result in gene segment mixing between the two viruses, resulting in progeny viruses containing a mixture of gene segments from the parental strains. This process of genetic reassortment is termed antigenic shift when the HA and NA gene segments are involved. Antigenic shift is likely responsible for the creation of most pandemic influenza strains (Bouvier and Palese 2008; Medina and Garcia-Sastre 2011).

Although influenza A virus is an RNA virus typically sensed by the RNA detecting PRRs of the innate immune system, recent work has established that the DNA-sensing STING pathway is also involved in control of influenza virus infection. Measurement of type-I IFN production in *cGAS*^{-/-} or *STING*^{-/-} THP-1 cells infected with influenza A virus showed that virally-induced interferon production was decreased in cells lacking STING, but

cGAS^{-/-} cells displayed no deficit in type-I IFN production (Holm, Rahbek et al. 2016). It was subsequently found that STING plays a role in detecting membrane fusion events within the cell, triggering type-I IFN production in cells exposed to fusogenic liposomes in a *cGAS*-independent manner (Holm, Jensen et al. 2012; Holm, Rahbek et al. 2016). In THP-1 cells infected with influenza A virus, HA was found to co-localize with a small pool of cellular STING. Further analysis revealed that the HA fusion peptide interacts with STING during the course of influenza virus infection and antagonizes type-I IFN production induced by influenza A virus fusion with host cells (Holm, Rahbek et al. 2016).

Influenza Pathology and Clinical Disease

Influenza A virus causes an acute respiratory disease characterized by the onset of high fever, cough, coryza, fatigue, malaise, muscle aches, and chills (Taubenberger and Morens 2008). Acute symptoms of influenza may last for ten days with fatigue and weakness persisting for weeks after infection. Influenza infection may result in severe complications such as hemorrhagic bronchitis and primary or secondary pneumonia, leading to death. Children and the elderly, along with individuals with chronic pulmonary or cardiac disease, are at the highest risk of developing severe complications (Taubenberger and Morens 2008). Effective preventative measures against influenza A virus infection include anti-viral drugs and vaccination. Anti-viral drugs against influenza target either the M2 ion channel (amantadine and rimantadine) or NA (zanamivir and oseltamivir) for inhibition (Medina and Garcia-Sastre 2011; Taubenberger and Kash 2010). Unfortunately, influenza A viruses have developed widespread resistance to the M2 ion channel blockers (Hayden and Pavia 2006; Medina and Garcia-Sastre 2011). The NA inhibitors, while effective against both influenza A

and B viruses, must be taken either prophylactically or within 48 hours of infection (Hayden and Pavia 2006). This leaves vaccination as the most effective means of preventing influenza infection. Induced by influenza vaccination, the generation of antibodies against the viral HA protein prevents receptor binding by the virus to host cells and is virus neutralizing (Bouvier and Palese 2008). These HA-specific antibodies therefore prevent initial infection or reinfection with the same strain of influenza A virus. Influenza-specific CD8⁺ T-cells are also important in controlling influenza infection, as CD8⁺ T-cell depletion in mice results in impaired protection against influenza virus infection (Topham, Tripp et al. 1997; Ulmer, Fu et al. 1998). However, traditional vaccine adjuvants typically stimulate a weak cellular adaptive immune response, favoring the generation of humoral immunity (Cunningham, Serre et al. 2004; Jankovic D 1997; Sokolovska, Hem et al. 2007). To achieve optimal protection, inactivated or live attenuated influenza vaccines are used (Taubenberger and Morens 2008). However, the process of generating these inactivated or live attenuated influenza vaccines is costly and time-consuming when compared to the use of a traditional protein subunit vaccine (Wong and Webby 2013). Finding a vaccine adjuvant capable of stimulating both a strong humoral and cellular immune response to influenza antigen would therefore simplify and expedite influenza vaccine design.

Influenza A virus infects and replicates within the respiratory epithelial cells of the upper and lower respiratory tract. Replication of influenza A virus peaks approximately 48 hours after infection and declines slowly over a period of days, with shedding of infectious virions falling to undetectable levels by roughly six days post-infection (Taubenberger and Morens 2008). During this period of acute infection, multifocal destruction of the

pseudostratified columnar epithelium of the tracheobronchial airways occurs. On histology, there is significant necrosis of airway epithelial cells with accompanying edema and vascular congestion. The lumen of airways is often filled with necrotic cell debris, and macrophages and neutrophils can be observed infiltrating the walls of airways to phagocytose cellular debris. A neutrophilic exudate may also be present in the lumen of airways. Immune cell recruitment often results in the presence of a mixed inflammatory cell infiltrate surrounding airways and blood vessels (Sanders, Johnson et al. 2013; Taubenberger and Morens 2008).

Systemic Lupus Erythematosus

SLE Epidemiology

Systemic lupus erythematosus (SLE) is a chronic inflammatory autoimmune disease that affects multiple organ systems and is associated with the production of autoantibodies directed against nuclear self-antigens (Anisur Rahman 2008; Fairhurst, Wandstrat et al. 2006; Tsokos 2011). Depending on location, the prevalence of SLE in the general population ranges from 20 to 150 cases per 100,000 people. The vast majority of SLE patients are women of child-bearing age. In the United States, SLE is more prevalent in African, Hispanic, and Asian ethnic groups (Tsokos 2011).

Clinical Presentation of SLE

SLE presents with a diverse array of heterogeneous symptoms that can affect every organ system of the body (Eloranta and Ronnblom 2016). Constitutional symptoms may include fever, fatigue, and weight loss. Musculoskeletal symptoms often include arthralgia, myalgia, or arthritis. Dermatological symptoms include photosensitivity and the presence of skin rashes like the classic malar rash. Neurological manifestations can include seizures and

psychosis, among others. Pulmonary, gastrointestinal, and cardiac involvement can also occur and may present as pleuritis, nausea, and pericarditis. Hematologic symptoms are also common and include any of multiple cytopenias like leukopenia, thrombocytopenia, or anemia. Renal involvement is the most common presentation and glomerular disease can result in acute or chronic renal failure (Anisur Rahman 2008; Banchereau and Pascual 2006; Crow 2014). Dysfunction in the immune system will often result in detectable antinuclear antibody (ANA) titers in the serum, and the presence of anti-Smith (Sm) or anti-dsDNA antibodies in the serum is considered pathognomonic for SLE (Banchereau and Pascual 2006; Rahman and Isenberg 1994). Some SLE patients also have elevated serum levels of type-I IFN (Pascual, Farkas et al. 2006). Numerous studies have identified a number of ISGs that are overexpressed in the peripheral blood of these SLE patients. The presence of this “IFN signature” is associated with increased disease severity (Eloranta and Ronnblom 2016; Rönnblom and Alm 2003). SLE patients are at higher risk of death from renal failure, myocardial infarction, or stroke as a result of their disease and also have an increased risk of death from infections due to the use of immunosuppressive drugs to treat SLE (Anisur Rahman 2008).

Mechanism of Organ Damage in SLE

SLE is classified as a type III hypersensitivity reaction, in addition to being an autoimmune disease (Eggleton 2001). In SLE, autoantibodies bind to soluble self-antigens, contributing to immune complex formation. Small immune complexes which are not cleared by macrophages deposit in tissues, triggering complement activation and local inflammation. This aberrant inflammatory response is aided by autoreactive immune cells and causes organ

damage and the subsequent expression of disease symptoms (Anisur Rahman 2008; Crispin, Liossis et al. 2010; Tsokos 2011). The kidneys are often affected in SLE and kidney damage manifests as glomerulonephritis, which is induced primarily by the deposition of pathogenic anti-dsDNA IgG antibody-nucleosome immune complexes in the renal glomerular basement membrane (Berden, Licht et al. 1999; Kramers C 1994; van Bruggen MC 1997). Anti-C1q, anti-Sm, and anti-chromatin IgG immune complexes also tend to accumulate in the kidney and cause renal damage (Anisur Rahman 2008; Tsokos 2011). Immune complexes, however, may deposit in any tissue of the body. Anti-Ro IgG immune complexes can deposit in the skin and are associated with the development of photosensitive rashes in cutaneous lupus. In addition, anti-Ro antibodies are associated with the development of neonatal lupus and congenital heart block. Anti-phospholipid (cardiolipin) IgG immune complexes can disrupt endothelial cell function and increase the risk of thrombosis. Additionally, anti-phospholipid antibodies can bind placental trophoblast cells and induce fetal loss through activation of complement (Anisur Rahman 2008; Tsokos 2011).

The generation of pathogenic IgG-class autoantibodies by B-cells and plasma cells is mediated by antibody class-switching, a process that is dependent upon T-cell help. Autoreactive T-cells are therefore critical in the pathogenesis of SLE (Crispin, Liossis et al. 2010). In SLE patients, T-cells often demonstrate dysfunctional antigen-mediated activation, with inappropriate amplification of signaling events through the TCR. This inappropriate signaling amplification is due to abnormal aggregation of TCRs in lipid rafts on the T-cell membrane combined with the improper downstream use of spleen tyrosine kinase (Syk) rather than canonical ζ -associated protein (ZAP-70) by the TCR to relay signaling events

(Deng and Tsokos 2008; Krishnan, Juang et al. 2008). These signaling changes make autoreactive T-cells in SLE patients more responsive to self-antigens. Cytokine production by T-cells in SLE patients is also defective, with deficient production of IL-2 and increased production of IL-17 observed (Crispin, Liossis et al. 2010). IL-2 deficiency impedes activation-induced cell death and may contribute to the increased lifespan of autoreactive T-cells in SLE patients (Tsokos 2011). IL-17, an inflammatory cytokine that functions to recruit other immune cells like neutrophils, is produced by a population of autoreactive T-cells which tend to home to the kidney in SLE patients and contribute to renal disease by promoting an inflammatory immune response (Crispín JC 2008).

APCs like dendritic cells and plasmacytoid dendritic cells also display dysfunctional behavior in SLE patients (Pascual, Farkas et al. 2006). Normally, pDCs recognize viral infections through various PRRs including TLR7, TLR9, and the cGAS-STING pathway. In response to virus, pDCs located in the peripheral blood secrete large quantities of type-I IFN to combat infection (Banchereau and Pascual 2006). However, in SLE patients, pDCs infiltrate organs like the skin and kidney and inappropriately react to self-antigens (Farkas, Beiske et al. 2001). It is likely that pDCs are the main source of type-I IFN production in SLE patients (Tsokos 2011). Type-I IFN, in the context of SLE, may have numerous effects. For example, studies have shown that type-I IFN can induce the maturation of DCs, and in SLE patients with IFN signatures the induced maturation of DCs facilitates the activation of autoreactive T-cells and the development of autoimmunity (Banchereau, Pascual et al. 2004; Blanco, Palucka et al. 2001).

Risk Factors for SLE Development

The question that is central to the development of SLE and other autoimmune diseases is how natural mechanisms of immune tolerance are compromised, allowing for the proliferation of autoreactive lymphocytes and other immune cells. The exact etiology of SLE is unknown. However, numerous studies have identified both genetic and environmental risk factors that contribute to disease development. The clinical concordance rate of SLE in monozygotic twins is 25%, while in dizygotic twins it is ~2%, indicating genetic contributions are important but insufficient to cause disease (Anisur Rahman 2008). Known environmental risk factors for SLE include certain medications (procainamide, hydralazine, and isoniazid), smoking, and exposure to ultraviolet radiation (Tsokos 2011). In addition, there is a correlation between Epstein–Barr virus (EBV) infection and the onset of SLE. A case-control study found that 99% of SLE patients had antibodies against EBV, a proportion that is much higher than what is observed in healthy controls (Anisur Rahman 2008; Crispin, Liossis et al. 2010).

Numerous studies utilizing both human SLE patients and murine models of lupus have identified a myriad of genetic risk alleles that contribute to disease development. As females are disproportionately affected by SLE, both hormones and the X chromosome contribute to SLE development through unknown mechanisms (Crispin, Liossis et al. 2010). In lupus-prone mice genetically manipulated to express XX, XO, XY, or XXY sex chromosome combinations, the presence of two X chromosomes resulted in more severe autoimmune disease (Smith-Bouvier, Divekar et al. 2008). MHC genes have also been linked to SLE, with HLA-A1, B8, and DR3 increasing the risk of SLE development (Walport, Black et al. 1982). As MHC molecules are critical in the process of antigen presentation to T-cells,

these particular MHC genes may unduly favor the binding of self-antigens and increase the risk of autoimmunity (Anisur Rahman 2008). Genome-wide association studies have further identified a wide variety and number of genes associated with SLE. These genes have functions in numerous cellular and immune processes including IFN signaling (e.g. TREX1, STAT4, IRAK1, IRF5, TLR8, etc.), immune complex clearance (e.g. C1QA, C2, C4A/B, FCGR2A/3A/3B, etc.), T-cell and B-cell signaling (e.g. PTPN22, TNFSF4, BANK1, BLK, etc.), transcriptional regulation (e.g. JAZF1, BCL6, MECP2, etc.), and apoptosis signaling (e.g. CASP10) (Tsokos 2011). Though there are rare cases of single-gene mutations causing SLE (e.g. C1q mutations), SLE is a predominantly polygenic disease (Crispin, Liossis et al. 2010). The combination of multiple risk alleles is presumed necessary to confer an increased risk of disease development.

Murine Models of SLE

The use of various mouse models of lupus to study the genes involved in SLE pathogenesis has greatly increased our understanding of the mechanisms underlying SLE development. These lupus-prone mouse strains serve as the predominant animal models for human SLE. Though there are differences in disease presentation between the commonly used lupus-prone mouse strains and human SLE, all of the murine models of lupus used meet the American College of Rheumatology's diagnostic criteria for SLE (Andrews BS 1978; Fairhurst, Wandstrat et al. 2006).

The MRL/MpJ-*Fas*^{lpr/lpr} (MRL.lpr) mouse was derived from a series of crosses involving multiple inbred strains. The MRL genome therefore consists of a combination of genes from the LG/J (75%), AKR/J (12.6%), C3H/HeDi (12.1%), and C57BL/6 (0.3%)

murine genetic backgrounds (Andrews BS 1978; Fairhurst, Wandstrat et al. 2006; Theofilopoulos and Dixon 1985). During the breeding process, a spontaneous mutation later found to be located in the *Fas* gene occurred (Takahashi, Tanaka et al. 1994). This mutation was termed lymphoproliferation (*lpr*) as MRL.*lpr* mice manifested an autoimmune phenotype characterized by the massive proliferation of lymphocytes in secondary lymphoid organs (Andrews BS 1978). The *Fas*^{*lpr*} mutation was discovered to alter transcription of the Fas receptor gene, resulting in a nonfunctional transcript (Watanabe-Fukunaga, Brannan et al. 1992). As T- and B-cells rely on Fas-FasL signaling to induce apoptosis, MRL.*lpr* mice demonstrated a defect in apoptosis of autoreactive lymphocytes (Waring and Mullbacher 1999). In addition to splenomegaly and lymphadenopathy, both male and female MRL.*lpr* mice develop high titers of ANAs by 2-3 months of age, as well as displaying immune complex deposition in various tissues by 4-5 months of age. MRL.*lpr* mice eventually develop severe glomerulonephritis, with mortality approaching 100% by 9 months of age (Andrews BS 1978). Introgression of the *lpr* mutation onto the C57BL/6 (B6) background generated the C57BL/6J-*Fas*^{*lpr*}/*Fas*^{*lpr*} (B6.*lpr*) mouse, which displays a significantly milder autoimmune phenotype compared to MRL.*lpr* mice (Fairhurst, Wandstrat et al. 2006; Theofilopoulos and Dixon 1985).

The B6.*SLE1*^{*NZM/NZM*} (B6.SLE1) mouse was derived from the introgression of the *SLE1* lupus susceptibility locus found in NZM2410 lupus-prone mice onto the B6 genetic background (Morel, Mohan et al. 1997). The *SLE1* genomic segment was found to confer a loss of tolerance to nuclear antigens, particularly nucleosomes and chromatin (Chandra Mohan 1998; Morel, Mohan et al. 1997). B6.SLE1 mice develop ANAs by 3 months of age,

as well as hypergammaglobinemia. There is an expansion of activated CD4⁺ T-cells and B-cells in the spleen, resulting in mild splenomegaly (Chen, Cuda et al. 2005; Fairhurst, Wandstrat et al. 2006). Unlike MRL.lpr mice, autoimmune disease in B6.SLE1 mice is strongly gender biased towards females. Female B6.SLE1 mice produce ANAs with much higher penetrance than males, although both male and female B6.SLE1 mice display fairly normal kidney histology. As a result of mild renal involvement, the lifespan of B6.SLE1 mice is comparable to that of wild-type B6 mice (Fairhurst, Wandstrat et al. 2006). However, the introduction of the *SLE2* and *SLE3* lupus susceptibility loci (also derived from NZM2410 lupus-prone mice) onto B6.SLE1 mice generated the B6.SLE1/2/3 mouse, which displays a severe autoimmune phenotype (Morel, Croker et al. 2000). B6.SLE1/2/3 mice develop high titers of ANAs and exhibit fatal immune complex-mediated glomerulonephritis, which affects both genders. It was discovered that the *SLE2* genomic interval lowers the activation threshold for B-cells, facilitating B-cell hyperactivity (Mohan, Morel et al. 1997). The *SLE3* genomic segment was found to mediate T-cell dysregulation (Mohan, Yu et al. 1999).

The Role of PRRs in SLE Pathogenesis

Although the molecular mechanisms driving SLE pathogenesis are still unclear, various studies have established that the PRRs of the innate immune system play a role in disease development (Crispin, Liou et al. 2010; Fairhurst, Wandstrat et al. 2006). PRRs are used by the innate immune system to recognize foreign danger signals like microbe-derived nucleic acids which signify microbial invasion. Activation of PRRs by nucleic acids leads to the production of type-I IFN and other proinflammatory cytokines which play a fundamental role in host defense against infection (Goubau, Deddouche et al. 2013; Pandey S 2014; Wu

and Chen 2014). However, the inadvertent activation of PRRs by endogenous nucleic acids can contribute to the development of autoimmune disease. Studies utilizing MRL.lpr lupus-prone mice demonstrated that TLR7 signaling is required for the production of anti-Sm autoantibodies and TLR7 deficiency partially ameliorated autoimmune disease severity (Christensen, Shupe et al. 2006). In addition, work utilizing the B6.SLE1 mouse model of lupus showed that B-cell expression of TLR7 promoted production of autoantibodies directed against RNA-associated antigens and exacerbated autoimmune disease (Hwang, Lee et al. 2012). In numerous murine models of lupus, TLR9 deficiency reduced production of anti-DNA autoantibodies, although disease severity was unexpectedly worsened (Christensen, Kashgarian et al. 2005; Christensen, Shupe et al. 2006; Ehlers M 2006; Lartigue, Courville et al. 2006; Nickerson, Christensen et al. 2010). It has also been shown that MRL.lpr mice lacking Myd88 do not develop autoantibodies to chromatin and some ribonucleoproteins, resulting in an ameliorated disease phenotype (Nickerson, Christensen et al. 2010). The nucleic acid-sensing PRRs of the innate immune system therefore play an important role in SLE pathogenesis.

The cGAS-STING pathway plays a critical role in the development of autoimmunity in the *Trex1*^{-/-} mouse model of autoimmune disease. In humans, mutations in the exonuclease *Trex1* results in the autoimmune disease Aicardi–Goutieres syndrome (AGS). AGS shares many characteristics with SLE (Crow, Hayward et al. 2006). *Trex1*^{-/-} mice also demonstrate an autoimmune and autoinflammatory phenotype caused by the defective clearance of self-DNA (Crow, Hayward et al. 2006; Morita, Stamp et al. 2004). The genetic ablation of cGAS or STING in this model completely rescues the autoimmune phenotype that would otherwise

be seen in *Trex1*^{-/-} mice (Gall, Treuting et al. 2012; Gao, Li et al. 2015). In addition, a subset of SLE patients express increased cGAS levels and cGAMP production within peripheral blood mononuclear cells (PBMCs), and this is correlated with an IFN signature and increased disease activity (An, Durcan et al. 2016). Recently, a gain-of-function mutation in STING was found to cause familial chilblain lupus in a multigenerational Greek family (Konig, Fiehn et al. 2016). This activating mutation in STING, G166E, causes constitutive production of type-I IFN and elevated ISG levels in affected cells. It is therefore possible that the cGAS-STING pathway may play a role in the development of autoimmunity in SLE. However, the potential role that the cGAS-STING cytosolic DNA sensing pathway plays in SLE pathogenesis remains to be elucidated.

Goal of Current Research

As cGAS is the upstream DNA sensor to the STING/TBK1/IRF3 pathway, I hypothesized that cGAS is responsible for sensing and mediating the adjuvant effects of plasmid DNA during the course of DNA vaccination. Here I sought to determine if the cGAS-STING DNA sensing pathway is responsible for mediating the adjuvant effect of plasmid DNA in vivo. In addition, I address whether 2'3'-cGAMP can substitute for DNA as a molecular vaccine adjuvant with the same immunostimulatory properties as DNA but without its potential drawbacks. Within an influenza vaccination model, I compared the efficacy of 2'3'-cGAMP as an adjuvant to the widely used adjuvant alum and also investigated methods for boosting the adjuvant activity of 2'3'-cGAMP.

Within the context of SLE, the potential recognition of self-DNA by cGAS would activate the cGAS-STING pathway and result in inflammatory cytokine production. In a

genetically susceptible host, the cGAS-STING pathway might contribute to the inflammatory milieu, giving rise to inflammation-associated immune cells which would result in autoantibody production and the aberrant host immune response observed in SLE. To test this hypothesis, I investigated the role that the cGAS-STING pathway plays in disease pathogenesis in multiple murine models of lupus. I characterized the effect that genetic ablation of cGAS or STING in C57BL/6J-*Fas*^{lpr}/*Fas*^{lpr}, B6.MRL/Mp-*Fas*^{lpr/lpr}, and B6.*SLE1*^{NZM/NZM}.*Fas*^{lpr/lpr} mice has on the development of the autoimmune phenotype.

CHAPTER TWO

The cGAS-STING pathway mediates DNA adjuvant activity and use of 2'3'-cGAMP as a vaccine adjuvant

RESULTS

The adjuvant effect of DNA is mediated by both cGAS and STING

To determine if cGAS and STING are required for innate immune signaling following plasmid DNA administration in vivo, C57BL/6 wild-type (B6 WT) mice, cGAS KO, and STING *gt/gt* mice were injected intramuscularly (i.m.) with an empty pcDNA3 vector and local injection site cytokine and interferon-stimulated gene production was measured by RT-PCR 6 or 12 hrs after injection. Quantification of IFN- α_1/β production showed that both IFN- α_1 and IFN- β levels were attenuated in cGAS KO and STING *gt/gt* mice compared to WT at both timepoints (**Fig. 1a, 1b**). Measurement of ISG transcript levels revealed a significant decrease in CXCL10, Ifit3, and ISG15 expression in both cGAS KO and STING *gt/gt* mice compared to WT at both timepoints (**Fig. 1c,d,e**). Comparing between timepoints, IFN- α_1/β and ISG15/Ifit3 transcript levels at 12 hrs post-injection were higher in B6 WT, cGAS KO, and STING *gt/gt* mice compared to their corresponding 6 hrs post-injection levels.

To test if the diminished innate immune response to plasmid DNA in cGAS KO and STING *gt/gt* mice would have a negative impact on generation of antigen-specific adaptive immunity, B6 WT, cGAS KO, and STING *gt/gt* mice were vaccinated with influenza A/PR/8/34 (H1N1 PR8) hemagglutinin (HA) antigen in combination with pcDNA3 plasmid adjuvant. Serum HA-specific IgG antibody levels were measured one week post-boost and showed that loss of cGAS or STING resulted in a marked decrease in total anti-HA IgG

levels compared to WT (**Fig. 2a**). In mice, the IgG class of antibodies can be broken down into Th1-related subclasses (IgG2a, IgG2b, and IgG3) and the Th2-related subclass IgG1. To determine what effect the adjuvant property of plasmid DNA has on the generation of a “Th1-like” or “Th2-like” humoral immune response, I measured anti-HA specific IgG1 and IgG2b levels in the sera from vaccinated mice gathered one week post-boost. Consistent with the observed result for anti-HA total IgG, deletion of cGAS or STING resulted in a significant decrease in both anti-HA IgG1 and IgG2b levels compared to WT (**Fig. 2b, 2c**). B6 WT mice produced both IgG1 and IgG2b in response to vaccination, suggesting plasmid DNA is capable of stimulating the Th1/2 CD4⁺ T-cell response and that this effect is greatly reduced with genetic deletion of cGAS or STING. Similar results to those observed with HA antigen were obtained using ovalbumin (OVA) as the vaccine antigen (**Fig. 3a,b,c,d**). Vaccination of control mice with H1N1 PR8 HA antigen alone resulted in an insignificant humoral immune response, suggesting the generation of HA-specific antibodies was promoted by the presence of plasmid DNA adjuvant (**Fig. 4a,b,c**). In addition, the serum from vaccinated cGAS KO and STING gt/gt mice demonstrated a significant loss in HA-neutralizing antibody titer as measured by HAI assay compared to WT (**Fig. 2d**). I then challenged immunized mice with a lethal dose of influenza H1N1 PR8 virus to assess the protective efficacy of vaccination utilizing plasmid DNA as an adjuvant. Consistent with the impaired immune response observed in cGAS KO and STING gt/gt mice, both cGAS KO and STING gt/gt mice demonstrated substantial bodyweight loss and succumbed to influenza virus infection by day 12 post-challenge. In contrast, immunized B6 WT mice demonstrated only mild bodyweight loss and survived lethal influenza virus challenge (**Fig. 2e, 2f**). Control

mice vaccinated with H1N1 PR8 antigen alone uniformly succumbed to lethal influenza virus challenge (**Fig. 4d,e**).

Activation of the cGAS-STING pathway via 2'3'-cGAMP induces stronger neutralizing antibody and T-cell responses compared to alum

Although DNA itself displays adjuvant activity, there are potential disadvantages to its use. These disadvantages include the theoretical risk of integration into the host cellular genome, the potential to develop antibiotic resistance, and the development of autoimmunity (Kutzler and Weiner 2008). Therefore, it would be preferable to use an adjuvant that displayed the same immunogenic properties as DNA while avoiding the potential risks. As the adjuvant property of DNA is dependent on the cGAS-STING pathway, I sought to assess the capability of 2'3'-cGAMP to function as an adjuvant in lieu of DNA. To this end, I compared the efficacy of 2'3'-cGAMP to alum, a commonly used adjuvant. B6 WT mice were immunized with H1N1 PR8 HA antigen together with varying amounts of 2'3'-cGAMP or alum. Serum HA-specific IgG antibody levels were subsequently measured one week post-boost. Mice that received vaccine containing 10 μ g 2'3'-cGAMP displayed significantly higher anti-HA IgG1 levels compared to mice vaccinated with alum, with total anti-HA IgG and IgG2b levels trending higher in the 10 μ g 2'3'-cGAMP group (**Fig. 5a,b,c**). Strikingly, mice vaccinated with 10 μ g 2'3'-cGAMP displayed markedly higher influenza neutralizing antibody titers compared to mice immunized with alum (**Fig. 5d**). Mice that received vaccine containing either 3 or 5 μ g 2'3'-cGAMP had similar humoral immune responses as alum adjuvanted mice. As the ideal vaccine adjuvant stimulates both humoral and cellular immunity, I then sought to determine the effect 2'3'-cGAMP has on the CD8⁺ T-cell response. B6 WT mice were immunized with 2'3'-cGAMP or alum in conjunction with

H1N1 PR8 nucleoprotein (NP) antigen. Mice that received 10 μg 2'3'-cGAMP displayed a significantly higher proportion of NP-specific CD8⁺ T-cells within the total CD8⁺ T-cell population compared to mice immunized with alum (**Fig. 5e**). To assess the protective efficacy of 2'3'-cGAMP as an adjuvant compared to alum, vaccinated mice were challenged with a 50xMLD₅₀ dose of H1N1 PR8 virus. Although vaccinated mice in both the 10 μg 2'3'-cGAMP and alum groups displayed significant bodyweight loss (**Fig. 5f**), mice in the 10 μg 2'3'-cGAMP group had dramatically improved survival over alum adjuvanted mice (**Fig. 5g**). Mice in the 3 or 5 μg 2'3'-cGAMP groups displayed similar survival to alum adjuvanted mice. Control mice vaccinated with H1N1 PR8 HA antigen alone succumbed to 50xMLD₅₀ influenza virus challenge (**Fig. 4f,g**). Examination of lung histopathology from immunized mice infected with H1N1 PR8 virus showed numerous lung lesions in control mice immunized with H1N1 PR8 HA antigen alone (**Fig. 6a**). These lesions were characterized by airway epithelial cell apoptosis and necrosis, neutrophil invasion through the airway epithelium, edema in surrounding alveoli, the presence of neutrophils and lymphocytes in alveoli and bronchioles, and inflammatory cell debris accumulation in airway spaces. Mice in the 10 μg 2'3'-cGAMP or alum adjuvanted groups also exhibited similar lung lesions. Quantitative lung histopathology scoring showed that mice in the 10 μg 2'3'-cGAMP immunized group had lung lesions of significantly less severity than mice in the H1N1 PR8 HA antigen alone control group, with alum immunized mice demonstrating lung lesions that were intermediate in severity compared to control and 10 μg 2'3'-cGAMP groups (**Fig. 6b**). Taken together, these results suggest 2'3'-cGAMP can indeed function as an adjuvant with

the same immunostimulatory properties as plasmid DNA, and that 2'3'-cGAMP is superior to alum in inducing protective humoral and cellular adaptive immune responses.

Degradation-resistant 2'3'-cGAMP induces stronger adaptive immune responses compared to free 2'3'-cGAMP

Influenza vaccination utilizing 2'3'-cGAMP as an adjuvant protected mice from death following high-dose influenza virus challenge. Despite being protected from death, these mice still displayed marked bodyweight loss, demonstrating room for improvement in the adjuvant properties of 2'3'-cGAMP. The recently identified ecto-nucleotide pyrophosphatase/phosphodiesterase, ENPP1, has been shown to have 2'3'-cGAMP hydrolyzing activity (Li, Yin et al. 2014). As ENPP1 is found in the serum and extracellular environment, it is possible that much of the 2'3'-cGAMP administered intramuscularly during vaccination may be degraded before it has a chance to act. In addition, free 2'3'-cGAMP can also diffuse away from the injection site, leading to suboptimal exposure of antigen-presenting cells (APCs) to adjuvant. Therefore, I wanted to test whether protecting 2'3'-cGAMP from hydrolysis and limiting diffusion in vivo would result in a stronger adjuvant effect, leading to a better immune response following vaccination. To test this, I used a non-hydrolyzable thio-cGAMP analog (2'3'-cGsAsMP) and 2'3'-cGAMP delivered encapsulated in invivofectamine [2'3'-cGAMP(invivo)]. The liposome encapsulation protects 2'3'-cGAMP from degradation and limits diffusion away from the injection site. B6 WT mice were vaccinated with H1N1 PR8 HA antigen in conjunction with free 2'3'-cGAMP, 2'3'-cGsAsMP, or 2'3'-cGAMP(invivo). One week post-boost, serum HA-specific IgG antibody levels were measured. Mice in the 10 µg 2'3'-cGsAsMP and 10 µg 2'3'-cGAMP(invivo) groups displayed markedly higher anti-HA total IgG and IgG2b responses

than mice that received 10 μg 2'3'-cGAMP. Mice which received 3 μg 2'3'-cGsAsMP displayed an antibody response similar to mice in the 10 μg 2'3'-cGAMP group. Serum anti-HA IgG1 levels were not significantly different between the vaccinated groups of mice. Vaccination using invivofectamine alone without 2'3'-cGAMP resulted in a negligible humoral immune response (**Fig. 7a,b,c**). Mice immunized using 10 μg 2'3'-cGsAsMP and 10 μg 2'3'-cGAMP(*invivo*) also generated significantly higher influenza neutralizing antibody titers compared to mice vaccinated with 10 μg 2'3'-cGAMP. Mice immunized with 3 μg 2'3'-cGsAsMP displayed similar HAI titers to mice adjuvanted with 10 μg 2'3'-cGAMP. Control mice that received vaccine adjuvanted with invivofectamine alone produced insignificant HAI titers (**Fig. 7d**). To measure the CD8⁺ T-cell response, B6 WT mice were vaccinated with H1N1 PR8 NP antigen in combination with free 2'3'-cGAMP, 2'3'-cGsAsMP, or 2'3'-cGAMP(*invivo*). Mice adjuvanted with 10 μg 2'3'-cGAMP(*invivo*) had a significantly higher proportion of NP-specific CD8⁺ T-cells within the total CD8⁺ T-cell population compared to mice vaccinated with 10 μg 2'3'-cGAMP. However, no significant difference was seen in NP-specific CD8⁺ T-cell populations between mice immunized with 10 μg 2'3'-cGsAsMP and 10 μg 2'3'-cGAMP. In addition, both cohorts of mice vaccinated with 3 μg cGsAsMP or invivofectamine only displayed negligible NP-specific CD8⁺ T-cell responses (**Fig. 7e**). Vaccinated mice were challenged with a 50xMLD₅₀ dose of H1N1 PR8 virus. Mice in the 10 μg 2'3'-cGsAsMP and 10 μg 2'3'-cGAMP(*invivo*) cohorts experienced significantly less bodyweight loss than mice that received 10 μg 2'3'-cGAMP. Mice immunized with 3 μg 2'3'-cGsAsMP also displayed less bodyweight loss than mice in the 10 μg 2'3'-cGAMP group. Mice vaccinated with invivofectamine alone

displayed little protection against virus challenge with severe bodyweight loss observed (**Fig. 7f**). All vaccinated mice in the 10 μg 2'3'-cGsAsMP, 2'3'-cGAMP, and 2'3'-cGAMP(*in vivo*) groups survived influenza virus challenge, whereas one mouse died in the 3 μg 2'3'-cGsAsMP group and none survived from the *in vivo* fectamine only group (**Fig. 7g**). Lung sections from immunized mice infected with H1N1 PR8 virus in the *in vivo* fectamine only group exhibited similar lung lesions to those seen in the control H1N1 PR8 HA antigen alone and 10 μg 2'3'-cGAMP adjuvanted groups (**Fig. 6a, 8a**). In contrast, vastly ameliorated lung lesions were observed in the tissues from 10 μg 2'3'-cGsAsMP and 2'3'-cGAMP(*in vivo*) immunized groups. Consistent with the observed histology, histopathology scores for both 10 μg 2'3'-cGsAsMP and 2'3'-cGAMP(*in vivo*) vaccinated groups were dramatically lower than the score for the 10 μg 2'3'-cGAMP immunized group (**Fig. 8b**). The histology score for the 2'3'-cGAMP(*in vivo*) adjuvanted group was significantly lower than that of the control *in vivo* fectamine only group. Interestingly, the *in vivo* fectamine only group had a less severe lung histology score than the H1N1 PR8 HA antigen alone control group, placing it on par with the mean composite histological score of the 10 μg 2'3'-cGAMP group.

2'3'-cGAMP adjuvant activity is synergistically enhanced when combined with TLR9 agonist

Previous studies have reported that the combined use of cyclic dinucleotides with CpG ODN produced a synergistic effect which significantly improved the immunostimulatory properties of both adjuvants (Temizoz, Kuroda et al. 2015; Yildiz, Alpdundar et al. 2015). To see if this effect extended to my vaccination model, I immunized B6 WT mice with H1N1 PR8 HA antigen in conjunction with free 2'3'-cGAMP, Class C

CpG ODN (CpG-C), or a combination of the two. Serum HA-specific IgG antibody levels were measured one week post-boost. Mice vaccinated with 10 μg CpG-C displayed modest anti-HA total IgG production, with IgG1 being the primary IgG subclass produced. A stronger effect was seen when 50 μg CpG-C was used in vaccinating the mice compared to 10 μg CpG-C. Similar to the 10 μg CpG-C group, mice immunized with 5 μg 2'3'-cGAMP displayed moderate levels of anti-HA total IgG, with primarily IgG1 subclass antibody production. However, mice adjuvanted with both 5 μg 2'3'-cGAMP and 10 μg CpG-C together produced significantly higher levels of serum anti-HA total IgG, IgG1, and IgG2b compared to mice adjuvanted with only 5 μg 2'3'-cGAMP or 10 μg CpG-C alone (**Fig. 9a,b,c**). In line with the anti-HA IgG antibody response, influenza neutralizing antibody titers were dramatically increased in mice vaccinated with the combination of 5 μg 2'3'-cGAMP and 10 μg CpG-C compared to mice adjuvanted with 5 μg 2'3'-cGAMP or 10 μg CpG-C alone. In addition, mice that received 50 μg CpG-C had a higher HAI titer compared to mice that received 10 μg CpG-C (**Fig. 9d**). These results suggest the combination of cGAMP and CpG ODN is indeed synergistic with respect to stimulating the humoral immune response. To see if the combination of cGAMP and CpG ODN has synergistic effects in stimulating the cellular immune response, B6 WT mice were immunized with H1N1 PR8 NP antigen in conjunction with free 2'3'-cGAMP and/or CpG-C. Mice adjuvanted with 5 μg 2'3'-cGAMP and 10 μg CpG-C together had a significantly higher proportion of NP-specific CD8⁺ T-cells within the total CD8⁺ T-cell population compared to mice vaccinated with 5 μg 2'3'-cGAMP or 10 μg CpG-C alone. There was no statistically significant difference in the NP-specific CD8⁺ T-cell population between mice vaccinated with 50 μg CpG-C or 10 μg CpG-C (**Fig.**

9e). Vaccinated mice were challenged with a 50xMLD₅₀ dose of H1N1 PR8 virus. Mice in the 5 µg 2'3'-cGAMP and 10 µg CpG-C group demonstrated significantly less bodyweight loss than mice adjuvanted with either 5 µg 2'3'-cGAMP, 10 µg CpG-C, or 50 µg CpG-C alone (**Fig. 9f**). All mice in the 5 µg 2'3'-cGAMP and 10 µg CpG-C group survived influenza virus challenge. None of the mice vaccinated with 10 µg CpG-C alone survived, whereas mice immunized with 5 µg 2'3'-cGAMP or 50 µg CpG-C demonstrated partial protection from lethal influenza challenge (**Fig. 9g**). Upon histopathological examination, the lung sections from 5 µg 2'3'-cGAMP, 10 µg CpG-C, and 5 µg 2'3'-cGAMP plus 10 µg CpG-C vaccinated groups infected with H1N1 PR8 virus showed the presence of lung lesions similar to those observed in the H1N1 PR8 HA antigen alone control group (**Fig. 6a, 10a**). Compared to H1N1 PR8 HA antigen alone control group, composite histology scores for the 5 µg 2'3'-cGAMP, 10 µg CpG-C, and 5 µg 2'3'-cGAMP plus 10 µg CpG-C vaccinated groups were significantly lower (**Fig. 10b**). Unexpectedly, there was no significant difference observed in histology score when comparing between the 5 µg 2'3'-cGAMP and 10 µg CpG-C immunized group and the 5 µg 2'3'-cGAMP alone immunized group. Similarly, no significant difference in histology score was found between the 5 µg 2'3'-cGAMP and 10 µg CpG-C group and the 10 µg CpG-C alone group.

CONCLUSIONS AND DISCUSSIONS

All vaccines must contain a protective antigen and an adjuvant component in order to be optimally immunogenic and efficacious. For DNA vaccines, the plasmid backbone constitutes the adjuvant component of the vaccine and is responsible for triggering innate immune activation. However, it is unclear which innate immune sensor is responsible for detecting the plasmid DNA adjuvant component of a DNA vaccine *in vivo*. Previous reports have shown that DNA vaccine immunogenicity is independent of the TLR pathways and instead dependent on the STING/TBK1/IRF3 pathway. In particular, type-I IFN production is crucial for induction of the immune response to B-form DNA and is also required for cellular immune responses following DNA vaccination (Ishii, Coban et al. 2005; Ishii, Kawagoe et al. 2008; Shirota, Petrenko et al. 2009; Stetson and Medzhitov 2006; Tudor, Riffault et al. 2001). Recent work has established cGAS as a nonredundant cytosolic DNA sensor that functions upstream of the STING/TBK1/IRF3 pathway (Li, Wu et al. 2013; Sun, Wu et al. 2012). This made cGAS a likely candidate for the DNA sensor responsible for mediating the adjuvant effects of plasmid DNA. My results show that deletion of cGAS in mice impairs type-I IFN and ISG production following plasmid DNA inoculation *in vivo* compared to WT mice. Both cGAS KO and STING *gt/gt* mice produced comparable levels of type-I IFN and ISG's to intramuscularly injected plasmid DNA (**Fig. 1**). This impairment in type-I IFN and ISG production ultimately lead to a diminished vaccination-induced immune response in cGAS KO and STING *gt/gt* mice compared to WT when plasmid DNA was used as the vaccine adjuvant (**Fig. 2; Fig. 3**). Unexpectedly, however, I observed that local post-plasmid DNA injection type-I IFN production rose over the course of 12 hours in

both cGAS KO and STING *gt/gt* mice (**Fig. 1a,b**). This increase in type-I IFN production was accompanied by modest increases in ISG production in both cGAS KO and STING *gt/gt* mice (**Fig. 1d,e**). This may explain why vaccination-induced immune responses were not completely abrogated in cGAS KO and STING *gt/gt* mice when plasmid DNA was used as the vaccine adjuvant. That cGAS KO and STING *gt/gt* mice were capable of mounting immune responses, albeit weakly, to an influenza antigen vaccine containing plasmid DNA adjuvant is surprising and suggests that when the cGAS-STING pathway is deleted, other pathways of DNA sensing may step in to partially fill the void. One possibility is that plasmid DNA is capable of activating endosomal TLR9 weakly, and that when the cGAS-STING pathway is intact and functioning, its effects are dominant over the TLR9/MyD88 pathway in terms of eliciting type-I IFN production. In the absence of cGAS or STING, however, the TLR9/MyD88 pathway would still be capable of initiating a weak innate immune response against plasmid DNA. It is also possible that other PRRs may play a role in sensing cytosolic DNA. A recent study has suggested a role for the Aim2-inflammasome pathway in mediating DNA vaccine immunogenicity (Suschak, Wang et al. 2015). The activation of these and other putative DNA sensors in the absence of the cGAS-STING pathway provides a possible explanation as to why cGAS KO and STING *gt/gt* mice are able to generate weak adaptive immune responses to a plasmid DNA adjuvanted vaccine. My work stands in contrast to a previously reported study which found that the immune response to DNA vaccination *in vivo* is not cGAS-dependent but rather STING/IRF7-dependent, with IRF3 playing a limited role in mediating DNA vaccine immunogenicity (Suschak, Wang et al. 2015). My results show a more significant role for cGAS in sensing the plasmid DNA

adjuvant component of DNA vaccines. This discrepancy in results may be due to the use of a different vaccination strategy in my study. Because I was interested solely in testing whether cGAS was the DNA sensor responsible for detecting the plasmid DNA adjuvant component of a DNA vaccine, I isolated the adjuvant property of plasmid DNA by using it as the vaccine adjuvant and delivering it with influenza protein antigen. This was done in order to mimic the effects of a traditional DNA vaccination while keeping the adjuvant and antigen components separate in order to avoid confounding factors. In this model of DNA vaccination, cGAS plays an important role in mediating the adjuvant properties of plasmid DNA. In the future, I can conduct DNA vaccination experiments where I immunize B6 WT, cGAS KO, and STING *gt/gt* mice with a traditional DNA vaccine to see if I can replicate the results I obtained utilizing DNA-adjuvanted vaccination. If the results are inconsistent, future work will be focused on identifying the potential differences between traditional DNA vaccination and DNA-adjuvanted vaccination. It is likely those potential differences would alter the dependency of the vaccination-induced immune response on cGAS-STING pathway signaling.

My results showed that the adjuvant property of DNA is both cGAS and STING dependent, suggesting that the immune response to plasmid DNA is driven by cGAS-STING pathway signaling. I found that plasmid DNA is capable of stimulating both a Th1-like and Th2-like humoral immune response, suggesting DNA stimulates both a Th1 and Th2 CD4⁺ T-cell response (**Fig. 2b,c; Fig. 3**). Although DNA as an adjuvant is capable of stimulating a balanced cellular and humoral immune response, there are potential downsides to the use of DNA plasmids to deliver vaccines. Therefore I wanted to find a vaccine adjuvant capable of

the same immunostimulatory properties as DNA but without its potential disadvantages.

2'3'-cGAMP, a small cyclic dinucleotide second messenger molecule, is found in the cGAS-STING pathway and is ideally positioned to be used as an adjuvant in lieu of DNA. Because 2'3'-cGAMP binds to STING and induces production of type-I IFN and other proinflammatory cytokines, it has the same effect on the innate immune system as plasmid DNA. Unlike the plasmid DNA used for DNA vaccines, however, 2'3'-cGAMP is unable to be accidentally integrated into the host genome, can be mass produced without the need for antibiotic resistance markers, and is too small of an endogenous molecule to elicit natural autoantibody production against itself. In addition, the presence of ENPP1 in the extracellular environment makes 2'3'-cGAMP a naturally metabolizable molecule, limiting its potential distribution and any unwanted inflammatory effects. Furthermore, mice vaccinated with 2'3'-cGAMP combined with the model antigen OVA develop robust OVA-specific humoral and cellular immune responses, indicating the potential of 2'3'-cGAMP to function as a vaccine adjuvant (Li, Wu et al. 2013). One of the major issues confronting traditionally used adjuvants like alum is that they are generally incapable of stimulating a strong Th1 CD4⁺/CD8⁺ T-cell response, and cellular adaptive immunity is critical for optimal protection against pathogens. In this study, I use an influenza vaccination model to demonstrate that 2'3'-cGAMP functions as a vaccine adjuvant capable of stimulating both protective humoral and cellular adaptive immune responses superior to that of the standard FDA-approved adjuvant alum. 2'3'-cGAMP elicits higher titers of influenza neutralizing antibodies and influenza-specific CD8⁺ T-cells compared to alum (**Fig. 5d,e**). However, when vaccinated mice are challenged with a lethal dose of influenza virus, 2'3'-cGAMP immunized mice

demonstrate significant bodyweight loss comparable to alum immunized mice, although survival of 2'3'-cGAMP immunized mice is superior (**Fig. 5f,g**). The dose response to 2'3'-cGAMP when used as an adjuvant is non-linear at the dosages I tested, with a possible explanation being that much of the 2'3'-cGAMP injected is likely degraded or diffuses away from the intramuscular injection site before it is able to act on APCs (**Fig. 5a,b,c**). In order to improve upon the performance of 2'3'-cGAMP as an adjuvant, I used three distinct strategies. The first strategy was to encapsulate 2'3'-cGAMP in a liposome particle in order to limit its diffusion and enhance uptake into target cells, the second strategy was to use a non-hydrolyzable analog to prevent its degradation and prolong exposure to target cells, and the third strategy was to combine it with a TLR9 agonist in order to achieve synergistic immunostimulatory effects. All three strategies were effective in enhancing the adjuvant properties of 2'3'-cGAMP, leading to higher influenza neutralizing antibody titers and influenza-specific CD8⁺ T-cell populations (with the exception of 2'3'-cGsAsMP) across the three vaccination strategies used (**Fig. 7d,e; Fig. 9d,e**). Mice receiving 2'3'-cGsAsMP, 2'3'-cGAMP(in vivo), or 2'3'-cGAMP + CpG-C all demonstrated significant boosts in their Th1-like humoral immune response compared to free 2'3'-cGAMP, suggesting these vaccination strategies were capable of enhancing the Th1 CD4⁺ T-cell response (**Fig. 7c; Fig. 9c**). In addition, vaccinated mice from these groups displayed striking protection against high-dose influenza virus challenge (50xMLD₅₀) compared to mice vaccinated with free 2'3'-cGAMP (**Fig. 7f,g; Fig. 9f,g**). Although these alternate strategies for overcoming the natural limitations of 2'3'-cGAMP as an adjuvant were effective, there are potential safety concerns inherent in potently stimulating the immune response in this manner. As 2'3'-cGAMP is a

naturally occurring, metabolizable, endogenous molecule it is expected to have little toxicity. However, the use of liposome encapsulated or non-hydrolyzable analogs of 2'3'-cGAMP prolongs the presence of 2'3'-cGAMP in injected tissue, raising the possibility of causing prolonged local inflammation at the injection site and its associated deleterious effects. Although the combination of 2'3'-cGAMP with CpG-C is expected to have short-term effects due to natural degradation mechanisms in place for both molecules, the synergistic effect of combining these two adjuvants together on the immune system may also cause adverse local injection site tissue reactions via stimulation of a strong inflammatory response. Further work will be needed to address the potential safety concerns of vaccination strategies intended to enhance the adjuvant effect of 2'3'-cGAMP. In the future, I can perform drug safety testing with mice that have been injected with 2'3'-cGAMP, 2'3'-cGsAsMP, 2'3'-cGAMP(in vivo), or 2'3'-cGAMP and CpG-C. These mice would be monitored for side effects and their organs can be examined for signs of drug toxicity. In addition to the methods tested in this study, there are other strategies to improve adjuvant potency including altering the injection site location. Previous studies have demonstrated that free cGAMP can function as an efficacious adjuvant via the mucosal and intradermal vaccination routes, eliciting a balanced antigen-specific humoral and cellular immune response with minimal toxicity (Skrnjug I. 2014; Wang, Li et al. 2016).

The use of 2'3'-cGsAsMP as a non-hydrolyzable analog did improve upon the adjuvant properties of 2'3'-cGAMP, significantly boosting the antigen-specific humoral immune response to vaccination. 2'3'-cGsAsMP has been reported to be approximately 40 times more resistant to ENPP1 hydrolysis than 2'3'-cGAMP, and in vitro stimulation of

THP-1 cells with 2'3'-cGsAsMP resulted in roughly ten-fold higher IFN- β production compared to cells stimulated with 2'3'-cGAMP. This effect of 2'3'-cGsAsMP was likely not due to tighter STING binding, but rather its increased biostability (Li, Yin et al. 2014). For this reason, I expected 2'3'-cGsAsMP to stimulate a stronger CD8⁺ T-cell response than 2'3'-cGAMP when used as a vaccine adjuvant. However, the antigen-specific CD8⁺ T-cell response to 2'3'-cGsAsMP did not appreciably differ from that of 2'3'-cGAMP, while the use of 2'3'-cGAMP(in vivo) did significantly boost the antigen-specific CD8⁺ T-cell response to vaccination compared to 2'3'-cGAMP (**Fig. 7e**). One explanation for this observed result is that while 2'3'-cGsAsMP would have increased biostability in vivo, unlike in vitro cell cultures, diffusion away from the inoculation site occurs and can result in decreased bioavailability of adjuvant to APCs located in the intramuscular injection site (Wang, Li et al. 2016). Since 2'3'-cGsAsMP and 2'3'-cGAMP have similar chemical properties and structures, it is likely that both adjuvants have comparable rates of diffusion away from the injection site, partially negating the advantage in biostability that 2'3'-cGsAsMP would otherwise have and dampening its adjuvant effect. Despite adjuvant diffusion, the enhanced biostability of 2'3'-cGsAsMP over 2'3'-cGAMP could still be harnessed over the course of multiple vaccination injections, which would maximize exposure of APCs to adjuvant. This would explain why 2'3'-cGsAsMP was effective in boosting vaccine-induced humoral immune responses but not CD8⁺ T-cell responses compared to 2'3'-cGAMP in my experiments, as I administered both priming and booster vaccine doses to mice before measuring antigen-specific humoral immune responses whereas only a priming vaccine dose was administered to mice prior to measurement of antigen-specific CD8⁺ T-cell responses.

One strategy to overcome the issue of 2'3'-cGAMP diffusion is the use of a nanoparticle/liposome-mediated adjuvant delivery mechanism, which has been shown to be effective for other cyclic dinucleotides like cyclic di-GMP (Hanson MC 2015).

Encapsulation of 2'3'-cGAMP in a liposome would limit its diffusion and enhance its cellular uptake. In addition, liposome encapsulation protects 2'3'-cGAMP from ENPP1 hydrolysis. These effects explain why 2'3'-cGAMP(*in vivo*) was superior to 2'3'-cGAMP as a vaccine adjuvant in inducing antigen-specific humoral and cellular immune responses and also explains why 2'3'-cGAMP(*in vivo*) induced a stronger antigen-specific CD8⁺ T-cell response than 2'3'-cGsAsMP.

Here I show that the cGAS-STING pathway mediates the adjuvant property of plasmid DNA during the course of DNA vaccination and that cGAS is the DNA sensor responsible for detection of the plasmid DNA adjuvant component of a DNA vaccine. I further demonstrate that 2'3'-cGAMP can function as an effective vaccine adjuvant with the same immunogenic properties as plasmid DNA. Using an influenza vaccination model, I show that 2'3'-cGAMP induces strong protective humoral and cellular immune responses to vaccination and that the adjuvant activity of 2'3'-cGAMP can be enhanced by liposome encapsulation, the use of non-hydrolyzable analogs, or co-administration with CpG-C DNA. My results provide further insight into the innate immune mechanisms involved in DNA vaccine immunogenicity, and demonstrate that 2'3'-cGAMP is a promising adjuvant that can be used to design vaccines which merit future clinical studies.

MATERIALS AND METHODS

Reagents

2'3'-cGAMP was synthesized and purified as previously described (Zhang, Shi et al. 2013). CpG-C DNA (ODN 2395) was purchased from InvivoGen. Imject Alum adjuvant was purchased from ThermoFisher Scientific. Invivofectamine 3.0 reagent was purchased from Invitrogen. Influenza A H1N1 (A/Puerto Rico/8/34) hemagglutinin (HA) and nucleoprotein (NP) antigens were purchased from Sino Biological Inc. Ovalbumin antigen was purchased from Sigma. Empty pcDNA3 plasmid was amplified in *E. coli* and purified for use using the Qiagen Endofree Plasmid Giga Kit.

Mice and Vaccinations

C57BL/6J and C57BL/6J-*Tmem173^{gt}*/J [STING *gt/gt*] mice were obtained from The Jackson Laboratory. *cGAS^{-/-}* (KO) mice were generated in our laboratory as previously described (Li, Wu et al. 2013). All mice were bred and maintained in the animal facilities of the University of Texas Southwestern Medical Center according to Institutional Animal Care and Use Committee-approved protocols.

For all influenza-related DNA, cGAMP, and CpG-C DNA adjuvant vaccination experiments, 6-8 week old female mice were primed on Day 0 with intramuscular (i.m.) injection in both hind quadriceps muscles with 50 μ l volume per quadriceps with antigen (2 μ g H1N1 HA or H1N1 NP per mouse) with or without adjuvant (100 μ g pcDNA3 plasmid; 3, 5, or 10 μ g cGAMP; 10 or 50 μ g CpG-C DNA; 3 or 10 μ g cGsAsMP; Alum; 10 μ g cGAMP packaged in invivofectamine [cGAMP (invivo)] per mouse). A booster dose was given on Day 10 with antigen (1 μ g H1N1 HA or H1N1 NP per mouse) with or without

adjuvant (the same amount of adjuvant was administered for both prime and boost). Alum was used at a 1:1 dilution in PBS containing antigen. cGAMP was packaged in invivojectamine according to manufacturer's protocol. For cGAMP (invivo) injections, the cGAMP packaged in invivojectamine was injected immediately prior to antigen injection. Serum was collected from the mice on Day 17 for antibody analysis.

For all OVA-related vaccination experiments, 8-10 week old female mice were primed on Day 0 with bilateral hind quadriceps (50 μ l volume/leg) i.m. injection with 10 μ g OVA antigen alone or together with 10 μ g pcDNA3 plasmid. An identical booster dose was given to mice on Day 10. Serum was collected from mice on Days 0, 10, 17, 20, and 24 for antibody analysis.

ELISA

96-well ELISA plates (greiner bio-one) were coated with recombinant H1N1 HA antigen at 5 μ g/mL in PBS overnight at 4°C. After blocking the plates with PBS-3% BSA (wt/vol), serum samples were added to plate at a 1:10000 dilution in PBS-1% BSA (wt/vol). After washing of plate, HRP-conjugated goat anti-mouse IgG (H+L) (Millipore) was added at a 1:2500 dilution. For IgG1 and IgG2b detection, HRP-conjugated goat anti-mouse IgG1 or IgG2b (Abcam) antibodies were added at a dilution of 1:5000. The plate was developed with 3,3',5,5'-tetramethylbenzidine substrate (Thermo Scientific), and the OD at 450 nm was measured.

For OVA-specific ELISAs, antibody titers were measured as previously described (Li, Wu et al. 2013).

Virus Challenge

For influenza challenge, Influenza A/PR/8/34 (H1N1) virus (Charles River Laboratories) was diluted in sterile PBS to either 10x (700 pfu/mouse) or 50xMLD₅₀ (3600 pfu/mouse) dosages. Mice were sedated using ketamine (30 mg/ml)/xylazine (4 mg/ml) intraperitoneally (i.p.) and virus was administered intranasally in a total volume of 40 µL, split evenly between nares. After virus challenge, mice received atipamezole (0.63 mg/ml) i.p. and were subsequently monitored for weight loss and mortality for 14 days. Mice were humanely sacrificed when weight loss exceeded 30%.

HAI Assay

Influenza A/PR/8/34 (H1N1)-specific neutralizing antibodies were detected using a hemagglutination inhibition assay. Serum samples were serially diluted 1:2 in 50 µL PBS-1% BSA in sterile v-bottom polystyrene microtiter plates. 50 µL Influenza A/PR/8/34 (H1N1) virus (4 HAU) was added to each well. After 45 minute incubation at room temperature, 50 µL of 0.15% chicken red blood cells (Lampire Biological Laboratories) were added to each well. After 1 hour incubation at room temperature, the HAI titer was assessed for each sample. The HAI titer was expressed as the reciprocal of the highest serum dilution that fully inhibited hemagglutination caused by the virus.

Flow Cytometry

For tetramer staining, 6-week old mice were immunized on Day 0 as indicated. On Day 10, mice received a 10xMLD₅₀ booster dose of Influenza A/PR/8/34 (H1N1) virus intranasally. Four days post-boost, spleens were harvested from mice and splenocytes isolated for surface staining. Briefly, cells were washed in ice-cold FACS staining buffer [10% FBS (wt/vol), 0.1% NaN₃ (wt/vol) in PBS]. Cell suspensions were then incubated with

Rat anti-mouse CD16/32 antibody (Biolegend) at a 1:200 dilution for 15 minutes on ice.

After washing cells with FACS staining buffer, cells were then surface stained with tetramer and antibodies against CD3 and CD8. The stained cells were analyzed using a FACSCalibur flow cytometer (BD Biosciences). Data were analyzed using FlowJo software. CD8-PE and CD3-FITC antibodies were purchased from eBioscience. H-2D(b) Influenza A Virus H1N1 PR8 Nucleoprotein (ASNENMETM) APC-labeled tetramer was provided by the NIH Tetramer Core Facility.

Quantitative RT-PCR

Mice were shaved and injected with 100 µg pcDNA3 plasmid i.m. in both tibialis anterior muscles (50 µl volume per leg). Injection site muscle tissue was harvested 6 or 12 hours post-injection and snap frozen. Muscle tissue samples were placed in Lysing Matrix D tubes (MP Biomedicals) and homogenized using a Precellys24 tissue homogenizer (Bertin Technologies). Total RNA was isolated from homogenized muscle tissue samples using an RNeasy Mini Kit (Qiagen) and cDNA was synthesized using the iScript cDNA synthesis kit (Bio-Rad). Real-time PCR (RT-PCR) reactions were carried out by using the iTaq Universal SYBR Green Supermix (Bio-Rad). RT-PCR was performed on an Applied Biosystems ViiA 7. Primers used: Rpl19 (AAATCGCCAATGCCAACTC; TCTTCCCTATGCCCATATGC), IFN-β (TCCGAGCAGAGATCTTCAGGAA; TGCAACCACCACTCATTCTGAG), IFN-α₁ (AGCCTTGACACTCCTGGTAC, TGGTGGAGGTCATTGCAGAA), CXCL10 (GCCGTCATTTTCTGCCTCA; CGTCCTTGCGAGAGGGATC), Ifit3 (TGGCCTACATAAAGCACCTAGATGG, CGCAAACCTTTTGGCAAACCTTGTCT), ISG15 (GGAACGAAAGGGGCCACAGCA, CCTCCATGGGCCTTCCCTCGA).

Pathology

Vaccinated mice were inoculated with 10xMLD₅₀ Influenza A/PR/8/34 (H1N1) virus intranasally. Four days post-infection, lungs were harvested from mice. The right middle lung lobe was isolated for histology and fixed in 4% (wt/vol) paraformaldehyde. Tissue samples were then paraffin-embedded, sectioned at 5 µm, and stained with hematoxylin and eosin (H&E). For histological scoring of lung lesions, H&E sections were blindly evaluated by a pathologist for airway and vascular inflammation according to the following scoring system: Airway Criteria Evaluated [1) Peribronchial Edema, 2) Peribronchial Inflammation, 3) Alveoli Inflammation, 4) Epithelial Airway Morphology Change, 5) Amount of inflammatory cell debris in all airways] and Vascular Criteria Evaluated [1) Perivascular Edema, 2) Perivascular Inflammation]. Each individual criterion was scored from 0-4 based on severity [0 = none, 1 = minimal, 2 = mild, 3 = moderate, 4 = severe]. The total composite lung histology score was derived by adding the score of each criterion together.

Virology

Influenza A/PR/8/34 (H1N1) virus stock was titered by plaque assay using Madin-Darby canine kidney cells using standard methods. The median lethal dose (MLD₅₀) was calculated in mice using standard methods (Cottey R. 2001).

Statistical Analysis

All data are presented as the mean of individual mice ± SEM. Statistical analysis of mouse survival was performed using the Mantel-Cox test. All other statistical analyses were performed by using a two-tailed, unpaired Student's *t* test.

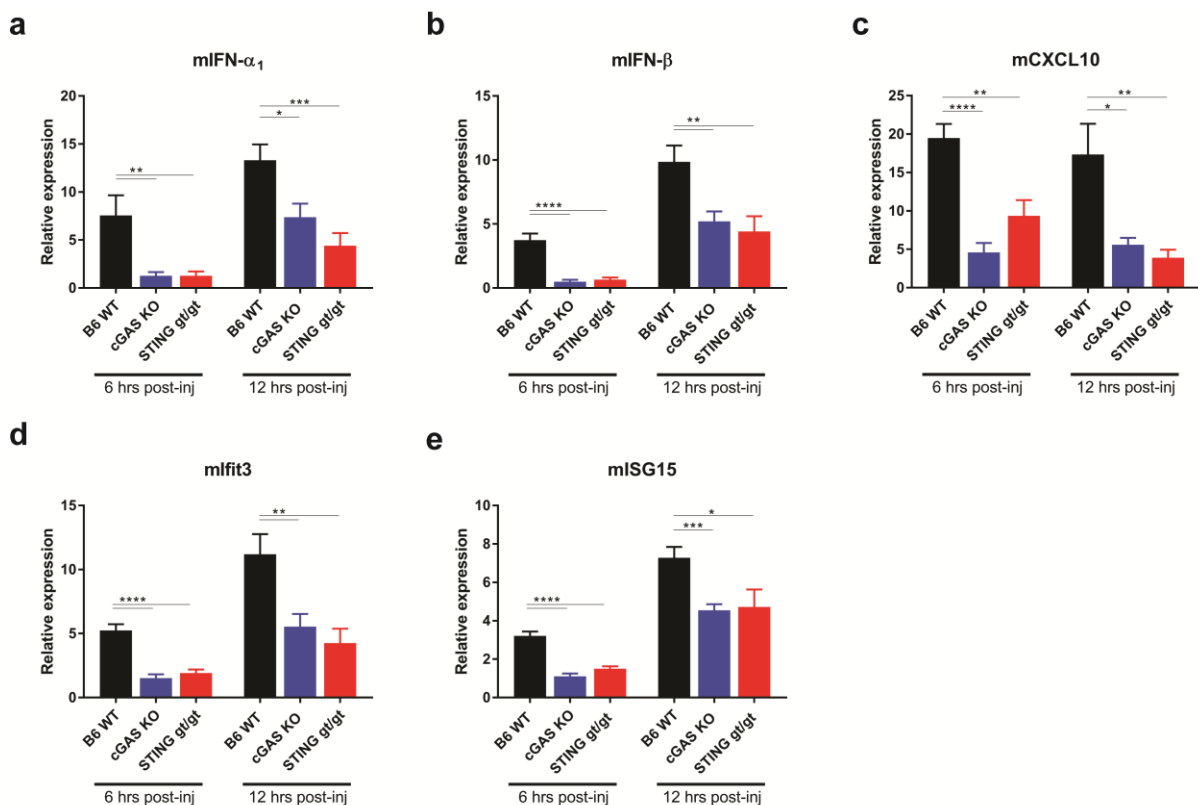


Figure 1: IFN- α_1/β and ISG production following intra-muscular DNA injection is dependent on cGAS and STING.

a,b,c,d,e, Cytokine production as measured by RT-PCR for mouse IFN- α_1 (**a**) and IFN- β (**b**) in local injection site tissue harvested from B6 WT, cGAS KO, or STING *gt/gt* mice that were injected intramuscularly with pcDNA3 plasmid. Injection site tissue was harvested 6 or 12 hrs post-injection. In addition, interferon-stimulated gene expression was measured for mouse CXCL10 (**c**), Ifit3 (**d**), and ISG15 (**e**). Data are presented as the mean \pm SEM from three independent experiments of three mice per group (total $n = 9/\text{genotype}$). Values are relative to naïve mouse gene expression. * $p < 0.05$, ** $p < 0.01$, *** $p < 0.001$, **** $p < 0.0001$ versus indicated group (two-tailed, unpaired Student's *t* test).

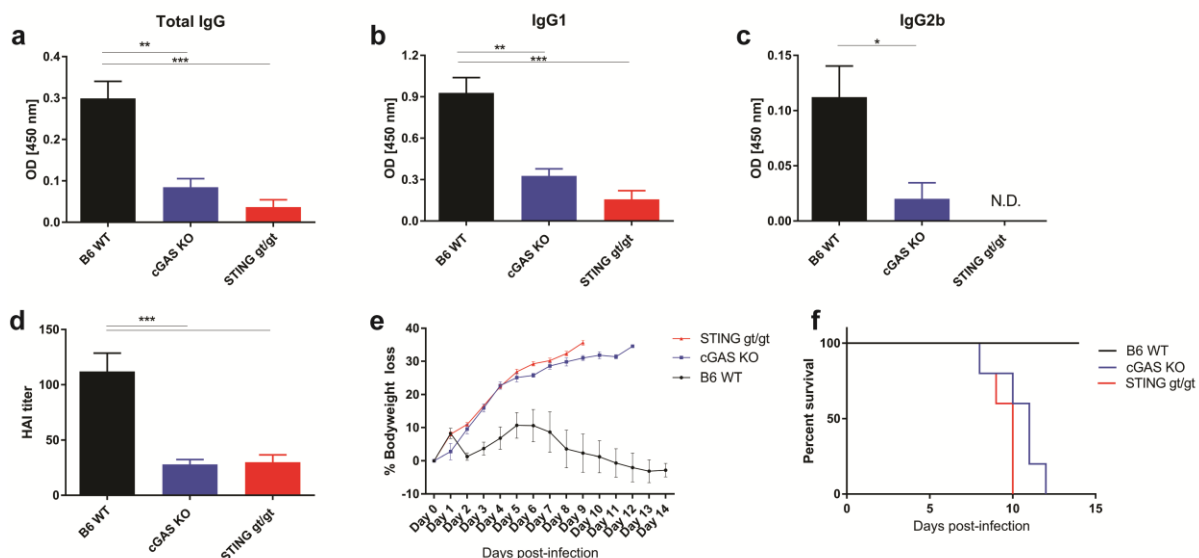


Figure 2: cGAS and STING are required for an immune response following vaccination utilizing DNA as an adjuvant.

a,b,c, Circulating anti-hemagglutinin (anti-HA) total IgG (**a**) levels were measured by ELISA in serum harvested from vaccinated mice one week post-boost. In addition, the circulating anti-HA IgG1 (**b**) and IgG2b (**c**) subclass levels in vaccinated mouse sera were also measured at one week post-boost. B6 WT ($n = 8$), cGAS KO ($n = 5$), and STING gt/gt ($n = 5$) mice were immunized i.m. with a pcDNA3 plasmid plus H1N1 PR8 HA priming dose. A booster dose was administered ten days post-prime. **d**, In a separate independent experiment ($n = 10$ /genotype), HAI titers were measured via hemagglutination inhibition assay (HAI assay) in serum harvested one week post-boost from vaccinated mice. Mice were vaccinated as previously described. **e,f**, Vaccinated mice ($n = 5$ /genotype) were intranasally challenged with 10xMLD₅₀ of Influenza A/PR/8/34 (H1N1) virus 1.5 weeks post-boost. Bodyweight (**e**) and survival (**f**) were tracked daily for two weeks. Data are presented as the mean \pm SEM. * $p < 0.05$, ** $p < 0.01$, *** $p < 0.001$ versus indicated group (two-tailed, unpaired Student's t test).

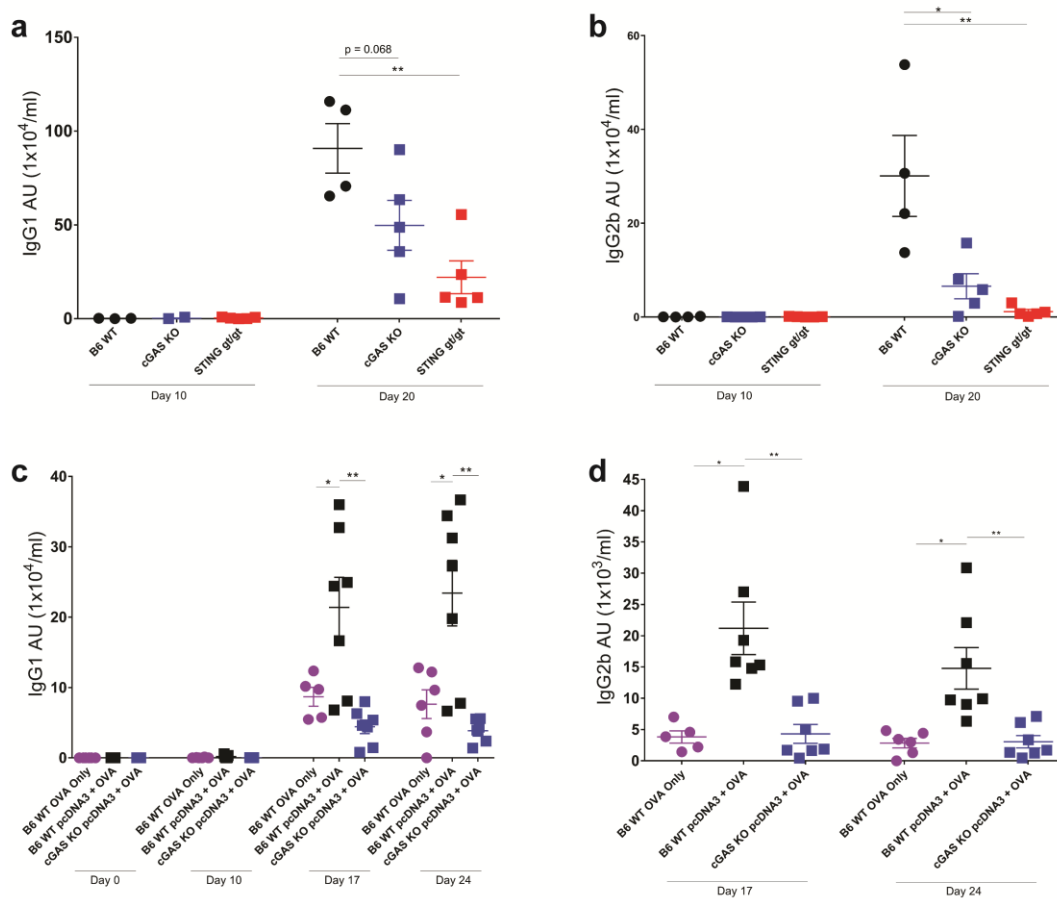


Figure 3: The cGAS-STING pathway is required for the humoral immune response to DNA-adjuvanted vaccination.

a,b, Circulating titers of anti-ovalbumin (OVA) IgG1 (**a**) and IgG2b (**b**) were measured by ELISA in serum harvested from immunized mice ten days post-prime and ten days post-boost. B6 WT, cGAS KO, and STING g/gt mice were vaccinated i.m. with a pcDNA3 plasmid together with OVA priming dose. A booster dose was administered to mice ten days post-prime. Each dot represents one mouse. **c,d**, Circulating titers of anti-OVA IgG1 (**c**) and IgG2b (**d**) in serum harvested from immunized mice as measured by ELISA. B6 WT mice were primed i.m. with OVA alone or together with pcDNA3 plasmid. cGAS KO mice were primed i.m. with OVA together with pcDNA3 plasmid. All mice were boosted ten days post-prime. Serum was harvested on day 0 (prime), 10, 17, and 24. Each dot represents one mouse. Data are presented as the mean \pm SEM. * $p < 0.05$, ** $p < 0.01$ versus indicated group (two-tailed, unpaired Student's t test).

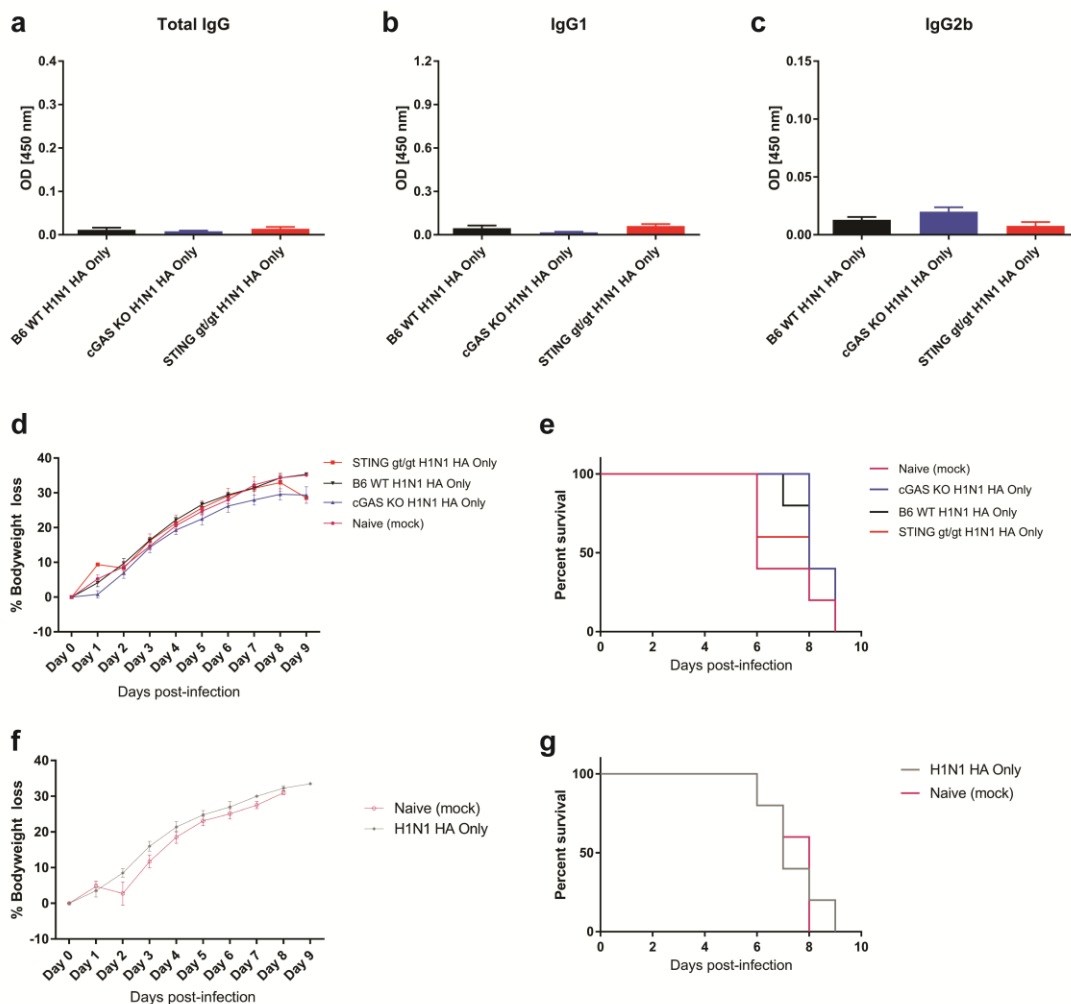


Figure 4: Vaccination with protein antigen alone induces negligible immune response in mice.

a,b,c, Serum was harvested from vaccinated mice one week post-boost and circulating levels of anti-HA total IgG (**a**), IgG1 (**b**), and IgG2b (**c**) were measured by ELISA. B6 WT ($n = 5$), cGAS KO ($n = 5$), and STING *gt/gt* ($n = 3$) mice were immunized i.m. with H1N1 PR8 HA alone. A booster dose was administered ten days post-prime. **d,e**, Vaccinated mice ($n = 5$ /genotype) were intranasally challenged with 10xMLD₅₀ of Influenza A/PR/8/34 (H1N1) virus 1.5 weeks post-boost. Bodyweight (**d**) and survival (**e**) were tracked daily for two weeks. Mice were vaccinated as previously described. A naïve group of B6 WT ($n = 5$) mice receiving mock injections of PBS was included for reference. **f,g**, Immunized mice ($n = 5$ /group) were intranasally challenged with 50xMLD₅₀ of Influenza A/PR/8/34 (H1N1) virus 1.5 weeks post-boost. Bodyweight (**f**) and survival (**g**) were tracked daily for two weeks. B6 WT mice were either given mock injections of PBS or were primed with H1N1 PR8 HA alone. A booster dose was administered ten days post-prime. Data are presented as the mean \pm SEM.

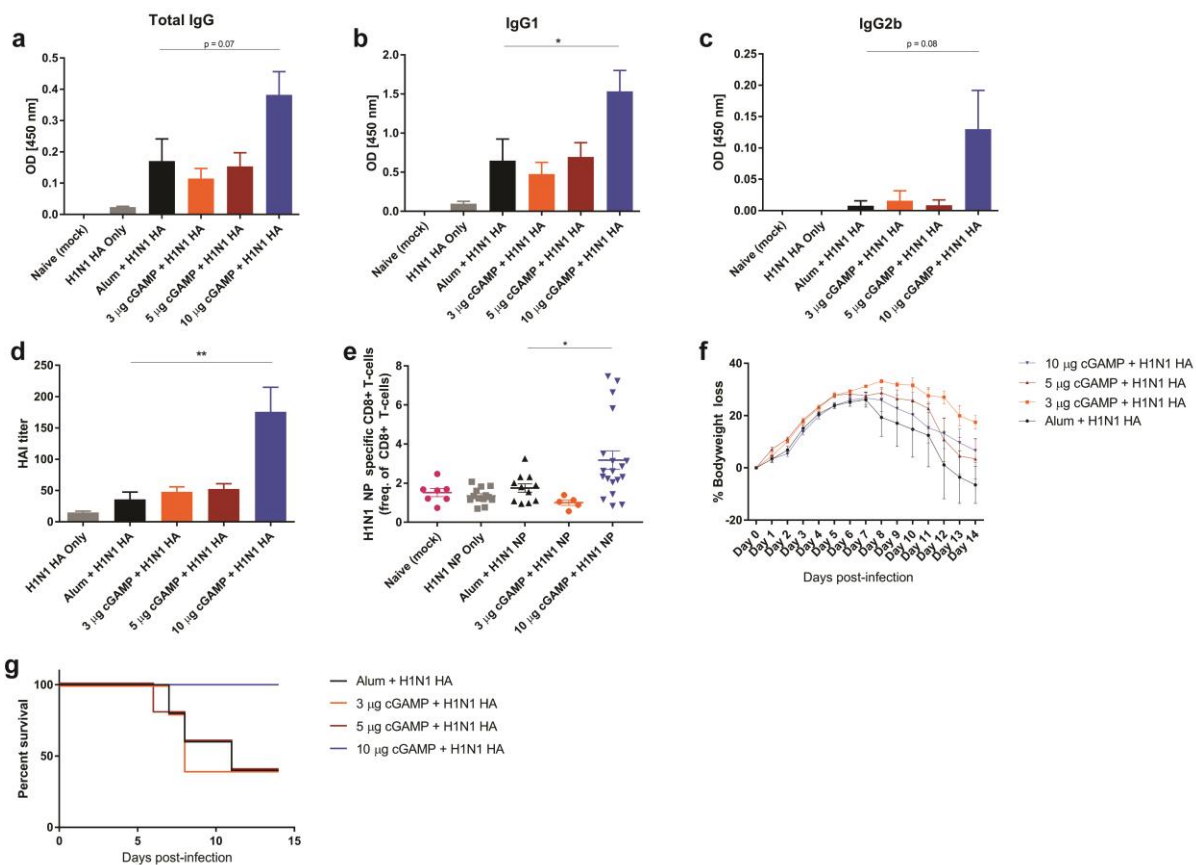


Figure 5: 2'3'-cGAMP demonstrates superior adjuvant effects compared to alum.

a,b,c, Circulating anti-HA total IgG (**a**) levels were measured by ELISA in serum harvested from vaccinated mice one week post-boost. Circulating anti-HA IgG1 (**b**) and IgG2b (**c**) subclass levels in vaccinated mouse sera were also measured. B6 WT mice ($n = 5/\text{group}$) were primed i.m. with H1N1 PR8 HA alone or in combination with alum or stated amount of 2'3'-cGAMP. A booster dose was administered ten days post-prime. **d**, In a separate independent experiment, HAI titers were measured one week post-boost via HAI assay in serum harvested from vaccinated mice. Mice were vaccinated as previously described. H1N1 HA Only ($n = 6$), alum and 3/10 μg cGAMP ($n = 5/\text{group}$), 5 μg cGAMP ($n = 8$). **e**, The amount of H1N1 Nucleoprotein (NP)-specific CD8⁺ T-cells (as a percentage of total CD8⁺ T-cells) found in the spleens of vaccinated mice that received a viral boost. Mice were immunized i.m. with H1N1 PR8 NP alone or in combination with indicated amount of 2'3'-cGAMP or alum. One week post-prime, mice received 10xMLD₅₀ Influenza A/PR/8/34 (H1N1) virus boost intranasally. Splenocytes were harvested four days post-viral boost and H1N1 NP-specific CD8⁺ T-cells were measured by flow cytometry using tetramer staining. Each dot represents one mouse. **f,g**, Vaccinated mice ($n = 5/\text{group}$) were intranasally challenged with 50xMLD₅₀ of Influenza A/PR/8/34 (H1N1) virus 1.5 weeks post-boost. Bodyweight (**f**) and survival (**g**) were tracked daily for two weeks. Data are presented as the mean \pm SEM. * $p < 0.05$, ** $p < 0.01$ versus indicated group (two-tailed, unpaired Student's *t* test).

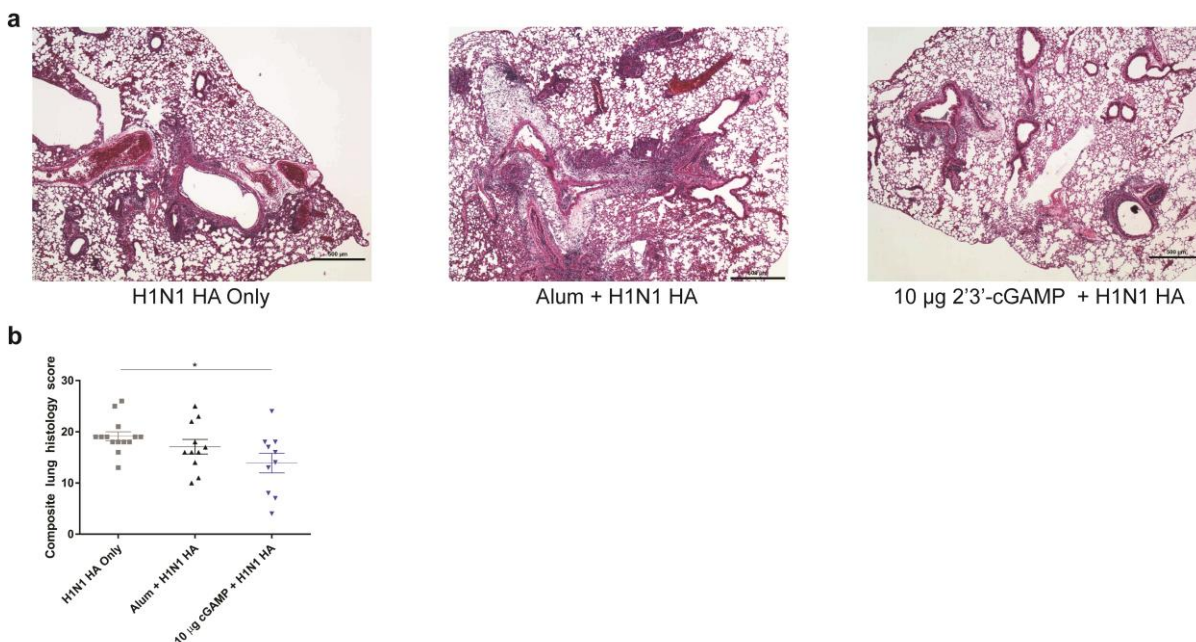


Figure 6: Histopathological damage to lungs of 2'3'-cGAMP and alum vaccinated mice infected with H1N1 PR8 virus.

a, Lung sections from immunized mice infected with Influenza A/PR/8/34 (H1N1) virus. Sections were hematoxylin-eosin stained and images taken at 4x magnification. Scale bar depicts 500 μ m. B6 WT mice were vaccinated i.m. with H1N1 PR8 HA alone or in combination with alum or 10 μ g 2'3'-cGAMP. Ten days post-prime, mice were given a booster dose. Vaccinated mice were infected with 10xMLD₅₀ Influenza A/PR/8/34 (H1N1) virus 1.5 weeks post-boost. Lungs were harvested four days post-infection. H1N1 HA Only ($n = 14$), alum ($n = 11$), 10 μ g 2'3'-cGAMP ($n = 10$). Images are representative of each depicted group. **b**, Composite histological scoring of airway and vascular lesions observed in lung sections from vaccinated mice infected with influenza virus. Mice were vaccinated and infected as previously described. Each dot represents one mouse. Data are presented as the mean \pm SEM. * $p < 0.05$ versus indicated group (two-tailed, unpaired Student's t test).

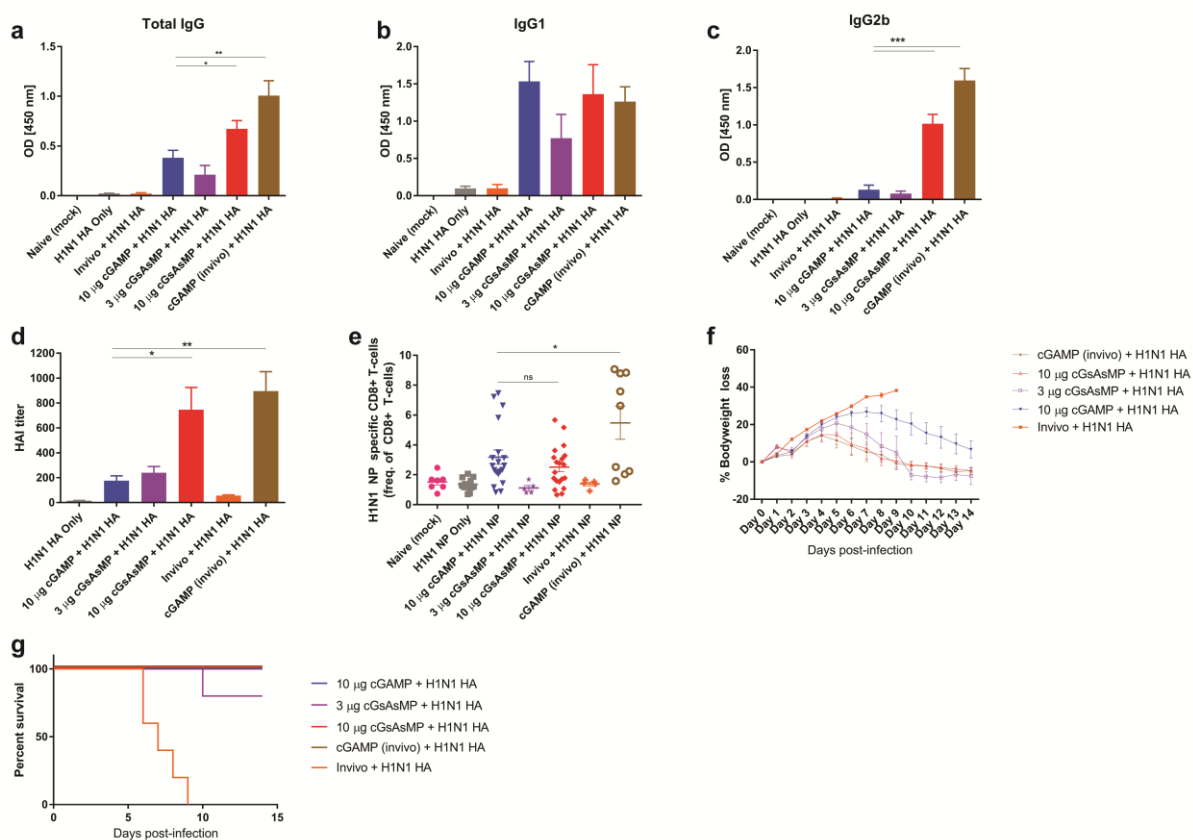


Figure 7: Both 2'3'-cGsAsMP and liposome-encapsulated 2'3'-cGAMP display enhanced adjuvant activity compared to free 2'3'-cGAMP.

a,b,c, Serum was harvested from vaccinated mice one week post-boost and levels of anti-HA total IgG (**a**), IgG1 (**b**), and IgG2b (**c**) were measured by ELISA. B6 WT mice ($n = 5/\text{group}$) were immunized i.m. with H1N1 PR8 HA alone or in combination with InvivoFectamine 3.0 (invivo), or the indicated amount of 2'3'-cGAMP/2'3'-cGsAsMP, or 10 μg 2'3'-cGAMP packaged in invivo [cGAMP(invivo)]. A booster dose was administered ten days post-prime. **d**, Serum HAI titers from vaccinated mice were measured one week post-boost in a separate independent experiment. Mice were vaccinated as previously described. H1N1 HA Only/10 μg 2'3'-cGsAsMP ($n = 6/\text{group}$), 10 μg 2'3'-cGAMP/3 μg 2'3'-cGsAsMP/10 μg cGAMP(invivo) ($n = 5/\text{group}$). **e**, The amount of H1N1 NP-specific CD8⁺ T-cells (as a percentage of total CD8⁺ T-cells) found in the spleens of vaccinated mice that received a viral boost. Mice were primed i.m. with H1N1 PR8 NP alone or in combination with the stated amount of 2'3'-cGAMP/2'3'-cGsAsMP, or invivo only, or 2'3'-cGAMP(invivo). One week post-prime, mice received 10xMLD₅₀ Influenza A/PR/8/34 (H1N1) virus boost intranasally. Splenocytes were harvested four days post-viral boost and H1N1 NP-specific CD8⁺ T-cells were measured by flow cytometry using tetramer staining. Each dot represents one mouse. **f,g**, Immunized mice ($n = 5/\text{group}$) were intranasally challenged with 50xMLD₅₀ of Influenza A/PR/8/34 (H1N1) virus 1.5 weeks post-boost. Bodyweight (**f**) and survival (**g**) were tracked daily for two weeks. Data are presented as the mean ± SEM. * $p < 0.05$, ** $p < 0.01$, *** $p < 0.001$ versus indicated group (two-tailed, unpaired Student's *t* test).

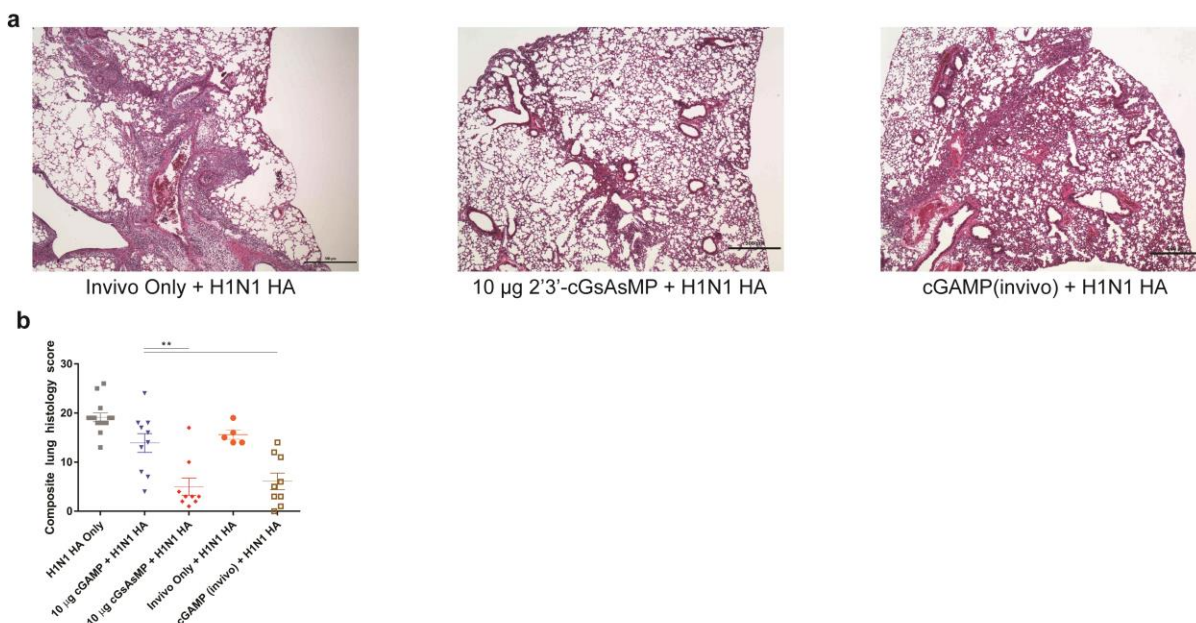


Figure 8: Ameliorated histopathological damage in lungs of 2'3'-cGsAsMP and cGAMP(invivo) vaccinated mice infected with H1N1 PR8 virus.

a, Lung sections from vaccinated mice challenged with Influenza A/PR/8/34 (H1N1) virus. Sections were hematoxylin-eosin stained and images taken at 4x magnification. Scale bar depicts 500 μ m. B6 WT mice were primed i.m. with H1N1 PR8 HA in combination with invivo only, 10 μ g 2'3'-cGsAsMP, or cGAMP(invivo). Ten days post-prime, a booster dose was administered to the mice. Vaccinated mice were infected with 10xMLD₅₀ Influenza A/PR/8/34 (H1N1) virus 1.5 weeks post-boost. Lungs were harvested four days post-infection. Invivo Only ($n = 5$), 10 μ g 2'3'-cGsAsMP/cGAMP(invivo) ($n = 9$ /group). Images are representative of each depicted group. **b**, Composite histological scoring of airway and vascular lesions observed in lung sections from immunized mice infected with influenza virus. Mice were immunized and infected as previously described. Each dot represents one mouse. Data are presented as the mean \pm SEM. $**p < 0.01$ versus indicated group (two-tailed, unpaired Student's t test).

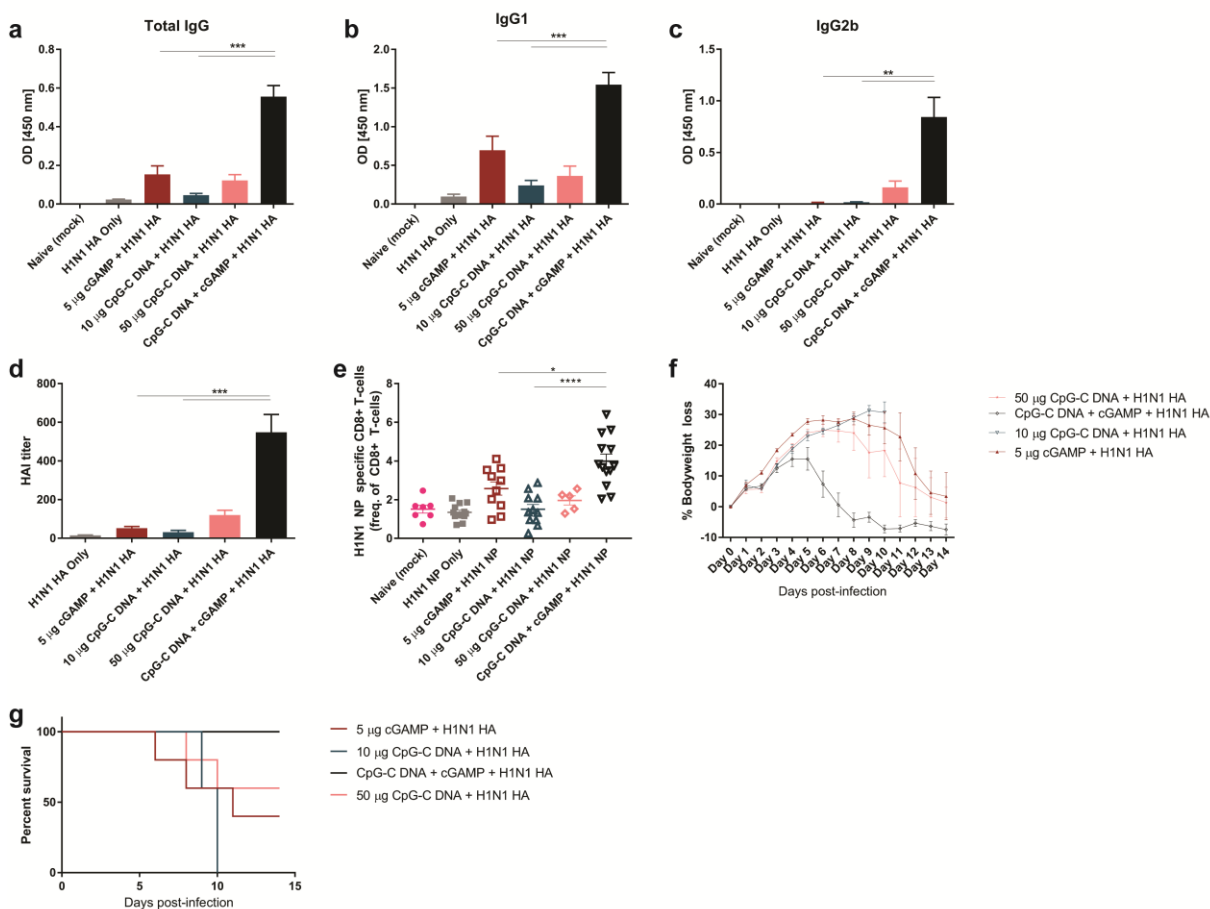


Figure 9: 2'3'-cGAMP adjuvant activity is enhanced in a synergistic manner when combined with TLR9 agonist.

a,b,c, One week post-boost, serum was harvested from immunized mice and circulating levels of anti-HA total IgG (**a**), IgG1 (**b**), and IgG2b (**c**) were measured by ELISA. B6 WT mice ($n = 5/\text{group}$) were vaccinated i.m. with H1N1 PR8 HA alone or in combination with the indicated amount of CpG-C, or 5 μg 2'3'-cGAMP, or 5 μg 2'3'-cGAMP and 10 μg CpG-C (CpG-C DNA+cGAMP) together. A booster dose was administered ten days post-prime. **d**, HAI titers from the sera of vaccinated mice harvested one week post-boost were measured in a separate independent experiment. Mice were vaccinated as previously described. H1N1 HA Only ($n = 6$), 5 μg 2'3'-cGAMP ($n = 8$), 10 μg CpG-C ($n = 7$), 50 μg CpG-C ($n = 5$), CpG-C DNA+cGAMP ($n = 14$). **e**, The amount of H1N1 NP-specific CD8⁺ T-cells (as a percentage of total CD8⁺ T-cells) found in the spleens of immunized mice that received a viral boost. Mice were vaccinated i.m. with H1N1 PR8 NP alone or in combination with the stated amount of 2'3'-cGAMP and/or CpG-C. One week later, primed mice received 10xMLD₅₀ Influenza A/PR/8/34 (H1N1) virus boost intranasally. Splenocytes were harvested four days post-viral boost and H1N1 NP-specific CD8⁺ T-cells were measured by flow cytometry using tetramer staining. Each dot represents one mouse. **f,g**, Vaccinated mice ($n = 5/\text{group}$) were intranasally challenged with 50xMLD₅₀ of Influenza A/PR/8/34 (H1N1) virus 1.5 weeks post-boost. Bodyweight (**f**) and survival (**g**) were tracked daily for two weeks. Data are presented as the mean \pm SEM. * $p < 0.05$, ** $p < 0.01$, *** $p < 0.001$ versus indicated group (two-tailed, unpaired Student's t test).

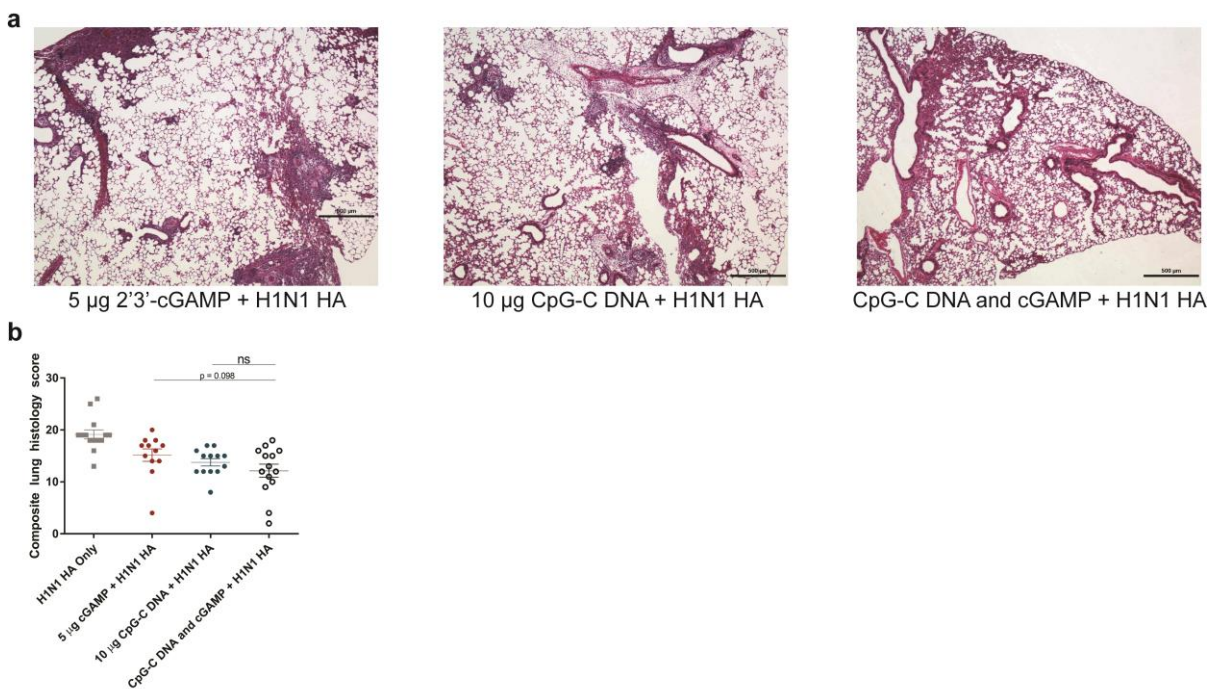


Figure 10: Synergy between 2'3'-cGAMP and CpG-C DNA is not reflected in the histopathological damage observed in lungs of vaccinated mice infected with H1N1 PR8 virus.

a, Lung sections from immunized mice challenged with Influenza A/PR/8/34 (H1N1) virus. Sections were hematoxylin-eosin stained and images taken at 4x magnification. Scale bar depicts 500 μm . B6 WT mice were vaccinated i.m. with H1N1 PR8 HA in combination with 5 μg 2'3'-cGAMP, 10 μg CpG-C, or 5 μg 2'3'-cGAMP plus 10 μg CpG-C (CpG-C DNA and cGAMP). Mice were given a booster dose ten days post-prime. Vaccinated mice were infected with 10xMLD₅₀ Influenza A/PR/8/34 (H1N1) virus 1.5 weeks post-boost. Lungs were harvested four days post-infection. 5 μg 2'3'-cGAMP ($n = 12$), 10 μg CpG-C ($n = 13$), CpG-C DNA and cGAMP ($n = 14$). Images are representative of each depicted group. **b**, Composite histological scoring of airway and vascular lesions observed in lung sections from vaccinated mice challenged with influenza virus. Mice were immunized and infected as previously described. Each dot represents one mouse. Data are presented as the mean \pm SEM.

CHAPTER THREE

The cGAS-STING pathway promotes autoantibody production and autoimmune inflammatory cell accumulation in C57BL/6J-*Fas*^{lpr}/*Fas*^{lpr} mice

RESULTS

Genetic ablation of cGAS or STING in C57BL/6J-*Fas*^{lpr}/*Fas*^{lpr} mice results in decreased autoantibody production

Autoantibodies directed against nuclear self-antigens are an important characteristic of SLE. Among the various autoantibody specificities, anti-DNA autoantibodies (in particular, anti-dsDNA autoantibodies) are considered pathognomonic for SLE (Anisur Rahman 2008; Fairhurst, Wandstrat et al. 2006). In some lupus patients, anti-dsDNA autoantibody titers have been shown to be correlated with greater disease severity (Anisur Rahman 2008). Mice harboring homozygous *Fas*^{lpr/lpr} mutations normally make autoantibodies specific for a number of autoantigens, including DNA (Andrews BS 1978; Braun 2003; Fairhurst, Wandstrat et al. 2006; Nickerson, Christensen et al. 2010; Schwarting, Paul et al. 2005; Tada, Kondo et al. 2011). To test if the cGAS-STING pathway is required for the production of pathogenic IgG autoantibodies against DNA, I generated C57BL/6J-*Fas*^{lpr}/*Fas*^{lpr} (B6.lpr) mice deficient in either cGAS (cGAS KO.lpr) or STING (Sgt.lpr). These mice were generated on a pure B6 background in order to avoid confounding genetic factors often introduced when genetic backgrounds are mixed. SLE is an autoimmune disease with a known gender bias, affecting females more commonly and severely than males (Anisur Rahman 2008; Tsokos 2011). Initially, I assessed anti-dsDNA/ssDNA IgG autoantibody levels in an assortment of 5 month old male and female B6.lpr, cGAS KO.lpr, and Sgt.lpr mouse sera to determine if a gender bias was present. Female B6.lpr mice showed significantly higher anti-DNA autoantibody production than male B6.lpr mice (**Fig. 11a,b**).

Initial results also demonstrated a significant decrease in anti-dsDNA and anti-ssDNA IgG autoantibody levels in the sera from cGAS KO.lpr females and Sgt.lpr males compared to their gender-matched B6.lpr controls (**Fig. 11a,b**). Although analysis of IgM autoantibody repertoire via autoantigen microarray showed an overall decrease in IgM autoantibodies in the sera from female cGAS KO.lpr and male Sgt.lpr mice compared to their gender-matched B6.lpr controls, analysis of IgG autoantibody repertoire via autoantigen microarray revealed only a significant global decrease in IgG autoantibodies when comparing female cGAS KO.lpr mice to female B6.lpr mice (**Fig. 12a,b**). Sera from male Sgt.lpr mice demonstrated similar reactivity as sera from male B6.lpr mice, and both male Sgt.lpr and B6.lpr sera demonstrated only mildly elevated reactivity compared to sera from B6 WT control (**Fig. 12b**). Because my initial results suggested that male B6 background mice with $Fas^{lpr/lpr}$ mutations only produce mildly elevated levels of pathogenic IgG autoantibodies compared to control B6 WT mice, further experiments utilizing B6.lpr mice were conducted solely with female mice in order to allow for any differences in autoantibody production between the various genotypes of mice tested to be observed clearly.

To verify my initial results, serum was harvested from 5 month old female B6.lpr, cGAS KO.lpr, Sgt.lpr, and control mice. For both anti-dsDNA and anti-ssDNA IgG autoantibody specificities, cGAS KO.lpr and Sgt.lpr mice showed a significant decrease in serum levels of anti-DNA autoantibodies compared to B6.lpr mice (**Fig. 11c,d**). cGAS KO.lpr mice produced similar levels of anti-dsDNA/ssDNA IgG autoantibodies as Sgt.lpr mice. All female mice harboring $Fas^{lpr/lpr}$ mutations, including cGAS KO.lpr and Sgt.lpr mice, demonstrated significantly elevated levels of anti-DNA autoantibodies in their sera

compared to B6 WT control mice (**Fig. 11c,d**). cGAS KO and STING *gt/gt* mice had similar levels of anti-DNA autoantibodies in their sera as B6 WT mice (data not shown). To gain a clearer understanding of the autoantibody repertoire and titers present in the sera of B6.lpr, cGAS KO.lpr, and Sgt.lpr mice, an autoantigen microarray containing 95 autoantigens was used. Autoantigen microarray analysis showed an overall decrease in both IgG and IgM autoantibody titers in the sera from cGAS KO.lpr and Sgt.lpr mice compared to B6.lpr mice (**Fig. 11e**). Autoantibodies decreased in cGAS KO.lpr and Sgt.lpr mice relative to B6.lpr mice had specificities against a number of autoantigens associated with SLE such as Sm (Smith antigen), DNA, RNA, C1q, nucleosome, Ro/SSA, chromatin, and cardiolipin. Chosen sera from Sgt.lpr mice appeared mildly more reactive than sera from cGAS KO.lpr mice on the autoantigen microarray (**Fig. 11e**). These results suggest that activation of the cGAS-STING pathway promotes the development of autoantibodies and contributes to autoimmune disease pathogenesis in B6.lpr mice.

The cGAS-STING pathway promotes autoimmune inflammatory cell accumulation in C57BL/6J-*Fas*^{lpr}/*Fas*^{lpr} mice

Activation of the cGAS-STING pathway initiates the host innate immune response, which is required for the further development of the adaptive immune response. Though the cGAS-STING pathway is broadly expressed in both immune and non-immune tissues, expression of the pathway in immune cells capable of reacting to self-antigens is critical for the development of autoimmunity (Gao, Li et al. 2015). Mice with *Fas*^{lpr/lpr} mutations accumulate a number of abnormal T-cells due to aberrant proliferation of lymphoid cells (Aicher, Fujihashi et al. 1992; Morse HC 3rd 1982). Therefore, I tested whether genetic deletion of cGAS or STING would impact the accumulation of inflammatory immune cells

in B6.lpr mice. Spleens harvested from 5 month old female cGAS KO.lpr mice showed significantly less splenomegaly and splenocyte numbers than spleens harvested from age and gender-matched B6.lpr mice (**Fig. 13a,b**). Spleens taken from 5 month old female Sgt.lpr mice demonstrated significantly less splenocyte numbers than spleens from age and gender-matched B6.lpr mice, with spleen weights trending lower in Sgt.lpr mice compared to B6.lpr mice (**Fig. 13a,b**). B6.lpr mice showed significantly greater splenomegaly and splenocyte numbers than B6 WT control mice, whereas cGAS KO.lpr mouse spleen weight and splenocyte numbers trended higher than cGAS KO control mice but the difference in weight and cell counts was not statistically significant. For Sgt.lpr mice, there was significant splenomegaly compared to STING gt/gt control mice with splenocyte numbers trending higher in Sgt.lpr mice compared to STING gt/gt mice (**Fig. 13a,b**). These results suggested that removal of cGAS or STING in the B6.lpr mouse causes a decrease in splenic inflammatory immune cell accumulation.

I further investigated the composition of the inflammatory immune cell populations present in the spleens of B6.lpr, cGAS KO.lpr, and Sgt.lpr mice. The lymphoid compartment in mice harboring *Fas*^{lpr/lpr} mutations contains a predominance of CD4/8 double negative TCR β ⁺B220⁺ T-cells (DN T-cell), a unique and unusual subset of T-cells that may play a role in autoimmune disease pathogenesis in *Fas*^{lpr/lpr} mice through the production of IL-17 and IFN- γ (Crispín JC 2008; Morse HC 3rd 1982). As expected, analysis of splenocytes obtained from 5 month old female B6.lpr and B6 WT mice showed a markedly increased percentage and number of DN T-cells present in the spleens of B6.lpr mice compared to B6 WT control mice (**Fig. 13c, Fig. 14a**). The frequency and number of DN T-cells present in the spleens of

5 month old female cGAS KO.lpr mice was significantly reduced compared to B6.lpr mice, whereas only the number but not the frequency of DN T-cells present in the spleens of Sgt.lpr mice was significantly reduced compared to B6.lpr mice (**Fig. 13c, Fig. 14a**). Interestingly, the percentage and number of DN T-cells present in the spleens of Sgt.lpr mice was significantly higher than what was observed in cGAS KO.lpr mice. cGAS KO.lpr and Sgt.lpr mice contained an elevated percentage and number of splenic DN T-cells compared to their respective non-*Fas*^{lpr/lpr} containing cGAS KO and STING *gt/gt* controls (**Fig. 13c, Fig. 14a**). In addition to DN T-cells, cGAS KO.lpr and Sgt.lpr mice contained significantly lower numbers of activated CD44⁺CD69⁺TCRβ⁺ T-cells and activated CD44⁺CD69⁺B220⁺ B-cells in their spleens compared to B6.lpr mice (**Fig. 13d,e**). The frequency of activated T-cells as a percentage of all TCRβ⁺ T-cells was also decreased in cGAS KO.lpr mice compared to B6.lpr mice (**Fig. 14b**). cGAS KO.lpr and Sgt.lpr mice displayed similar percentages and numbers of activated T/B-cells to each other. B6.lpr mice consistently displayed elevated frequencies and numbers of activated T/B-cells compared to control B6 WT mice (**Fig. 13d,e; Fig. 14b,c**). cGAS KO.lpr mice demonstrated a significant difference from cGAS KO control mice in frequency of activated T-cells, which was higher in cGAS KO.lpr mice compared to cGAS KO mice (**Fig. 14b**). Sgt.lpr mice demonstrated a higher frequency of both activated T and B-cells compared to control STING *gt/gt* mice (**Fig. 14b,c**). Consistent with my previously observed autoantibody data, cGAS KO.lpr and Sgt.lpr mice contained lower numbers of B220⁺CD138⁺ plasma cells in their spleens compared to B6.lpr mice (**Fig. 13f**). In addition to splenic plasma cell numbers, cGAS KO.lpr mice also demonstrated a significant reduction in the percentage of splenic plasma cells present compared to B6.lpr

mice, with the frequency of plasma cells found in the spleens of Sgt.lpr mice trending lower than what was observed for B6.lpr mice (**Fig. 14d**). Of note, the spleens of Sgt.lpr mice contained a higher percentage of plasma cells than spleens from cGAS KO.lpr mice, though plasma cell numbers were similar between the two genotypes (**Fig. 13f; Fig. 14d**). B6.lpr, cGAS KO.lpr, and Sgt.lpr mice displayed a higher percentage of plasma cells in their spleens compared to their respective B6 WT, cGAS KO, and STING *gt/gt* controls (**Fig. 14d**). However, only B6.lpr mice had a higher splenic plasma cell count than control (**Fig. 13f**). These results suggest that the activation of the cGAS-STING pathway promotes inflammatory lymphocyte accumulation in the spleens of B6.lpr mice.

I also investigated whether cGAS or STING deficiency in B6.lpr mice would affect accumulation of myeloid compartment inflammatory immune cells, although myeloid-lineage cell proliferation is minimally affected in mice with *Fas*^{*lpr/lpr*} mutations (Fecho K 1998). Myeloid cell populations that express the leukocyte adhesion and migration molecule CD11b include monocytes, neutrophils, granulocytes, and macrophages (Solovjov, Pluskota et al. 2005). These CD11b⁺ myeloid cells contribute to the inflammatory response. Dendritic cells, on the other hand, express high levels of CD11c and are critical antigen-presenting cells that bridge the innate and adaptive immune systems (Shortman and Liu 2002). Spleens were harvested from 5 month old female B6.lpr, cGAS KO.lpr, and Sgt.lpr mice and the frequency and number of splenic CD86⁺CD11b⁺ or CD86⁺CD11c⁺ myeloid cells was measured. Curiously, cGAS KO.lpr mice exhibited a higher frequency of CD11b⁺ myeloid cells compared to either B6.lpr or Sgt.lpr mice (**Fig. 14e**). However, there was no significant difference seen in CD11b⁺ myeloid cell numbers when comparing between B6.lpr, cGAS

KO.lpr, and Sgt.lpr mice (**Fig. 13g**). One B6.lpr mouse displayed an unusually high number of CD11b⁺ myeloid cells relative to the rest of the B6.lpr cohort. B6.lpr, cGAS KO.lpr, and Sgt.lpr mice had similar frequencies and numbers of CD11b⁺ myeloid cells compared to their respective control B6 WT, cGAS KO, and STING gt/gt mice (**Fig. 13g; Fig. 14e**).

Interestingly, cGAS KO.lpr and Sgt.lpr mice had lower numbers of CD11c⁺ myeloid cells in their spleens compared to B6.lpr mice, although the frequency of CD11c⁺ myeloid cells was similar between the three genotypes (**Fig. 13h; Fig. 14f**). B6.lpr and Sgt.lpr mice displayed elevated percentages and numbers of CD11c⁺ myeloid cells compared to their respective B6 WT and STING gt/gt controls. cGAS KO.lpr mice displayed elevated numbers, but not frequencies, of CD11c⁺ myeloid cells compared to cGAS KO control mice (**Fig. 13h; Fig. 14f**). There are a number of inflammation-associated myeloid cell populations, including F4/80⁺Ly6c^{HI}CD11c⁺CD11b⁺ inflammatory dendritic cells (infDC's), CD11b⁺Ly6c^{HI} inflammatory monocytes, and CD11b⁺Ly6G^{HI}Ly6c^{INT} inflammatory N1 neutrophils (Fridlender ZG 2009; Hespel and Moser 2012). The frequency of infDC's was similar between B6.lpr, cGAS KO.lpr, and Sgt.lpr mice, although cGAS KO.lpr mice displayed a lower number of splenic infDC's than B6.lpr mice (**Fig. 13i; Fig. 14g**). B6.lpr and cGAS KO.lpr mice had elevated frequencies of infDC's compared to their respective B6 WT and cGAS KO controls, while the percentage of splenocytes that were infDCs in Sgt.lpr mice trended higher than in STING gt/gt mice (**Fig. 14g**). The number of splenic infDCs was similar between B6.lpr, cGAS KO.lpr, and Sgt.lpr mice and their respective B6 WT, cGAS KO, and STING gt/gt controls (**Fig. 13i**). The percentage of inflammatory monocytes in the CD11b⁺ myeloid cell population was significantly lower in cGAS KO.lpr mice compared to

B6.lpr mice, while Sgt.lpr mice exhibited similar frequencies of inflammatory monocytes as B6.lpr mice (**Fig. 14h**). Splenic inflammatory monocyte numbers were similar between B6.lpr, cGAS KO.lpr, and Sgt.lpr mice (**Fig. 13j**). B6.lpr mice displayed a higher frequency of inflammatory monocytes than control B6 WT mice, whereas the frequency of inflammatory monocytes in the spleens of cGAS KO.lpr and Sgt.lpr mice trended higher than that of control cGAS KO and STING gt/gt mice (**Fig. 14h**). Inflammatory monocyte numbers were not significantly different comparing between B6.lpr, cGAS KO.lpr, and Sgt.lpr mice and their respective B6 WT, cGAS KO, and STING gt/gt controls (**Fig. 13j**). N1 neutrophil frequencies as a percentage of CD11b⁺ cells and cell numbers were not significantly different comparing between B6.lpr and cGAS KO.lpr or Sgt.lpr mice (**Fig. 13k; Fig. 14i**). However, cGAS KO.lpr mice displayed a significantly higher percentage and number of splenic N1 neutrophils than Sgt.lpr mice. cGAS KO.lpr mice also exhibited an elevated frequency of N1 neutrophils compared to control cGAS KO mice while B6.lpr and Sgt.lpr mice exhibited similar frequencies of N1 neutrophils compared to their respective B6 WT and STING gt/gt controls (**Fig. 14i**). N1 neutrophil numbers were higher in Sgt.lpr mice compared to STING gt/gt controls but similar in B6.lpr and cGAS KO.lpr mice compared to their respective B6 WT and cGAS KO controls (**Fig. 13k**). These results show that although genetic ablation of cGAS or STING in B6.lpr mice causes a decrease in CD11c⁺ myeloid cell numbers, the effect of cGAS-STING pathway removal on other inflammation-associated myeloid cell populations is inconsistent and minor. Taken together, these results suggest the cGAS-STING pathway contributes primarily to accumulation of inflammatory immune cells in the

lymphoid compartment, with a slight contribution made to accumulation of inflammatory immune cells in the myeloid compartment.

cGAS or STING deficiency has no effect on IFN signature, cytokine levels, or lupus nephritis in C57BL/6J-*Fas*^{lpr}/*Fas*^{lpr} mice

Type-I IFNs have been shown to play an important role in SLE pathogenesis in the B6.lpr murine model of lupus. Treatment of female B6.lpr mice with polyinosinic:polycytidylic acid (poly I:C) strongly induces systemic type-I IFN production, which results in accelerated autoimmune disease development and amplification of autoimmune disease severity (Braun 2003). Conversely, crossing B6.lpr mice with an IFNAR knockout strain significantly ameliorates autoimmune disease symptoms in these animals. As activation of the cGAS-STING pathway results in type-I IFN production, it is likely that the reduction in autoantibody levels and inflammatory immune cell populations I observed in cGAS KO.lpr and Sgt.lpr mice is due to abrogated type-I IFN production. To test this, I isolated PBMCs and splenocytes from 7 month old female B6.lpr, cGAS KO.lpr, and Sgt.lpr mice in order to measure type-I IFN and ISG production within these cells. Consistent with my results obtained using 5 month old female mice, spleens isolated from 7 month old female B6.lpr mice were grossly enlarged compared to spleens taken from 7 month old female cGAS KO.lpr and Sgt.lpr mice (**Fig. 15a**). However, spleens from 7 month old female B6.lpr, cGAS KO.lpr, and Sgt.lpr mice were all demonstrably larger than spleen harvested from control B6 WT mouse. Measurement of IFN- α_1/β production in PBMCs showed that relative to B6 WT control, type-I IFN production trends higher in B6.lpr and Sgt.lpr mice while cGAS KO.lpr and B6 WT mice produce comparable levels of type-I IFN (**Fig. 15b,c**). However, comparing type-I IFN levels between B6.lpr, cGAS KO.lpr, and Sgt.lpr mice

revealed no statistically significant differences. Measurement of ISG transcript levels in PBMCs revealed no statistically significant differences in CXCL10, Ifit3, ISG15, and IRF7 production when comparing between B6.lpr, cGAS KO.lpr, and Sgt.lpr mice (**Fig. 15d,e,f,g**). As lymphocytes abnormally accumulate in secondary lymphoid organs in *Fas*^{lpr/lpr} mutation containing mice, I also measured type-I IFN production in splenocytes. IFN- α_1/β transcript levels, relative to B6 WT control, were comparable in B6.lpr, cGAS KO.lpr, and Sgt.lpr mice (**Fig. 16a,b**). Similarly, measurement of ISG production in splenocytes showed no difference in CXCL10, Ifit3, ISG15, and IRF7 levels between B6.lpr, cGAS KO.lpr, and Sgt.lpr mice (**Fig. 16c,d,e,f**). These results indicate that B6.lpr mice do not generate an obviously detectable IFN signature, and genetic ablation of cGAS or STING in B6.lpr mice has a negligible effect on type-I IFN and ISG production within PBMCs and splenocytes.

The cytokine IL-12 plays an important role in mediating T-cell responses during inflammation, inducing the production of Th1-associated cytokines like IFN- γ and IL-2 (Trinchieri 1995). Some SLE patients have high serum levels of IL-12, which correlates with high serum IFN- γ levels and pulmonary involvement during disease flares (Y TOKANO 1999). As the cGAS-STING pathway can modulate production of IL-12, I wanted to test whether cGAS or STING deficiency in B6.lpr mice could result in decreased levels of circulating IL-12 (Murphy, Cleveland et al. 1995). Serum was harvested from 5 month old female B6.lpr, cGAS KO.lpr, and Sgt.lpr mice and circulating titers of IL-12 were measured. Serum IL-12 titers did not differ between B6.lpr mice and cGAS KO.lpr or Sgt.lpr mice (**Fig. 16g**). However, cGAS KO.lpr mice did have less IL-12 present in the sera compared to Sgt.lpr mice.

Since cGAS KO.lpr and Sgt.lpr mice exhibit lower levels of pathogenic IgG autoantibodies than B6.lpr mice, I evaluated the extent of renal disease in these strains although it is known that B6.lpr mice generally have minimal renal pathology (Kelley and Roths 1985). Kidneys were harvested from 5 month old female B6.lpr, cGAS KO.lpr, Sgt.lpr, and control mice. Glomerular pathology and the degree of inflammatory cell infiltration into the kidneys were evaluated. Assessment of glomeruli revealed few signs of glomerulonephritis, and glomerular inflammation histology scores were not significantly different between B6.lpr mice and cGAS KO.lpr or Sgt.lpr mice (**Fig. 17a**). In addition, control B6 WT, cGAS KO, and STING gt/gt mice displayed similar glomerular pathology to their respective *Fas*^{lpr/lpr} mutation containing counterparts. Evaluation of the extent of inflammatory cell infiltration into the kidneys of B6.lpr, cGAS KO.lpr, and Sgt.lpr mice revealed no difference between the three strains (**Fig. 17b**). Although some B6.lpr, cGAS KO.lpr, and Sgt.lpr mice had higher histological scores for inflammatory cell infiltrate compared to their respective B6 WT, cGAS KO, and STING gt/gt controls, overall there was no difference seen between the *Fas*^{lpr/lpr} mutation containing strains and their wild-type counterparts.

Absence of cGAS or STING in B6.MRL/Mp-*Fas*^{lpr/lpr} and B6.SLE1^{NZM/NZM}.*Fas*^{lpr/lpr} mice does not recapitulate the phenotype of C57BL/6J-*Fas*^{lpr}/*Fas*^{lpr} mice

Although genetic ablation of cGAS or STING in B6.lpr mice results in a reduction in potentially pathogenic IgG autoantibodies and reduces splenic accumulation of inflammatory immune cells, assessment of disease severity parameters like extent of lupus nephritis or serum IL-12 levels in these strains revealed only negligible phenotypes. The genetic background of mice harboring *Fas*^{lpr/lpr} mutations has a major effect on disease severity, with

B6.lpr mice displaying delayed onset and reduced severity of symptoms relative to MRL/MpJ-*Fas*^{lpr}/J (MRL.lpr) mice (Kelley and Roths 1985). On a B6 background, the combination of the NZM2410 strain-derived *SLE1* lupus susceptibility locus with *Fas*^{lpr/lpr} results in more severe autoimmune disease than what is observed in B6.lpr mice (Shi, Xie et al. 2002). As I was unable to determine if the reduction in IgG autoantibodies and inflammatory immune cell accumulation in cGAS KO.lpr and Sgt.lpr mice translated into reduced disease symptoms due to the mild autoimmune disease phenotype present in B6.lpr mice, I generated cGAS or STING deficient MRL.lpr mice to test if the cGAS KO.lpr and Sgt.lpr phenotypes could be recapitulated on a mixed B6.MRL/Mp genetic background. In addition, I generated B6 background cGAS or STING deficient *SLE1*^{NZM/NZM}.*Fas*^{lpr/lpr} mice to test if the cGAS KO.lpr and Sgt.lpr phenotypes could be recapitulated in a B6 background model of lupus with more severe disease. Serum was harvested from 3 month old *cGAS*^{+/+}.*Tmem173*^{+/+}.MRL/Mp-*Fas*^{lpr/lpr} (B6.MRL/lpr), *Tmem173*^{gt/+}.MRL/Mp-*Fas*^{lpr/lpr} [Sgt(het).MRL/lpr], *Tmem173*^{gt/gt}.MRL/Mp-*Fas*^{lpr/lpr} (Sgt.MRL/lpr), *cGAS*^{+/-}.MRL/Mp-*Fas*^{lpr/lpr} [cGAS(het).MRL/lpr], and *cGAS*^{-/-}.MRL/Mp-*Fas*^{lpr/lpr} (cGAS KO.MRL/lpr) mice and circulating levels of anti-dsDNA and anti-ssDNA IgG autoantibodies was measured. Comparing between genders, only cGAS KO.MRL/lpr mice demonstrated a gender bias with female mice producing higher levels of anti-DNA autoantibodies than male mice (**Fig. 18a,b**). Comparing between female mice, cGAS(het).MRL/lpr and cGAS KO.MRL/lpr mice produced higher levels of anti-DNA autoantibodies than B6.MRL/lpr mice (**Fig. 18a,b**). Comparing between male mice, B6.MRL/lpr mice had higher serum levels of anti-dsDNA IgG than Sgt.MRL/lpr mice (**Fig. 18a**). Combining male and female mice into mixed gender

cohorts for each strain revealed no significant differences in circulating anti-dsDNA and anti-ssDNA IgG autoantibody levels when comparing between B6.MRL/lpr, Sgt.MRL/lpr, and cGAS KO.MRL/lpr mice (**Fig. 18c,d**). Mixed gender Sgt(het).MRL/lpr mice had higher serum levels of anti-dsDNA IgG than mixed gender Sgt.MRL/lpr mice (**Fig. 18c**). Serum levels of anti-dsDNA and anti-ssDNA IgG autoantibodies were also measured in 3 month old $cGAS^{+/+}.Tmem173^{+/+}.SLE1^{NZM/NZM}.Fas^{lpr/lpr}$ (SLE1.lpr), $cGAS^{+/-}.SLE1^{NZM/NZM}.Fas^{lpr/lpr}$ [cGAS(het).SLE1.lpr], $cGAS^{-/-}.SLE1^{NZM/NZM}.Fas^{lpr/lpr}$ (cGAS KO.SLE1.lpr), $Tmem173^{gt/+}.SLE1^{NZM/NZM}.Fas^{lpr/lpr}$ [Sgt(het).SLE1.lpr], and $Tmem173^{gt/gt}.SLE1^{NZM/NZM}.Fas^{lpr/lpr}$ (Sgt.SLE1.lpr) mice. No gender bias was seen for anti-DNA IgG autoantibody levels when comparing between male and female SLE1.lpr, cGAS(het).SLE1.lpr, Sgt(het).SLE1.lpr, and Sgt.SLE1.lpr mice (**Fig. 19a,b**). Circulating levels of anti-dsDNA and anti-ssDNA IgG autoantibodies were not significantly different between SLE1.lpr mice and Sgt(het).SLE1.lpr, cGAS(het).SLE1.lpr, or Sgt.SLE1.lpr mice (**Fig. 19c,d**). In addition, the survival curves and mortality rates for SLE1.lpr, Sgt(het).SLE1.lpr, and Sgt.SLE1.lpr mice were similar (**Fig. 19e**). These results show that the removal of cGAS or STING from B6.MRL/Mp- $Fas^{lpr/lpr}$ mice or B6. $SLE1^{NZM/NZM}.Fas^{lpr/lpr}$ mice does not result in recapitulation of the phenotypes observed in cGAS KO.lpr and Sgt.lpr mice, suggesting that the interplay of various genes within either the *SLE1* congenic interval with $Fas^{lpr/lpr}$ or within mixed B6.MRL/Mp background $Fas^{lpr/lpr}$ mice may influence the contribution of the cGAS-STING pathway to autoimmune disease pathogenesis.

CONCLUSIONS AND DISCUSSIONS

The presence of autoantibodies directed against nucleic acids is a hallmark of SLE (Anisur Rahman 2008; Tsokos 2011). In addition, a significant portion of SLE patients demonstrate excessive type-I IFN production in the form of an IFN signature in their peripheral blood. Type-I IFN signaling has been implicated in SLE disease pathogenesis, implying a role for the innate immune system in SLE development (Banchereau and Pascual 2006; Crow 2014; Eloranta and Ronnblom 2016; Pascual, Farkas et al. 2006; Thibault, Graham et al. 2009). Self-DNA, perhaps engulfed by macrophages or dendritic cells while contained in circulating immune complexes, is capable of triggering cGAS-STING pathway activation, leading to the robust production of type-I IFNs and other inflammatory cytokines. Chronic production of type-I IFN can subsequently provoke the development of autoinflammation and autoimmunity (Konig, Fiehn et al. 2016; Liu, Jesus et al. 2014). My work investigating the role of the cGAS-STING pathway in SLE pathogenesis using the B6.lpr mouse shows that genetic ablation of cGAS or STING results in a dramatic reduction in autoantibody production (**Fig. 11**). B6.lpr mice deficient in cGAS or STING produce not only less anti-DNA autoantibodies than wild-type B6.lpr mice, but also less autoantibodies directed against other nuclear antigens like Sm, RNA, nucleosome, Ro/SSA, and chromatin. This indicates that cGAS is a PRR capable of influencing autoantibody production in mice with *Fas*^{lpr/lpr} mutations, adding cGAS to a list containing PRRs like TLR2, TLR4, TLR7, and TLR9 that are implicated in the development of murine autoimmunity (Christensen, Kashgarian et al. 2005; Christensen, Shupe et al. 2006; Fairhurst, Hwang et al. 2008; Hwang, Lee et al. 2012; Nickerson, Christensen et al. 2010; Summers, Hoi et al. 2010; Urbonaviciute,

Starke et al. 2013). Interestingly, I observed less circulating plasma cells present in the spleens of cGAS KO.lpr and Sgt.lpr mice compared to B6.lpr mice, providing an explanation as to why autoantibody production was decreased in B6.lpr mice lacking cGAS or STING (**Fig. 13f**). Although cGAS KO.lpr and Sgt.lpr mice display significantly reduced levels of anti-DNA autoantibodies in their sera compared to B6.lpr mice, anti-DNA autoantibody levels were still elevated in cGAS KO.lpr and Sgt.lpr mice compared to B6 WT controls (**Fig. 11c,d**). This suggests that anti-DNA autoantibody production is only partially dependent on cGAS-STING pathway signaling, implying the presence of other innate immune receptors in generation of the anti-DNA humoral immune response. Previous studies have implicated TLR9 as having a role in anti-DNA antibody generation in the MRL.lpr mouse, and anti-nucleosome antibody generation in the B6.lpr mouse (Lartigue, Courville et al. 2006; Nickerson, Christensen et al. 2010). I cannot rule out the potential contribution of TLR9 pathway signaling to the development of anti-DNA autoantibodies in the B6.lpr mouse in the absence of the cGAS-STING pathway. However, TLR9 appeared to solely contribute to anti-DNA autoantibody production in the MRL.lpr mouse, whereas cGAS-STING pathway signaling appears to play a broader role in overall autoantibody generation in the B6.lpr mouse. More work is needed to further understand the relative contributions of various innate immune receptors to autoantibody generation within B6.lpr mice, and it may be possible that production of some autoantibodies is independent of PRR signaling. In the future, I can generate B6.lpr mice deficient in cGAS or STING and TLR9. These cGAS or STING and TLR9 double knockout B6.lpr mice would allow me to determine whether anti-DNA autoantibody production is dependent on both the cGAS-STING and TLR9 pathways.

It would also be possible to generate other double knockout B6.lpr mice in which cGAS or STING is genetically ablated along with another PRR implicated in SLE pathogenesis (e.g. TLR7). Characterizing the ANA profiles of these mice would allow me to determine the relative contribution of different PRRs to autoantibody generation in B6.lpr mice in the absence of the cGAS-STING pathway.

Although it is well-documented that a majority of human SLE patients display an increased expression of ISGs in their peripheral blood, the B6.lpr mouse is not known to exhibit this IFN signature (Zhuang, Szeto et al. 2015). My results looking at type-I IFN and ISG production in PBMCs isolated from B6.lpr mice show that, relative to B6 WT mice, B6.lpr mice display a roughly four-fold increase in peripheral blood type-I IFN levels (**Fig. 15b,c**). In addition, transcript levels of the ISGs CXCL10, Ifit3, and IRF7 are modestly increased in B6.lpr mice relative to B6 WT mice (**Fig. 15d,e,g**). Expression of ISG15 in PBMCs from B6.lpr mice was approximately ten-fold higher than wild-type control (**Fig. 15f**). These modest increases in type-I IFN and ISG production suggest that B6.lpr mice may indeed express a weak IFN signature. However, it is not possible for me to come to a definite conclusion as the sample size used in my experiment was small and the variation in type-I IFN and ISG production between individual B6.lpr mice was large. In the future, I can test more mice of each strain in order to increase the experimental group sample sizes, which would allow me to be more confident in my conclusions.

Since cGAS-STING pathway activation leads to robust type-I IFN production, the genetic ablation of cGAS or STING in B6.lpr mice should lower type-I IFN levels in circulating immune cells. However, measurement of type-I IFN and ISG transcript levels in

PBMCs and splenocytes from cGAS KO.lpr and Sgt.lpr mice revealed no significant differences from B6.lpr mice (**Fig. 15; Fig. 16**). One possible explanation for this observation is that the sample sizes used in my experiment were small, and the variation between individual mice of a given genotype was large. This would make it difficult to see any statistically significant differences between genotypes. In the future, I can test more mice in order to increase the sample size of each experimental group, which would allow me to draw a more definitive conclusion. Another possible explanation for this observation is that because type-I IFN and ISG levels are already relatively low in B6.lpr mice, any further decreases caused by cGAS or STING deficiency may be too difficult to detect. Although it is known that type-I IFN plays a critical role in the development of autoimmune disease in B6.lpr mice, it is possible that this endogenous type-I IFN is produced locally rather than systemically. Plasmacytoid dendritic cells are thought to be the primary source of type-I IFN in SLE, and in SLE patients pDCs infiltrate organs such as the skin and kidney (Tsokos 2011). Therefore it is possible that in B6.lpr mice, much of the type-I IFN generated by pDCs acts locally within the tissue. This would also make detection of type-I IFN and ISG production difficult, providing another explanation as to why I was unable to see reduced type-I IFN and ISG production in cGAS KO.lpr and Sgt.lpr mice compared to B6.lpr mice.

How cGAS-STING pathway signaling affects circulating plasma cell numbers in B6.lpr mice is unclear, but likely involves the production of type-I IFNs. Within the context of host defense, type-I IFNs play a critical role in defense against viral infections by stimulating dendritic cell and macrophage activation. These APCs further activate the anti-viral immune response by promoting the activation, differentiation, and survival of antigen-

specific T and B-cells (Eloranta and Ronnblom 2016). Type-I IFN production by plasmacytoid dendritic cells is critical for plasma cell differentiation and generation (Jego, Palucka et al. 2003). In addition to affecting APC activity, type-I IFNs have been shown to interact directly with T and B-cells to enhance their activation during viral infection (Pascual, Farkas et al. 2006). Autoimmune diseases like SLE can be characterized as a chronic, pathologic, and over-active anti-viral immune response that targets self-antigens rather than exogenous viral antigens. In SLE, it is known that type-I IFNs can act directly on B-cells to increase plasma cell differentiation and isotype switching, enhancing the production of autoantibodies (Eloranta and Ronnblom 2016; Pascual, Farkas et al. 2006). Exposing lupus-prone mice to IFN- α results in the sustained proliferation of B-cells, as well as the generation of antibody-secreting cells within secondary lymphoid organs (Mathian, Gallegos et al. 2011). This provides a possible explanation as to why cGAS or STING deficiency in B6.lpr mice results in lower circulating plasma cell numbers (**Fig. 13f**). The lack of cGAS or STING would impair production of type-I IFNs in response to self-DNA within APCs like pDCs, thereby impairing the ability of APCs to stimulate plasma cell differentiation from autoreactive B-cells. My results are consistent with previous findings demonstrating that IFN- α/β receptor-deficient mixed background B6/129.lpr mice have decreased B-cell activation and lower numbers of autoantibody-secreting cells (Braun 2003).

During inflammatory responses, type-I IFNs have been shown to inhibit activation-induced T-cell death, promoting CD4⁺ and CD8⁺ T-cell survival. Type-I IFNs also promote a Th1-skewed CD4⁺ T-cell response, enhancing the cytotoxic CD8⁺ T-cell response. Finally, type-I IFNs also stimulate the development of CD4⁺ and CD8⁺ memory T-cells (Eloranta and

Ronnlblom 2016; Pascual, Farkas et al. 2006). I would predict that lower levels of type-I IFNs produced by APCs or other immune cells in cGAS KO.lpr and Sgt.lpr mice should result in less memory T and B-cell generation and activation when compared to B6.lpr mice. Indeed, I observed that activated CD44⁺CD69⁺ T and B-cell numbers in cGAS KO.lpr and Sgt.lpr mice were reduced compared to B6.lpr mice (**Fig. 13d,e**). The unusual DN T-cell population found exclusively in mice with *Fas*^{lpr/lpr} mutations was also dramatically reduced in cGAS KO.lpr and Sgt.lpr mice compared to B6.lpr mice (**Fig. 13c**). The generation of DN T-cells within B6.lpr mice appears to be dependent on defective Fas-FasL pathway signaling, so it is unclear why cGAS or STING deficiency would affect the DN T-cell population in B6.lpr mice although altered type-I IFN production may play an indirect role in influencing DN T-cell formation and survival. It is also possible that cGAS-STING pathway signaling has immune cell-intrinsic effects on lymphocyte proliferation and survival.

In addition to its effects on the lymphoid compartment, type-I IFN also influences activity of cells within the myeloid compartment. IFN- α promotes the differentiation of monocytes and immature dendritic cells into mature APCs while simultaneously enhancing expression of MHC-II and co-stimulatory molecules like CD40 or CD86 on the surface of APCs (Eloranta and Ronnlblom 2016; Fairhurst, Wandstrat et al. 2006). When stimulated by type-I IFNs, NK cells increase their cytolytic activity (Eloranta and Ronnlblom 2016). While I observed no significant change in splenic CD86⁺CD11b⁺ myeloid cell numbers in cGAS KO.lpr and Sgt.lpr mice compared to B6.lpr mice, I did observe a significant reduction in splenic CD86⁺CD11c⁺ myeloid cell numbers in cGAS KO.lpr and Sgt.lpr mice compared to B6.lpr mice (**Fig. 13g,h**). Numerous leukocyte populations including monocytes,

macrophages, neutrophils, and NK cells express CD11b on their cell surface (Solovjov, Pluskota et al. 2005). Dendritic cells are the primary myeloid-lineage cells that express CD11c on their cell surface, although a subset of NK cells also express CD11c (Shortman and Liu 2002). These cells are all responsive to type-I IFN stimulation, and their function and activity are enhanced through exposure to type-I IFNs (Eloranta and Ronnblom 2016). However, in the B6.lpr mouse, my results suggest that cGAS or STING deficiency and the concomitant reduction of type-I IFN production in response to self-DNA that follows has a minimal impact on the accumulation of mature, CD86-expressing, CD11b⁺ myeloid cells. Instead, cGAS or STING deficiency in B6.lpr mice appears to impact accumulation of mature CD11c⁺ myeloid cells. It is possible that in the B6.lpr mouse, type-I IFN produced by cGAS-STING pathway activation favors the maturation and accumulation of CD11c⁺ dendritic cells over CD11b⁺ myeloid-lineage cells. Inflammatory dendritic cells, inflammatory monocytes, and N1 neutrophils comprise unique inflammatory myeloid cell populations. InfDC's are thought to derive from monocytes that differentiate in situ at the site of inflammation. They are capable APCs and, in models of tumor immunity, a major source of inflammatory cytokines (Hespel and Moser 2012). Both CD11b⁺Ly6C^{HI} inflammatory monocytes and CD11b⁺Ly6G^{HI}Ly6C^{INT} N1 neutrophils traffic selectively to sites of inflammation, contributing to the local inflammatory milieu (Fridlender ZG 2009; Hespel and Moser 2012). These populations of inflammatory myeloid cells were not significantly altered in a consistent manner in cGAS KO.lpr or Sgt.lpr mice when compared to B6.lpr mice, and were inconsistently elevated in B6.lpr, cGAS KO.lpr, and Sgt.lpr mice compared to their respective wild-type controls (**Fig. 13i,j,k; Fig. 14g,h,i**). The *Fas*^{lpr/lpr} mutation

causes lymphoproliferation mainly in the lymphocyte compartment, and myeloid cell populations are not as affected (Fecho K 1998; Morse HC 3rd 1982). This may explain why I did not observe significant accumulation of inflammatory myeloid cell populations within B6.lpr mouse spleens, as these cell populations are relatively rare and detection of any differences in these cell populations between my mouse strains is difficult without abnormal accumulation of cells. This is also a possible explanation as to why I was able to see differences in lymphocyte accumulation more clearly compared to myeloid cell accumulation, since disease is more readily apparent in the lymphocyte compartment in B6.lpr mice.

Renal disease in SLE is mediated by the deposition of IgG immune complexes within glomeruli, causing activation of complement and the subsequent induction of inflammation, which causes tissue damage as inflammatory immune cells are recruited to the kidneys (Anisur Rahman 2008; Tsokos 2011). The onset of renal disease in B6.lpr mice typically occurs around 5-6 months of age and is mild in severity. Complement component 3 (C3) and IgG immune complex deposition in the glomeruli of B6.lpr mice is slightly elevated compared to wild-type B6 mice at 4 months of age. However, glomerulonephritis symptoms such as glomerular enlargement, hypercellularity, and mesangial thickening are mild in B6.lpr mice compared to wild-type B6 mice even at 14-16 months of age (Braun 2003; Kelley and Roths 1985). It is therefore not surprising that at 5 months of age, female B6.lpr, cGAS KO.lpr, and Sgt.lpr mice exhibit glomerular inflammation and renal inflammatory cell infiltrate histology scores roughly equivalent to that of their respective wild-type controls (**Fig. 17a,b**). As antinuclear antibodies in SLE are nephrophilic, a decrease in circulating IgG

autoantibodies against nuclear antigens like dsDNA would be predicted to result in an amelioration of renal pathology (Anisur Rahman 2008; Berden, Licht et al. 1999; Kramers C 1994; Tsokos 2011; van Bruggen MC 1997). Although cGAS KO.lpr and Sgt.lpr mice demonstrate reduced serum levels of antinuclear antibodies and less accumulation of splenic inflammatory lymphocytes compared to B6.lpr mice, this did not translate into an observable phenotype with respect to renal pathology. As the differences in renal pathology between B6.lpr and B6 WT mice are already minor, changes in glomerular structure and accumulation of inflammatory cell infiltrates in kidneys from cGAS KO.lpr and Sgt.lpr mice relative to B6.lpr mice could not be easily observed. I conclude that the mild form of renal disease present in B6.lpr mice made any alleviation in renal disease severity by genetically ablating cGAS or STING too challenging to detect.

In order to investigate whether cGAS or STING deficiency in *Fas*^{lpr/lpr} mutation containing mice results in amelioration of renal pathology, I crossed MRL.lpr mice with cGAS KO or STING *gt/gt* mice to generate mixed genetic background B6.MRL/Mp-*Fas*^{lpr/lpr} mice lacking cGAS or STING. On a MRL/Mp background, the *Fas*^{lpr/lpr} mutation results in severe autoimmune disease characterized by high titers of antinuclear autoantibodies, high serum levels of circulating immune complexes, massive lymphoproliferation within secondary lymphoid organs, and severe glomerulonephritis with mortality approaching 100% by 9 months of age (Andrews BS 1978; Hewicker, Kromschroder et al. 1990; Kelley and Roths 1985). As B6.lpr mice display a much milder disease phenotype than MRL.lpr mice, disease initiated by the *Fas*^{lpr/lpr} mutation is accelerated by alleles present within the MRL/Mp background (Fairhurst, Wandstrat et al. 2006). Therefore, *Fas*^{lpr/lpr} mice with a

mixed B6.MRL/Mp background would be predicted to have more severe autoimmune disease than B6.lpr mice, allowing any amelioration in renal disease caused by genetic ablation of cGAS or STING to be more easily observed. This would require that the antinuclear antibody phenotype I observed in cGAS KO.lpr and Sgt.lpr mice be recapitulated in cGAS KO.MRL/lpr and Sgt.MRL/lpr mice. However, I found no difference in serum levels of nephrophilic anti-DNA IgG autoantibodies when comparing cGAS KO.MRL/lpr and Sgt.MRL/lpr mice to B6.MRL/lpr mice (**Fig. 18c,d**). I was therefore unable to recapitulate the phenotype of cGAS KO.lpr and Sgt.lpr mice in cGAS KO.MRL/lpr and Sgt.MRL/lpr mice. One possible explanation for this result is that the mixing of B6 and MRL/Mp genetic backgrounds generated unknown confounding factors which influenced the contribution of the cGAS-STING pathway on autoantibody generation and inflammatory lymphocyte accumulation in B6.MRL/Mp-*Fas*^{lpr/lpr} mice. In the B6.lpr model, administration of polyI:C to mice causes potent induction of type-I IFN which results in a dramatic enhancement of autoimmune disease severity (Braun 2003). However, administration of IFN- β to MRL.lpr mice with either early or advanced disease dramatically ameliorated clinical, serological, and histological autoimmune phenotypes (Schwartz, Paul et al. 2005). In addition, IFNAR deficient MRL.lpr mice demonstrated more severe renal pathology accompanied by higher autoantibody titers (Hron and Peng 2004). This indicates that the MRL/Mp genetic background negates the typically proinflammatory nature of type-I IFNs through an unknown mechanism, while in B6 background mice type-I IFN acts canonically to enhance the autoimmune response initiated by the *Fas*^{lpr/lpr} mutation. It is therefore likely in my mixed background B6.MRL/Mp-*Fas*^{lpr/lpr} mice that the MRL/Mp background's

negative effect on type-I IFN signaling neutralizes the stimulating effect of type-I IFN on the immune system that would otherwise be observed in pure B6 background *Fas^{lpr/lpr}* mice. This confounding factor would then negatively impact the cGAS-STING pathway's contribution to autoantibody production and inflammatory lymphocyte accumulation, as these effects are most likely driven through type-I IFN production. Another explanation is that there may be epistatic interactions between unknown modifier gene(s) in the MRL/Mp background and the cGAS-STING pathway, and these interactions may alter cGAS-STING pathway activity in B6.MRL/Mp-*Fas^{lpr/lpr}* mice. My results using cGAS KO.MRL/lpr and Sgt.MRL/lpr mice are different from those found in a recent study in which B6.STING^{-/-}.MRL/Mp-*Fas^{lpr/lpr}* mice displayed accelerated mortality, elevated autoantibody production, increased severity of glomerulonephritis, and increased serum cytokine levels compared to controls (Sharma, Campbell et al. 2015). This discrepancy in results can likely be attributed to the heterogeneous genetic composition of the mice used in both studies, as it is unlikely that the contributions of the B6 and MRL/Mp backgrounds to the genomes of my mouse strains are identical to the genetic makeup of the B6.STING^{-/-}.MRL/Mp-*Fas^{lpr/lpr}* mice used in the recent study. This would explain the differences in phenotypes observed.

In order to avoid confounding factors resulting from mixing genetic backgrounds, I also crossed B6.SLE1 mice with cGAS KO.lpr and Sgt.lpr mice to generate pure B6 background mice harboring the *SLE1* lupus susceptibility locus and *Fas^{lpr/lpr}*. Although B6.SLE1 mice produce antinuclear antibodies starting around 3 months of age and develop mild splenomegaly with expansion of splenic CD4⁺ T-cell and B-cell populations, they demonstrate predominantly normal renal pathology and mortality is comparable with healthy

B6 mice (Chandra Mohan 1998; Fairhurst, Wandstrat et al. 2006). However, the combination of *SLE1* with *Fas*^{lpr/lpr} in B6 mice results in a severe autoimmune phenotype characterized by elevated levels of antinuclear antibodies, prominent lymphadenopathy and splenomegaly, and severe renal disease causing accelerated mortality (Shi, Xie et al. 2002). I predicted that the recapitulation of the cGAS KO.lpr and Sgt.lpr phenotypes in the B6.*SLE1*^{NZM/NZM}.*Fas*^{lpr/lpr} mouse would result in amelioration of renal disease in this murine model of lupus. However, similar to the phenotypes observed in cGAS KO.MRL/lpr and Sgt.MRL/lpr mice, Sgt.SLE1.lpr mice produced similar levels of anti-DNA IgG autoantibodies as control B6.SLE1.lpr mice (**Fig. 19c,d**). In addition, mortality was comparable between Sgt.SLE1.lpr and B6.SLE1.lpr mice, indicating the contribution of the cGAS-STING pathway to disease pathogenesis and severity is minimal in the B6.SLE1.lpr mouse (**Fig. 19e**). One explanation for the failure of Sgt.SLE1.lpr mice to recapitulate the phenotype of Sgt.lpr mice is that the *SLE1* lupus susceptibility locus contains an entire genomic segment derived from chromosome 1 of lupus-prone NZM2410 mice, which confers the potential for numerous epistatic interactions between *SLE1* and other genes. Indeed, epistatic interactions between *SLE1* and other lupus susceptibility loci *SLE2/3* or the *Fas*^{lpr/lpr} mutation are responsible for the severe autoimmune disease phenotypes observed in B6.SLE1/2/3 and B6.SLE1.lpr mice (Fairhurst, Wandstrat et al. 2006). It is therefore possible that epistatic interactions between *SLE1* and STING modulate cGAS-STING pathway activity in Sgt.SLE1.lpr mice, reducing the contribution of cGAS-STING pathway signaling to autoimmune disease development and severity. Another explanation may be that the autoimmune disease which develops from the epistatic interaction of *SLE1* and *Fas*^{lpr/lpr} is not as dependent on type-I IFN as disease caused

solely by $Fas^{lpr/lpr}$ mutation. The *SLE1* lupus susceptibility locus is critical in the breaching of tolerance to chromatin, whereas the $Fas^{lpr/lpr}$ mutation impairs activation-induced lymphocyte death and apoptosis (Fairhurst, Wandstrat et al. 2006). The combination of *SLE1* with $Fas^{lpr/lpr}$ on autoimmune disease development and severity is synergistic, with $Fas^{lpr/lpr}$ mediated generation of autoreactive lymphocytes aided by the decreased threshold needed to break tolerance conferred by *SLE1*. In this murine model of lupus, removal of type-I IFN production by the cGAS-STING pathway through the genetic ablation of STING may only have a minimal impact on the generation of autoreactive lymphocytes.

For some experimental groups like cGAS KO.SLE1.lpr and cGAS(het).MRL/lpr, my sample sizes were small. I was therefore unable to draw any definitive conclusions regarding anti-DNA autoantibody production in these strains of mice. Therefore, future work will focus on increasing the sample sizes of these experimental groups. In addition, future work will also focus on studying the role cGAS-STING pathway signaling has on autoimmune disease development in other murine models of lupus that have established IFN signatures (e.g. pristane-induced lupus).

Though the cGAS-STING pathway and type-I IFN play crucial roles in the pathogenesis of autoimmune and autoinflammatory disease in both mice and humans, it is clear that the complex genetic interplay between numerous lupus susceptibility genes within a given lupus-prone murine genetic background can influence the importance of type-I IFN and therefore the contribution of the cGAS-STING pathway to disease development. Further work will be required to unravel these intricate epistatic interactions, and a more complete

understanding of the relationship between different lupus susceptibility genes and the cGAS-STING pathway will provide substantial insight into the molecular pathogenesis of SLE.

MATERIALS AND METHODS

Mice

C57BL/6J (B6 WT), C57BL/6J-*Tmem173*^{gt}/J (STING gt/gt), MRL/MpJ-*Fas*^{lpr}/J (MRL.lpr), and C57BL/6J-*Fas*^{lpr}/*Fas*^{lpr} (B6.lpr) mice were obtained from The Jackson Laboratory. *cGAS*^{-/-} (KO) mice were generated in our laboratory as previously described (Li, Wu et al. 2013). B6.*SLE1*^{NZM/NZM} (B6.SLE1) mice were from Edward Wakeland (University of Texas Southwestern Medical Center). All mice were bred and maintained in the animal facilities of the University of Texas Southwestern Medical Center according to Institutional Animal Care and Use Committee-approved protocols.

B6 background *cGAS* KO.lpr and STING gt/gt.lpr (Sgt.lpr) mice (expressing either *cGAS*^{-/-} or *Tmem173*^{gt/gt} alleles in combination with *Fas*^{lpr/lpr}, all homozygously) were generated by breeding B6.*cGAS* KO or B6.STING gt/gt mice with B6.lpr mice for two generations, and then selecting for F2 progeny homozygous at both loci.

For the generation of mixed B6.MRL/Mp background *cGAS* KO.MRL/lpr and STING gt/gt.MRL/lpr (Sgt.MRL/lpr) mice, B6.*cGAS* KO or B6.STING gt/gt mice were crossed with MRL.lpr mice. The *cGAS*^{+/-} or *Tmem173*^{gt/+} and *Fas*^{lpr/+} heterozygous littermates were then intercrossed and F2 progeny homozygous at both loci were selected. In addition, where indicated, mice heterozygous for *Tmem173*^{gt/+} but homozygous for *Fas*^{lpr/lpr} [Sgt(het).MRL/lpr] and mice heterozygous for *cGAS*^{+/-} but homozygous for *Fas*^{lpr/lpr} [cGAS(het).MRL/lpr] were also studied. F2 progeny expressing wild-type *cGAS*^{+/+} or *Tmem173*^{+/+} and homozygous for *Fas*^{lpr/lpr} (B6.MRL/lpr) were kept as controls.

Mice expressing *Tmem173^{gt/gt}*, *SLE1^{NZM/NZM}*, and *Fas^{lpr/lpr}* (Sgt.SLE1.lpr) all homozygously on a B6 background were derived by crossing Sgt.lpr mice with B6.SLE1 mice. The *Tmem173^{gt/+}*, *Fas^{lpr/+}*, and *SLE1^{NZM/+}* heterozygous littermates were then backcrossed with B6.SLE1 mice and F2 progeny heterozygous for *Tmem173^{gt/+}* and *Fas^{lpr/+}* but homozygous for *SLE1^{NZM/NZM}* were intercrossed. The F3 progeny homozygous at all three loci were then selected. In addition, F3 progeny expressing wild-type *Tmem173^{+/+}* or heterozygous *Tmem173^{gt/+}* but homozygous for *SLE1^{NZM/NZM}* and *Fas^{lpr/lpr}* [SLE1.lpr or Sgt(het).SLE1.lpr] were also studied. Utilizing the same crossing strategy used to create Sgt.SLE1.lpr mice, mice expressing *cGAS^{-/-}*, *SLE1^{NZM/NZM}*, and *Fas^{lpr/lpr}* (cGAS KO.SLE1.lpr) all homozygously on a B6 background were generated by crossing cGAS KO.lpr mice with B6.SLE1 mice. F3 progeny expressing heterozygous *cGAS^{+/-}* but homozygous *SLE1^{NZM/NZM}* and *Fas^{lpr/lpr}* [cGAS(het).SLE1.lpr] were also studied.

ELISA

96-well ELISA plates (greiner bio-one) were coated with either 50 µg/mL herring-testis DNA (for anti-dsDNA IgG detection) or 5 µg/mL single-stranded calf thymus DNA (Sigma-Aldrich) (for anti-ssDNA IgG detection) in PBS overnight at 4°C. After blocking the plates with PBS-3% BSA (wt/vol), diluted serum samples were added to plate in PBS-1% BSA (wt/vol). For serum samples from B6.lpr, cGAS KO.lpr, and Sgt.lpr mice a 1:50 serum dilution was used. For serum samples from B6.MRL/lpr, cGAS(het).MRL/lpr, cGAS KO.MRL/lpr, Sgt(het).MRL/lpr, and Sgt.MRL/lpr mice a 1:100 serum dilution was used. For serum samples from SLE1.lpr, cGAS(het).SLE1.lpr, cGAS KO.SLE1.lpr, Sgt(het).SLE1.lpr, and Sgt.SLE1.lpr mice a 1:400 serum dilution was used. After washing of plate, secondary

HRP-conjugated goat anti-mouse IgG (H+L) antibody (Millipore) was added at a 1:2500 dilution. The plate was developed with 3,3',5,5'-tetramethylbenzidine (TMB) substrate (Thermo Scientific), and the OD at 450 nm was measured.

For detection of IL-12 in mouse sera, a sandwich ELISA was employed. A 96-well ELISA plate was coated with rat anti-mouse IL-12 p40/p70 antibody (BD Biosciences) diluted in 0.05M carbonate-bicarbonate buffer (pH 9.6) at a concentration of 1 µg/mL. The ELISA plate was subsequently incubated overnight at 4°C. After blocking the plate with PBS-3% BSA, serum samples diluted 1:4 in PBS-1% BSA were added to plate. After washing of plate, biotin-conjugated rat anti-mouse IL-12 p40/p70 detection antibody (BD Biosciences) was added to the plate at a concentration of 1 µg/mL. The plate was washed again and avidin-HRP conjugated antibody (Biolegend) was added at a 1:1000 dilution. The plate was developed with TMB substrate and the OD at 450 nm was measured.

Autoantibody Array Analysis

IgG and IgM anti-nuclear autoantibodies in mouse sera were detected by autoantigen microarray as previously described (Li QZ 2005). Autoantigen microarray data analysis was performed as previously described (Dozmorov and Lefkovits 2009; Dozmorov, Jarvis et al. 2011).

Flow Cytometry

Spleens were harvested from 5 month-old female B6 WT, cGAS KO, STING *gt/gt*, B6.lpr, cGAS KO.lpr, and Sgt.lpr mice and splenocytes were isolated for surface staining. Briefly, splenocytes were washed in ice-cold FACS staining buffer [10% FBS (wt/vol), 0.1% NaN₃ (wt/vol) in PBS]. Cell suspensions were then incubated with rat anti-mouse CD16/32

antibody (Biolegend) at a 1:200 dilution for 15 minutes on ice. After washing cells with FACS staining buffer, cells were then surface stained. The stained cells were analyzed using a FACSCalibur flow cytometer (BD Biosciences). Data were analyzed using FlowJo software. Ly6c-APC, TCR β -APC, CD44-PE, CD138-PE, CD4-FITC, CD86-APC antibodies were purchased from Biolegend. CD11c-PE, F4/80-FITC, CD11b-FITC, CD8-PE, B220-PerCP-Cy5.5, CD69-FITC, Ly6G-PE antibodies were purchased from eBioscience.

Pathology

Kidneys were harvested from 5 month-old female B6 WT, cGAS KO, STING *gt/gt*, B6.lpr, cGAS KO.lpr, and Sgt.lpr mice and tissues were fixed in 4% paraformaldehyde (wt/vol). Fixed kidneys were paraffin-embedded then sectioned at 3 μ m and stained with hematoxylin & eosin and periodic acid-Schiff. Kidney section histology was blindly evaluated by a pathologist.

Glomerular inflammation was assessed according to the following histology scoring criteria: 100 glomeruli were counted for each animal. Each glomerulus received a score of 0-4 dependent on the amount of observed PAS positive deposition, cell proliferation, membranous hypertrophy, and/or adhesion to the parietal layer of the renal corpuscle. A score of 0 indicates no glomerular lesions, a score of 1 indicates <30% of glomerular tuft is affected, a score of 2 indicates 30-70% of glomerular tuft is affected, a score of 3 indicates 70-90% of glomerular tuft is affected, and a score of 4 indicates >90% of glomerular tuft is affected. The individual glomeruli scores were then averaged together into a glomerular inflammation score for each animal.

Inflammatory cell infiltrate was assessed according to the following histology scoring criteria: For each animal, the amount of infiltrating peripelvic and/or perivascular inflammatory immune cells was ascertained and the extent of inflammatory cell infiltrate in the kidneys was scored from 0 to 3. A score of 0 was given for no inflammatory cell infiltrate, a score of 1 was given for mild inflammatory cell infiltrate, a score of 2 was given for moderate inflammatory cell infiltrate, and a score of 3 was given for severe inflammatory cell infiltrate.

Quantitative RT-PCR

In order to isolate PBMCs for use in RT-PCR, whole blood was collected from mice and mixed with heparin. Red blood cells were lysed using Red Blood Cell Lysing Buffer Hybri-Max (Sigma) and isolated PBMCs were pelleted and flash frozen in liquid nitrogen. Spleens were harvested from mice and splenocytes were obtained following red blood cell lysis. Total RNA was isolated from PBMCs and splenocytes using an RNeasy Mini Kit (Qiagen) and cDNA was synthesized using the iScript cDNA synthesis kit (Bio-Rad). RT-PCR reactions were carried out by using the iTaq Universal SYBR Green Supermix (Bio-Rad). RT-PCR was performed on an Applied Biosystems ViiA 7. Primers used: Rpl19 (AAATCGCCAATGCCAACTC; TCTTCCCTATGCCCATATGC), IFN- β (TCCGAGCAGAGATCTTCAGGAA; TGCAACCACCACTCATTCTGAG), IFN- α_1 (AGCCTTGACACTCCTGGTAC, TGGTGGAGGTCATTGCAGAA), CXCL10 (GCCGTCATTTTCTGCCTCA; CGTCCTTGCGAGAGGGATC), Ifit3 (TGGCCTACATAAAGCACCTAGATGG, CGCAAACCTTTTGGCAAACCTTGTCT),

ISG15 (GGAACGAAAGGGGCCACAGCA, CCTCCATGGGCCTTCCCTCGA), IRF7 (ATGCACAGATCTTCAAGGCCTGGGC, GTGCTGTGGAGTGACACAGCGGAAGT).

Statistical Analysis

All data are presented as the mean of individual mice \pm SEM. Statistical analysis of autoantibody levels was performed using the Mann-Whitney U-test. All other statistical analyses were performed by using a two-tailed, unpaired Student's *t* test. * $p < 0.05$, ** $p < 0.01$, *** $p < 0.001$, **** $p < 0.0001$ versus indicated group.

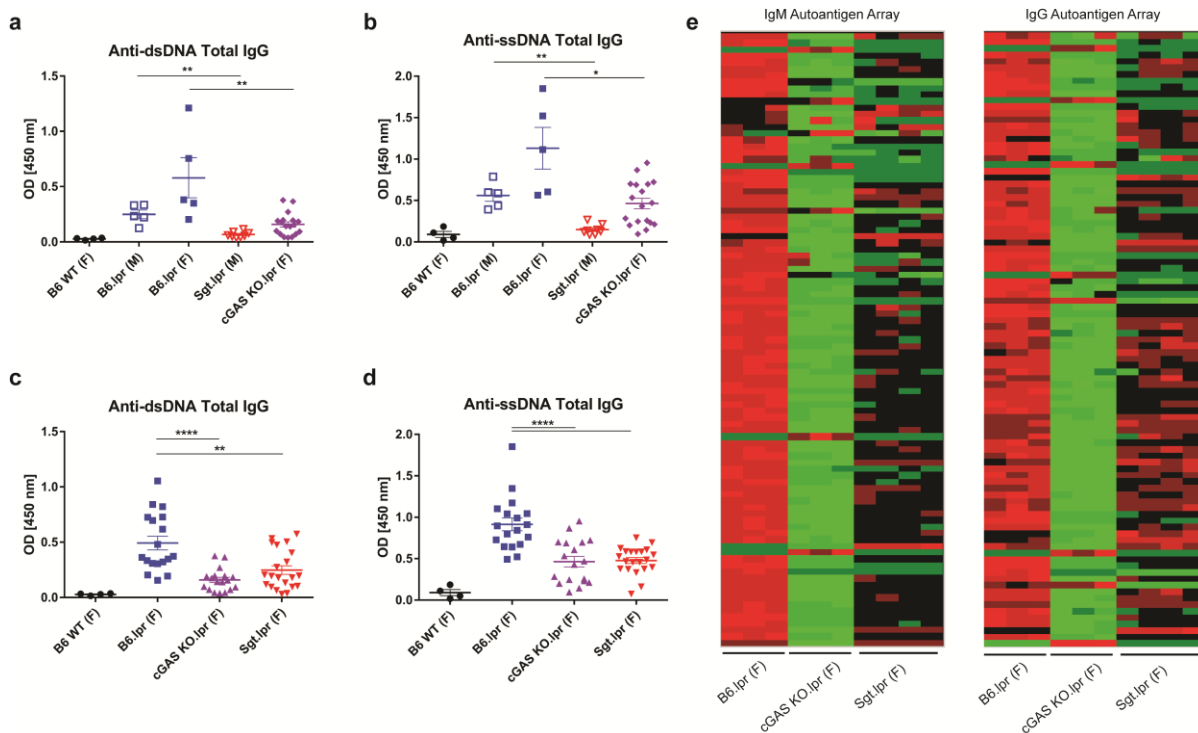


Figure 11: cGAS or STING deficiency in B6.lpr mice results in less autoantibody production.

a,b, Serum was harvested from 5 month old female B6 WT, B6.lpr, and cGAS KO.lpr mice and 5 month old male B6.lpr and Sgt.lpr mice and circulating levels of anti-dsDNA IgG (**a**) or anti-ssDNA IgG (**b**) autoantibodies were measured. Each dot represents one mouse. **c,d**, Serum was harvested from 5 month old female B6 WT, B6.lpr, cGAS KO.lpr, and Sgt.lpr mice and circulating levels of anti-dsDNA IgG (**c**) or anti-ssDNA IgG (**d**) autoantibodies were measured. Each dot represents one mouse. **e**, IgM and IgG autoantibody repertoire and titers were determined by binding of sera harvested from 5 month old female B6.lpr ($n = 3$), cGAS KO.lpr ($n = 3$), and Sgt.lpr ($n = 4$) mice to a predefined autoantigen microarray. Heatmaps summarizing IgM and IgG autoantibody levels are shown. Each column represents an individual mouse.

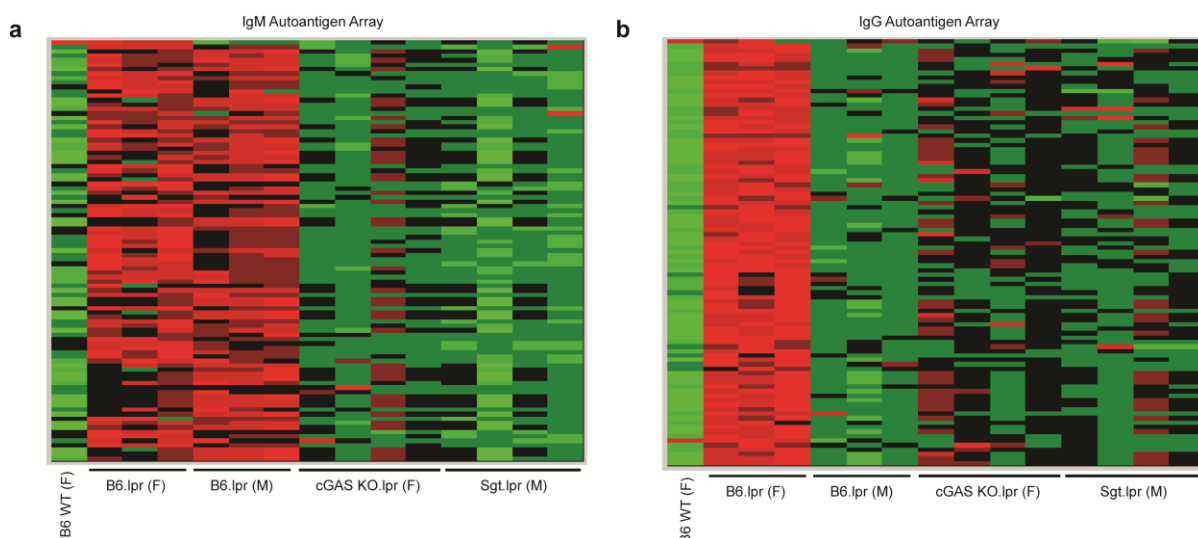


Figure 12: The effect of cGAS or STING deficiency on autoantibody production in B6.lpr mice.
a,b, Serum was harvested from 5 month old female B6 WT ($n = 1$), B6.lpr ($n = 3$), and cGAS KO.lpr ($n = 4$) mice and 5 month old male B6.lpr ($n = 3$) and Sgt.lpr ($n = 4$) mice and the IgM and IgG autoantibody repertoire and titers were determined by binding of sera to a predefined autoantigen microarray. Heatmaps summarizing IgM (**a**) and IgG (**b**) autoantibody levels are shown. Each column represents an individual mouse.

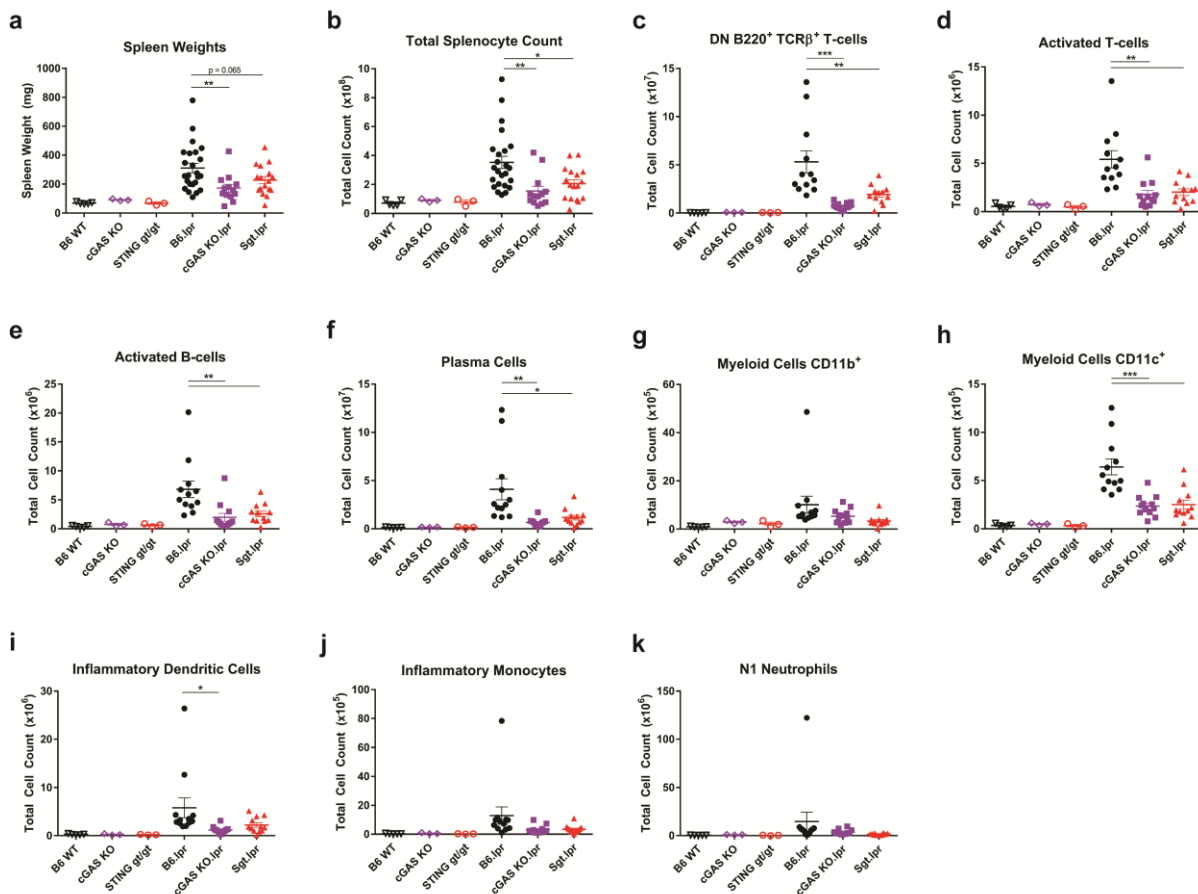


Figure 13: The effect of genetic ablation of cGAS or STING in B6.lpr mice on inflammatory immune cell accumulation.

a,b, Spleens were harvested from 5 month old female B6 WT, cGAS KO, STING gt/gt, B6.lpr, cGAS KO.lpr, and Sgt.lpr mice and spleen weight (**a**) and total splenocyte count (**b**) for each spleen was determined. **c,d,e,f,** Spleens were harvested from 5 month old female B6 WT, cGAS KO, STING gt/gt, B6.lpr, cGAS KO.lpr, and Sgt.lpr mice and lymphoid compartment total cell counts were determined for DN T-cells (**c**), activated memory T-cells (**d**), activated memory B-cells (**e**), and plasma cells (**f**). **g,h,i,j,k,** Spleens were harvested from 5 month old female B6 WT, cGAS KO, STING gt/gt, B6.lpr, cGAS KO.lpr, and Sgt.lpr mice and myeloid compartment total cell counts were determined for all CD11b⁺ myeloid cells (**g**), all CD11c⁺ myeloid cells (**h**), inflammatory dendritic cells (**i**), inflammatory monocytes (**j**), and N1 neutrophils (**k**). For all graphs, each dot represents one mouse.

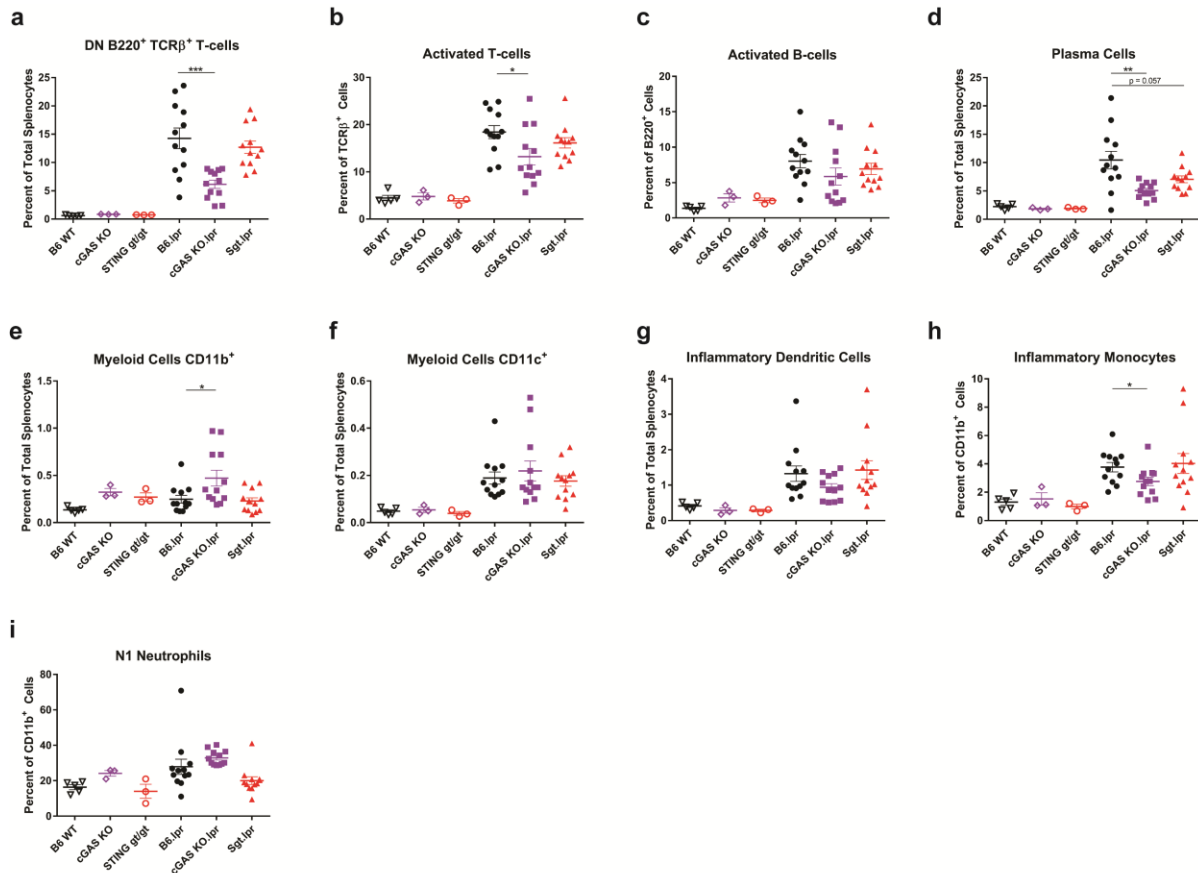


Figure 14: The effect of genetic ablation of cGAS or STING on splenic inflammatory immune cell populations in B6.lpr mice.

a,b,c,d, Spleens were harvested from 5 month old female B6 WT, cGAS KO, STING *gt/gt*, B6.lpr, cGAS KO.lpr, and Sgt.lpr mice and lymphoid compartment cell frequencies were determined for DN T-cells (**a**), activated memory T-cells (**b**), activated memory B-cells (**c**), and plasma cells (**d**). **e,f,g,h,i,** Spleens were harvested from 5 month old female B6 WT, cGAS KO, STING *gt/gt*, B6.lpr, cGAS KO.lpr, and Sgt.lpr mice and myeloid compartment cell frequencies were determined for all CD11b⁺ myeloid cells (**e**), all CD11c⁺ myeloid cells (**f**), inflammatory dendritic cells (**g**), inflammatory monocytes (**h**), and N1 neutrophils (**i**). For all graphs, each dot represents one mouse.

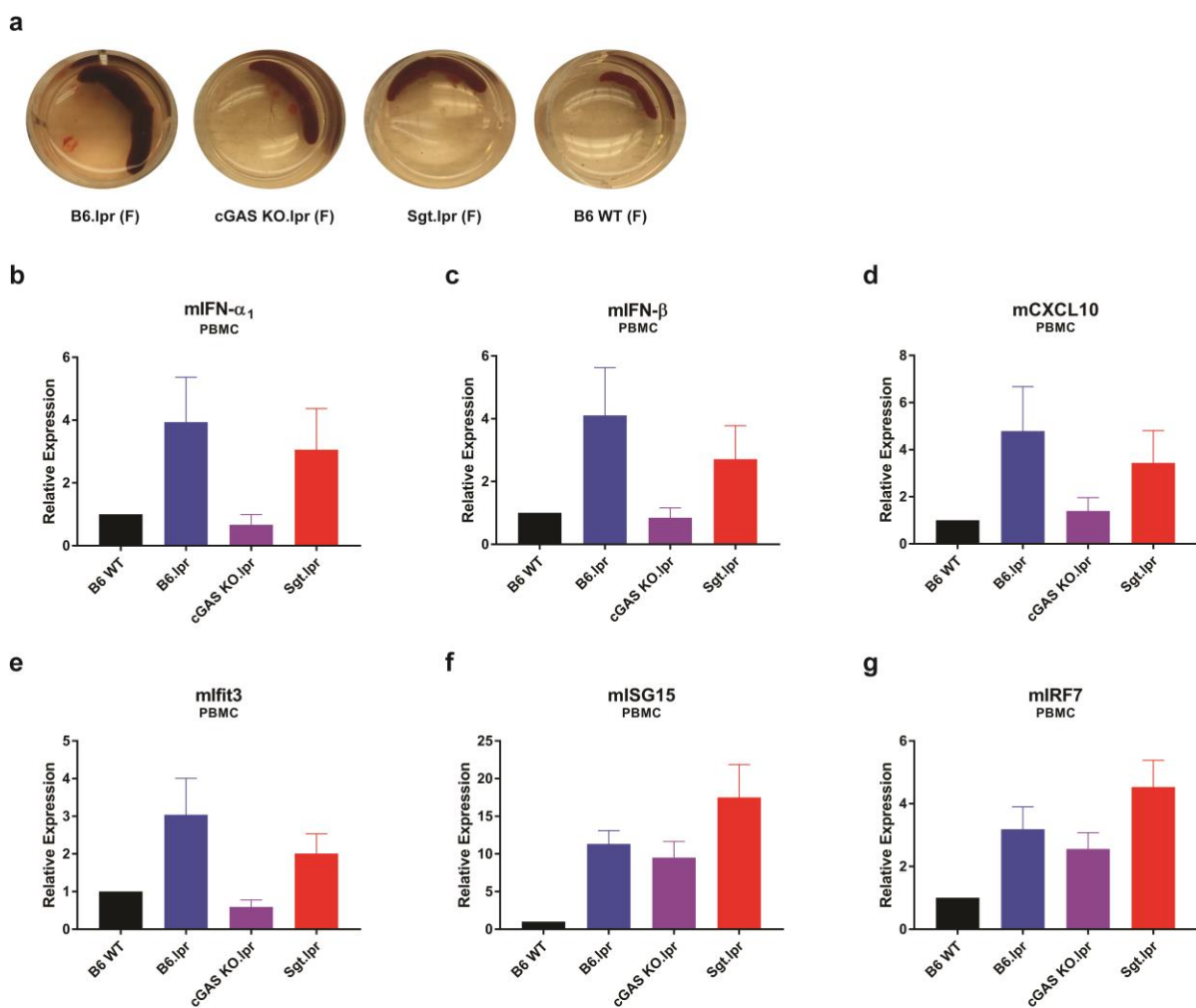


Figure 15: Splenomegaly and characterization of the IFN signature in B6.lpr, cGAS KO.lpr, and Sgt.lpr mice.

a, Spleens were harvested from 7 month old female B6.lpr ($n = 4$), cGAS KO.lpr ($n = 3$), and Sgt.lpr ($n = 3$) mice. A spleen from a female control B6 WT mouse is shown for reference. Images are representative of each group. **b,c,d,e,f,g**, PBMCs from 7 month old female B6.lpr ($n = 4$), cGAS KO.lpr ($n = 3$), Sgt.lpr ($n = 3$), and B6 WT ($n = 1$) mice were isolated and cytokine production was measured by RT-PCR for mouse IFN- α_1 (**b**) and IFN- β (**c**). In addition, transcript levels for mouse interferon-stimulated genes CXCL10 (**d**), Ifit3 (**e**), ISG15 (**f**), and IRF7 (**g**) were measured. Values are relative to B6 WT mouse gene expression.

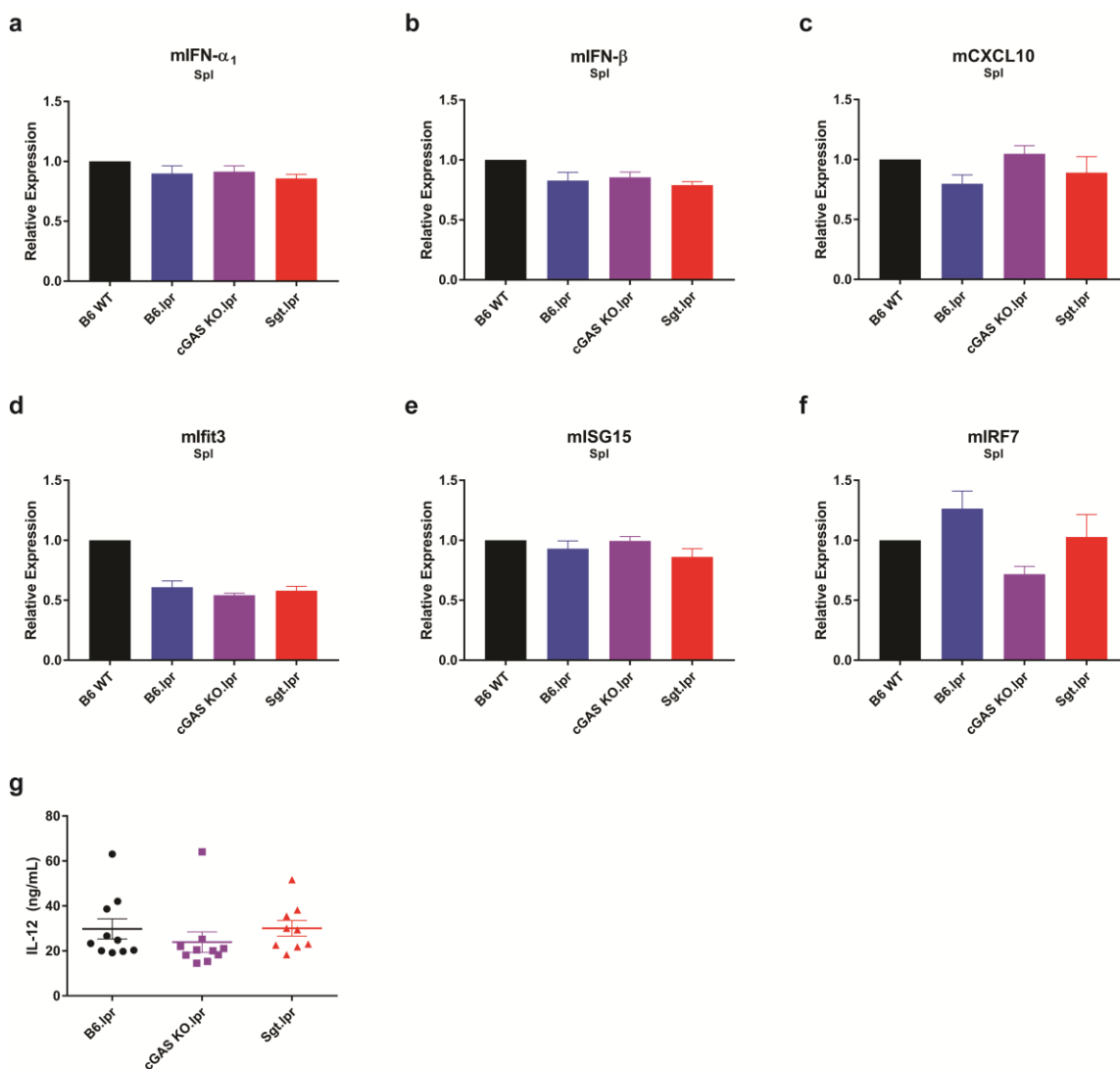


Figure 16: B6.lpr, cGAS KO.lpr, and Sgt.lpr mice show comparable levels of splenic cytokine and ISG production and similar levels of serum IL-12.

a,b,c,d,e,f, Spleens were harvested from 7 month old female B6.lpr ($n = 4$), cGAS KO.lpr ($n = 3$), Sgt.lpr ($n = 3$), and B6 WT ($n = 1$) mice. Cytokine production in isolated splenocytes was measured by RT-PCR for mouse IFN- α_1 (**a**) and IFN- β (**b**). In addition, transcript levels for mouse interferon-stimulated genes CXCL10 (**c**), Ifit3 (**d**), ISG15 (**e**), and IRF7 (**f**) were measured. Values are relative to B6 WT mouse gene expression. **g**, Serum was harvested from 5 month old female B6.lpr, cGAS KO.lpr, and Sgt.lpr mice and circulating levels of IL-12 were measured by ELISA. Each dot represents one mouse.

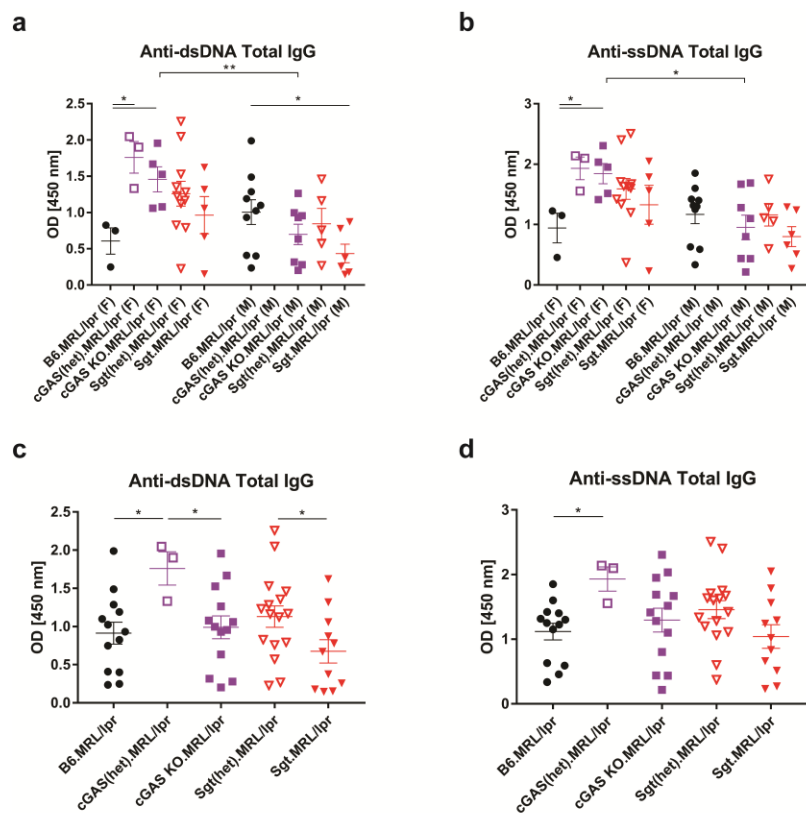


Figure 18: The effect that genetically ablating cGAS or STING in B6.MRL/Mp-*Fas*^{lpr/lpr} mice has on generation of anti-DNA autoantibodies.

a,b, Serum was harvested from 3 month old B6.MRL/lpr, Sgt(het).MRL/lpr, Sgt.MRL/lpr, cGAS(het).MRL/lpr, and cGAS KO.MRL/lpr mice and circulating levels of anti-dsDNA IgG (**a**) or anti-ssDNA IgG (**b**) autoantibodies was measured by ELISA. Results segregated by gender are shown. **c,d,** Mixed gender results obtained by combining gender-segregated (**a**) and (**b**) graphs are shown for anti-dsDNA IgG (**c**) and anti-ssDNA IgG (**d**) autoantibodies. For all graphs, each dot represents one mouse.

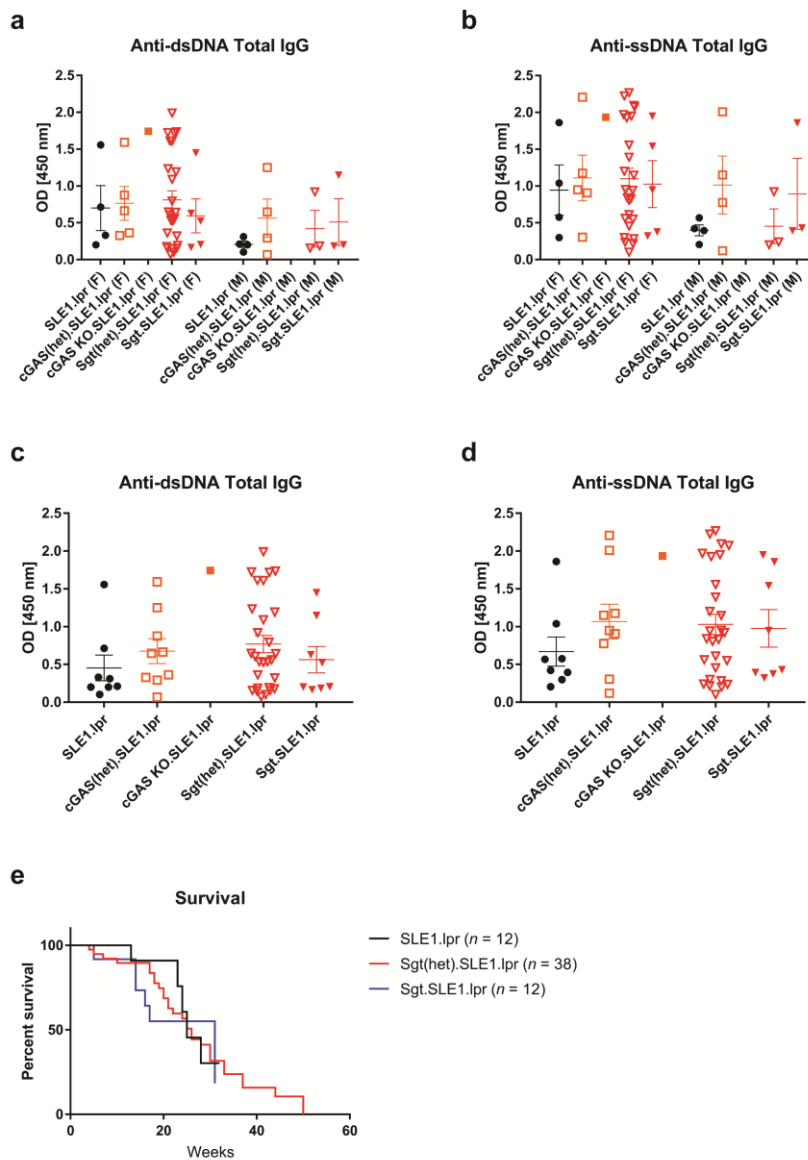


Figure 19: cGAS or STING deficiency in B6.SLE1.lpr mice does not alter the course of autoimmune disease.

a,b, Serum was harvested from 3 month old SLE1.lpr, cGAS(het).SLE1.lpr, cGAS KO.SLE1.lpr, Sgt.SLE1.lpr, and Sgt(het).SLE1.lpr mice and circulating levels of anti-dsDNA IgG (**a**) or anti-ssDNA IgG (**b**) autoantibodies was measured by ELISA. Results segregated by gender are shown. **c,d,** Mixed gender results obtained by combining gender-segregated (**a**) and (**b**) graphs are shown for anti-dsDNA IgG (**c**) and anti-ssDNA IgG (**d**) autoantibodies. Each dot represents one mouse. **e,** Survival of SLE1.lpr, Sgt.SLE1.lpr, and Sgt(het).SLE1.lpr mice. Mice were observed until the time of death.

CHAPTER FOUR

Miscellaneous experiments investigating the adjuvant effects of ultra-pH sensitive nanoparticles loaded with 2'3'-cGAMP and investigating the potential role cGAS-STING pathway signaling may play in the immune response to influenza infection in vivo

RESULTS

Ultra-pH sensitive nanoparticles function as an effective vaccine adjuvant with or without 2'3'-cGAMP cargo

It is known that 2'3'-cGAMP can function as an effective vaccine adjuvant, stimulating a balanced humoral and cellular immune response to protective antigens (Li, Wu et al. 2013; Skrnjug I. 2014; Wang, Li et al. 2016). However, in order to exert its immunostimulatory effects, 2'3'-cGAMP must enter the cytosol where it can bind to and activate STING. One potential method of enhancing 2'3'-cGAMP delivery into the cytoplasm of cells is via the use of nanotechnology. Recently, a series of tunable ultra-pH sensitive (UPS) nanoparticles was developed (Wang, Zhou et al. 2014; Zhou, Liu et al. 2012). These UPS nanoparticles can be selectively activated within acidic organelles of the cell like the endosome or lysosome. In addition, these UPS nanoparticles form micelles which can be used to encapsulate small molecules for delivery into cells. Therefore, it is possible for UPS nanoparticle-encapsulated 2'3'-cGAMP to be taken up into cells via either receptor-mediated endocytosis or phagocytosis. Once inside the endosome or phagolysosome, the acidic environment would trigger activation of the UPS nanoparticles, causing disassembly of the micelle structure and the subsequent delivery of 2'3'-cGAMP inside the cell. UPS nanoparticle micelle disassembly may also disrupt the endosomal or phagolysosomal membrane, further enhancing cytosolic delivery of 2'3'-cGAMP.

To test whether UPS nanoparticles can indeed function as an effective delivery mechanism for 2'3'-cGAMP as a vaccine adjuvant, I vaccinated B6 WT mice with H1N1 PR8 NP antigen in combination with either free 2'3'-cGAMP, alum, or a UPS nanoparticle micelle. The particular UPS nanoparticle formulation used was termed pc7a, which has an activating pH of 6.9. The pc7a nanoparticle would therefore activate once a pH of less than 6.9 was encountered within the cell (early endosome-activatable composition). I used pc7a nanoparticles with or without 2'3'-cGAMP loading (pc7a-cGAMP or pc7a, respectively) as adjuvants and compared their efficacy as vaccine adjuvants to free 2'3'-cGAMP and alum. Serum was harvested from vaccinated mice one week post-boost and serum levels of anti-NP specific total IgG were measured by ELISA. Mice immunized with pc7a-cGAMP demonstrated higher serum levels of anti-NP IgG antibodies than mice immunized with pc7a (**Fig. 20a**). Compared to mice in the alum vaccinated group, mice immunized with free 2'3'-cGAMP or pc7a-cGAMP had significantly higher serum levels of anti-NP IgG. However, no significant difference was seen in anti-NP IgG levels in sera taken from free 2'3'-cGAMP immunized mice and pc7a-cGAMP immunized mice (**Fig. 20a**). In addition, pc7a and alum immunized mice generated roughly comparable anti-NP total IgG responses. Mice in both the pc7a-cGAMP and free 2'3'-cGAMP immunized groups had significantly higher levels of serum anti-NP IgG1 than mice in the alum vaccinated group (**Fig. 20b**). However, no significant difference in anti-NP IgG1 levels was seen between either the pc7a and pc7a-cGAMP cohorts or the free 2'3'-cGAMP and pc7a-cGAMP cohorts. Similar to the total anti-NP IgG response, mice in the alum and pc7a immunized groups had comparable

anti-NP IgG1 responses (**Fig. 20b**). Mice in the pc7a-cGAMP cohort generated significantly higher anti-NP IgG2b serum antibody levels than mice in the pc7a, free 2'3'-cGAMP, and alum cohorts (**Fig. 20c**). In addition, mice vaccinated with free 2'3'-cGAMP had higher serum anti-NP IgG2b levels than mice immunized with alum. Also, pc7a immunized mice had higher serum anti-NP IgG2b levels than mice immunized with alum (**Fig. 20c**).

In order to see protection from influenza virus challenge, I subsequently repeated the vaccination experiments utilizing pc7a nanoparticles with H1N1 PR8 HA antigen. Measurement of anti-HA specific total IgG from sera harvested from vaccinated mice one week post-boost showed that mice in both the pc7a and pc7a-cGAMP immunized cohorts generated significantly higher anti-HA IgG antibody levels than mice in the free 2'3'-cGAMP or alum immunized cohorts (**Fig. 21a**). There was no significant difference seen in anti-HA IgG levels comparing between pc7a and pc7a-cGAMP immunized groups. The same results as those observed for anti-HA total IgG were seen when looking at anti-HA specific IgG1 and IgG2b levels in sera from vaccinated mice (**Fig. 21b,c**). To test the protective effect of vaccination utilizing pc7a nanoparticles, I challenged vaccinated mice with a lethal dose of influenza virus. Mice in the pc7a and pc7a-cGAMP immunized groups showed a dramatic reduction in bodyweight loss compared to mice in the free 2'3'-cGAMP or alum immunized groups (**Fig. 21d**). Control mice vaccinated with HA antigen alone or PBS mock injections showed severe bodyweight loss. All control mice succumbed to influenza challenge by day 10 post-infection, whereas mice in both the alum and 2'3'-cGAMP vaccinated groups showed partial protection from lethal influenza

virus challenge (**Fig. 21e**). Mice in both the pc7a and pc7a-cGAMP immunized cohorts showed full protection from influenza virus challenge, with all mice in these two groups surviving. These results indicate that both pc7a nanoparticles loaded with 2'3'-cGAMP and pc7a nanoparticles alone are capable vaccine adjuvants.

C57BL/6J mice deficient in cGAS, STING, or MAVS respond similarly to in vivo influenza infection

To test what effect genetically ablating cGAS, STING, or the cytosolic RNA-sensing pathway adaptor protein MAVS might have on the in vivo response to influenza infection, I challenged B6 WT, cGAS KO, STING *gt/gt*, and MAVS KO mice with H1N1 PR8 influenza virus. Following influenza infection, mice in all four genotypes tested demonstrated significant bodyweight loss (**Fig. 22a**). In addition, there was significant mortality observed in mice from all four genotypes tested following influenza infection (**Fig. 22b**). However, no significant difference was seen in survival curves when comparing between B6 WT, cGAS KO, STING *gt/gt*, and MAVS KO mice following influenza infection.

CONCLUSIONS AND DISCUSSIONS

When H1N1 PR8 NP was used as the vaccine antigen, pc7a nanoparticles alone functioned as an effective vaccine adjuvant. Mice immunized with pc7a-adjuvanted vaccine mounted humoral immune responses to NP antigen that were comparable to the humoral immune responses seen in mice immunized with alum-adjuvanted vaccine (**Fig. 20**). Compared to pc7a nanoparticles alone, pc7a-cGAMP was superior in stimulating anti-NP IgG2b production, resulting in a higher serum level of anti-NP specific total IgG in pc7a-cGAMP vaccinated mice (**Fig. 20a,c**). However, compared to the use of an equivalent amount of free 2'3'-cGAMP, pc7a-cGAMP only stimulated a greater production of anti-NP specific IgG2b (**Fig. 20c**). Anti-NP specific IgG1 and total anti-NP IgG responses were similar between the free 2'3'-cGAMP and pc7a-cGAMP immunized groups (**Fig. 20a,b**). When H1N1 PR8 HA antigen was used instead, both pc7a nanoparticles alone and pc7a-cGAMP induced strong anti-HA IgG1 and IgG2b production (**Fig. 21b,c**). In this experiment, both pc7a and pc7a-cGAMP cohorts displayed superior humoral immune responses to HA antigen than alum or free 2'3'-cGAMP immunized cohorts (**Fig. 21a,b,c**). This superior humoral immune response translated to better protection against influenza virus challenge for pc7a and pc7a-cGAMP immunized groups (**Fig. 21d,e**). Therefore, both pc7a and pc7a-cGAMP were similarly efficacious as vaccine adjuvants in this experiment. I expected that the use of pc7a-cGAMP to encapsulate and subsequently enhance cytosolic delivery of 2'3'-cGAMP into cells would result in a stronger humoral immune response to antigen compared to the use of pc7a nanoparticles alone or free 2'3'-cGAMP. In the experiment

in which HA antigen was used, pc7a-cGAMP did function as a superior adjuvant compared to free 2'3'-cGAMP. However, in the experiment in which NP antigen was used, pc7a-cGAMP was only superior to free 2'3'-cGAMP as a vaccine adjuvant in stimulating anti-NP IgG2b production. When I used HA antigen for my experiment, I saw no difference in the vaccine adjuvant efficacy of pc7a and pc7a-cGAMP. When I used NP antigen for my experiment, I saw that pc7a-cGAMP was superior to pc7a in inducing anti-NP IgG2b and overall anti-NP total IgG production. These results are therefore inconsistent with each other. It is possible that these inconsistencies are due to the use of different vaccination antigens between experiments, although I believe that is unlikely as all my subsequent experiments utilizing H1N1 PR8 NP or HA antigen have yielded consistent results when the same adjuvants are used between experiments. I did use different batches of pc7a and pc7a-cGAMP nanoparticles between the two experiments shown, and I believe this provides a more likely explanation for the inconsistencies I observed between the two experiments. Different batches of nanoparticles may have differing levels of cGAMP incorporation into micelles and it is also possible that a newer batch of nanoparticles would have less micelle degradation and loss of cGAMP compared to an older batch. This would account for the inconsistencies in the results I observed.

Although there were some inconsistencies in my results obtained from the nanoparticle experiments, I can confidently conclude that pc7a nanoparticles by themselves display adjuvant activity (**Fig. 20; Fig. 21**). This result was unexpected. However, there are some possible explanations as to why pc7a nanoparticles alone can

function effectively as an adjuvant. One explanation is that because I mixed pc7a nanoparticles and my protective antigen of interest together prior to injecting the vaccination mixture into mice, it is possible that some antigen becomes encapsulated within pc7a nanoparticle micelles. This would enhance both the lysosomal and cytosolic delivery of antigen into APCs, which would augment both the MHC-I and MHC-II antigen-processing pathways, resulting in an overall enhancement of APC antigen-presentation to both CD4⁺ and CD8⁺ T-cells. It has been shown that membrane fusion events can activate STING in a cGAS-independent manner (Holm, Jensen et al. 2012; Holm, Rahbek et al. 2016). It is possible that pc7a micelles may fuse with cell membranes inadvertently, which could trigger activation of STING and result in induction of type-I IFN and proinflammatory cytokines. If this phenomenon occurred in an APC that concurrently picked up the protective antigen, it would induce the activation and maturation of that APC. Subsequently, that mature APC would be capable of inducing an antigen-specific adaptive immune response. This would explain why pc7a nanoparticles alone can function as a vaccine adjuvant.

Influenza virus infection is typically sensed by the RNA-detecting PRRs of the innate immune system (Bahadoran, Lee et al. 2016). In addition to TLR7-mediated sensing in the endosome, influenza virus RNA can be detected in the cytoplasm by the cytosolic RNA-sensing protein retinoic acid inducible gene I (RIG-I). MAVS functions as the essential signaling adaptor protein that is downstream of RIG-I. Following RIG-I binding to viral single-stranded RNA (ssRNA), MAVS is activated (Wu and Chen 2014). Activated MAVS initiates further downstream signaling events, culminating in the

activation of TBK1 and IKK. Activation of TBK1 and IKK leads to the translocation of transcription factors IRF3 and NF- κ B into the nucleus. The end result of RIG-I-MAVS pathway signaling is the production of type-I IFN and proinflammatory cytokines, which function to initiate the host innate immune response. In addition to RNA-sensing PRRs, STING has recently been implicated as a detector of influenza virus-mediated membrane fusion events (Holm, Rahbek et al. 2016). Therefore, I predicted that MAVS KO and STING *gt/gt* mice would exhibit impaired innate immune sensing of influenza virus *in vivo*, which should result in the accelerated morbidity and mortality of MAVS KO and STING *gt/gt* mice compared to B6 WT or cGAS KO mice when infected with influenza A virus. However, when I challenged B6 WT, cGAS KO, STING *gt/gt*, and MAVS KO mice with H1N1 PR8 influenza virus, all mice (regardless of genotype) lost significant weight (**Fig. 22a**). Ultimately, survival of mice across all genotypes tested was similar, with the majority of mice in each genotype succumbing to influenza infection (**Fig. 22b**). These results were unexpected, with a possible explanation being that B6 background mice (like most inbred strains) have a functionally deleted Mx1 [Myxovirus (Influenza Virus) Resistance 1] gene (Sanders, Johnson et al. 2013). The Mx1 protein is a critical ISG that induces an antiviral state within cells, thereby conferring resistance to influenza virus infection. Without the Mx1 gene, mice are more susceptible to influenza virus infection. This would explain why B6 WT and cGAS KO mice had a similar response to influenza virus challenge as STING *gt/gt* and MAVS KO mice, because even though B6 WT and cGAS KO mice should be capable of sensing influenza virus and inducing type-I IFN production in response to infection, the lack of Mx1 protein in these mice would

severely attenuate the innate immune response to influenza virus *in vivo*. Mx1 deficiency would therefore explain why the bodyweight loss and survival of B6 WT, cGAS KO, STING *gt/gt*, and MAVS KO mice were similar following influenza virus infection. Another possible explanation for the results I observed is that although I used gender-matched mice for this experiment, the mice were not age-matched. Older mice tend to weigh more and are also more resistant to influenza virus infection, so the age differences between my different genotypes of mice may have unduly influenced the results. In the future, I can repeat the experiment with age and gender-matched mice.

MATERIALS AND METHODS

Reagents

2'3'-cGAMP was synthesized and purified as previously described (Zhang, Shi et al. 2013). UPS nanoparticles pc7a and pc7a-cGAMP were provided by Jinming Gao. Inject Alum adjuvant was purchased from ThermoFisher Scientific. Influenza A H1N1 (A/Puerto Rico/8/34) hemagglutinin (HA) and nucleoprotein (NP) antigens were purchased from Sino Biological Inc.

Mice and Vaccinations

C57BL/6J, B6;129-*Mavs*^{tm1Zjc}/J (MAVS KO), and C57BL/6J-*Tmem173*^{gt}/J [STING gt/gt] mice were obtained from The Jackson Laboratory. cGAS^{-/-} (KO) mice were generated in our laboratory as previously described (Li, Wu et al. 2013). All mice were bred and maintained in the animal facilities of the University of Texas Southwestern Medical Center according to Institutional Animal Care and Use Committee-approved protocols.

For vaccinations utilizing H1N1 NP antigen, 8 week old B6 WT female mice were primed on Day 0 with intramuscular (i.m.) injection in both hind quadriceps muscles with 50 μ l volume per quadriceps with antigen (3 μ g H1N1 NP per mouse) with or without adjuvant (10 μ g free 2'3'-cGAMP; Alum; 200 μ g pc7a; 10 μ g 2'3'-cGAMP packaged in 200 μ g pc7a [pc7a-cGAMP] per mouse). A booster dose was given on Day 10 with antigen (1 μ g H1N1 NP per mouse) with or without adjuvant (the same amount of adjuvant was administered for both prime and boost). Alum was used at a 1:1 dilution

in PBS containing antigen. Serum was collected from the mice on Day 17 for antibody analysis.

For vaccinations utilizing H1N1 HA antigen, 8 week old B6 WT female mice were primed on Day 0 with intramuscular (i.m.) injection in both hind quadriceps muscles with 50 μ l volume per quadriceps with antigen (1 μ g H1N1 HA per mouse) with or without adjuvant (10 μ g free 2'3'-cGAMP; Alum; 200 μ g pc7a; 10 μ g 2'3'-cGAMP packaged in 200 μ g pc7a [pc7a-cGAMP] per mouse). A booster dose was given on Day 10 with antigen (0.5 μ g H1N1 HA per mouse) with or without adjuvant (the same amount of adjuvant was administered for both prime and boost). Alum was used at a 1:1 dilution in PBS containing antigen. Serum was collected from the mice on Day 17 for antibody analysis.

ELISA

96-well ELISA plates (greiner bio-one) were coated with recombinant H1N1 HA or NP antigen at 5 μ g/mL in PBS overnight at 4°C. After blocking the plates with PBS-3% BSA (wt/vol), serum samples were added to plate at a 1:10000 dilution in PBS-1% BSA (wt/vol). After washing of plate, HRP-conjugated goat anti-mouse IgG (H+L) (Millipore) was added at a 1:2500 dilution. For IgG1 and IgG2b detection, HRP-conjugated goat anti-mouse IgG1 or IgG2b (Abcam) antibodies were added at a dilution of 1:5000. The plate was developed with 3,3',5,5'-tetramethylbenzidine substrate (Thermo Scientific), and the OD at 450 nm was measured.

Virus Challenge

For influenza challenge, Influenza A/PR/8/34 (H1N1) virus (Charles River Laboratories) was diluted in sterile PBS to either 10xMLD₅₀ (700 pfu/mouse for vaccinated mice) or 100 pfu/mouse (non-vaccinated mice) dosages. Mice were sedated using ketamine (30 mg/ml)/xylazine (4 mg/ml) intraperitoneally (i.p.) and virus was administered intranasally in a total volume of 40 µL (vaccinated mice) or 20 µL (non-vaccinated mice), split evenly between nares. After virus challenge, mice received atipamezole (0.63 mg/ml) i.p. and were subsequently monitored for weight loss and mortality for 14 days. Mice were humanely sacrificed when weight loss exceeded 30%.

Statistical Analysis

All data are presented as the mean of individual mice \pm SEM. Statistical analysis of mouse survival was performed using the Mantel-Cox test. All other statistical analyses were performed by using a two-tailed, unpaired Student's *t* test. **p* < 0.05, ***p* < 0.01, ****p* < 0.001, *****p* < 0.0001 versus indicated group.

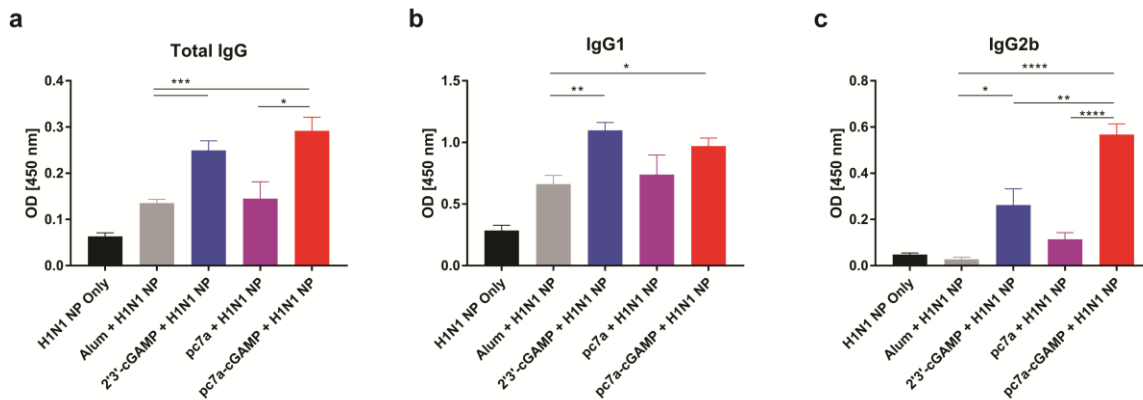


Figure 20: Characterizing the adjuvant effect of pc7a nanoparticles on the humoral immune response to vaccination.

a,b,c, Circulating anti-nucleoprotein (anti-NP) total IgG (**a**) levels were measured by ELISA in serum harvested from vaccinated mice one week post-boost. In addition, the circulating anti-NP IgG1 (**b**) and IgG2b (**c**) subclass levels in vaccinated mouse sera were also measured at one week post-boost. B6 WT mice ($n = 5/\text{group}$) were primed i.m. with H1N1 PR8 NP alone or in combination with alum, free 2'3'-cGAMP, pc7a, or pc7a-cGAMP. A booster dose was administered ten days post-prime. Data are presented as the mean \pm SEM.

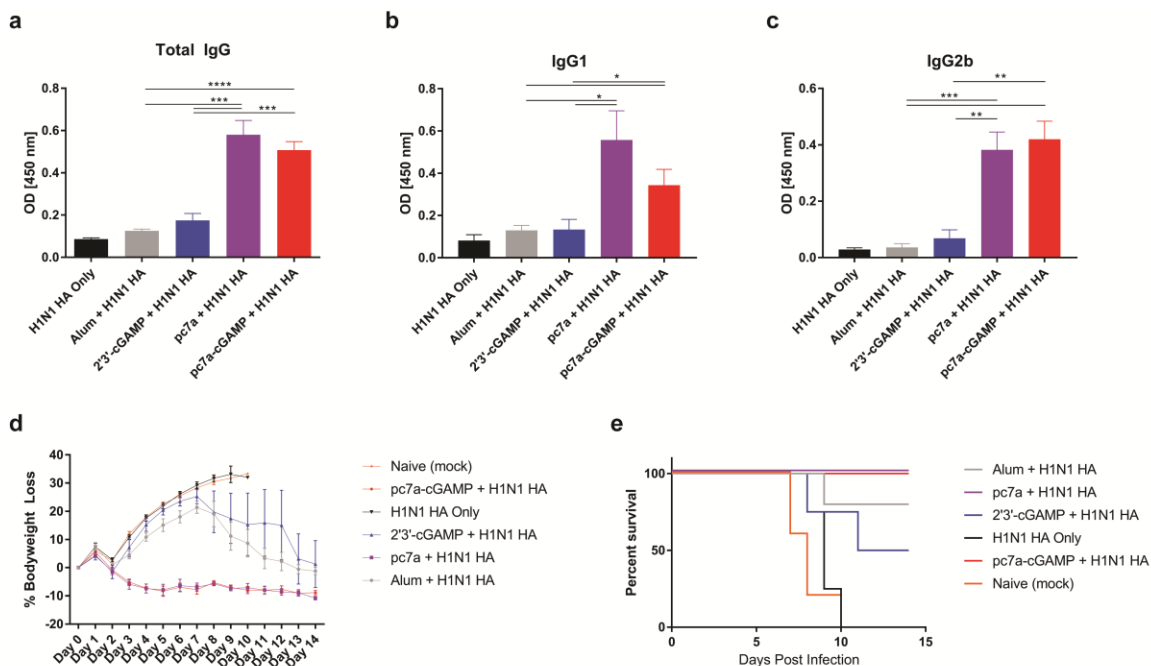


Figure 21: pc7a nanoparticles with or without encapsulated 2'3'-cGAMP demonstrate superior adjuvant effects compared to alum or free 2'3'-cGAMP.

a,b,c, Circulating anti-HA total IgG (**a**) levels were measured by ELISA in serum harvested from vaccinated mice one week post-boost. In addition, the circulating anti-HA IgG1 (**b**) and IgG2b (**c**) subclass levels in vaccinated mouse sera were also measured at one week post-boost. B6 WT mice ($n = 5/\text{group}$) were primed i.m. with H1N1 PR8 HA alone or in combination with alum, free 2'3'-cGAMP, pc7a, or pc7a-cGAMP. A booster dose was administered ten days post-prime. **d,e**, Vaccinated mice ($n = 5/\text{group}$) were intranasally challenged with $10 \times \text{MLD}_{50}$ of Influenza A/PR/8/34 (H1N1) virus 1.5 weeks post-boost. Bodyweight (**d**) and survival (**e**) were tracked daily for two weeks. Data are presented as the mean \pm SEM.

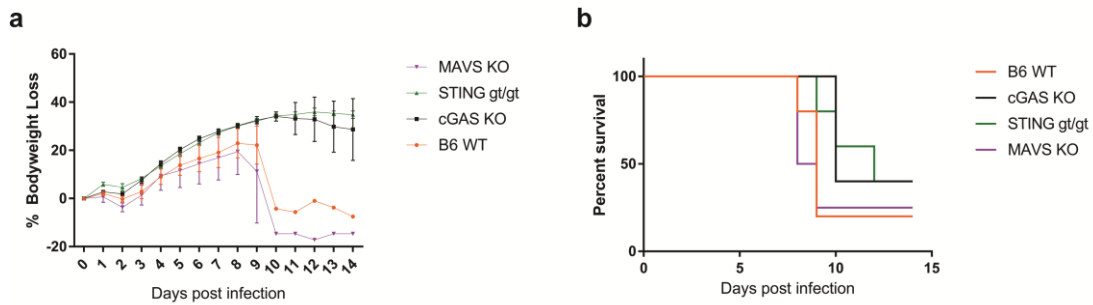


Figure 22: The responses of B6 WT, cGAS KO, STING gt/gt, and MAVS KO mice to influenza virus challenge.

a,b, B6 WT ($n = 5$), cGAS KO ($n = 5$), STING gt/gt ($n = 5$), and MAVS KO ($n = 4$) mice were intranasally challenged with 100 pfu/mouse of Influenza A/PR/8/34 (H1N1) virus. Bodyweight (**a**) and survival (**b**) were tracked daily for two weeks. Data are presented as the mean \pm SEM.

REFERENCES

- Abe, T., A. Harashima, et al. (2013). "STING recognition of cytoplasmic DNA instigates cellular defense." Molecular cell **50**(1): 5-15.
- Aicher, W. K., K. Fujihashi, et al. (1992). "Effects of the *lpr/lpr* mutation on T and B cell populations in the lamina propria of the small intestine, a mucosal effector site." Int Immunol **4**(9): 959-968.
- Akira, S. and K. Takeda (2004). "Toll-like receptor signalling." Nature reviews. Immunology **4**(7): 499-511.
- An, J., L. Durcan, et al. (2016). "cGAS Expression in Patients with Systemic Lupus Erythematosus." Arthritis & rheumatology.
- Andrade, W. A., S. Agarwal, et al. (2016). "Type I Interferon Induction by *Neisseria gonorrhoeae*: Dual Requirement of Cyclic GMP-AMP Synthase and Toll-like Receptor 4." Cell reports **15**(11): 2438-2448.
- Andrews BS, E. R., Theofilopoulos AN, Izui S, Wilson CB, McConahey PJ, Murphy ED, Roths JB, Dixon FJ (1978). "Spontaneous murine lupus-like syndromes. Clinical and immunopathological manifestations in several strains." J Exp Med **148**: 1198-1215.
- Anisur Rahman, D. A. I. (2008). "Systemic Lupus Erythematosus." The New England Journal of Medicine **358**: 929-939.
- Babiuk, S., N. Mookherjee, et al. (2004). "TLR9^{-/-} and TLR9^{+/+} mice display similar immune responses to a DNA vaccine." Immunology **113**(1): 114-120.
- Bahadoran, A., S. H. Lee, et al. (2016). "Immune Responses to Influenza Virus and Its Correlation to Age and Inherited Factors." Frontiers in microbiology **7**: 1841.
- Banchereau, J. and V. Pascual (2006). "Type I interferon in systemic lupus erythematosus and other autoimmune diseases." Immunity **25**(3): 383-392.
- Banchereau, J., V. Pascual, et al. (2004). "Autoimmunity through cytokine-induced dendritic cell activation." Immunity **20**(5): 539-550.
- Berden, J. H., R. Licht, et al. (1999). "Role of nucleosomes for induction and glomerular binding of autoantibodies in lupus nephritis." Curr Opin Nephrol Hypertens **8**(3): 299-306.
- Blanco, P., A. K. Palucka, et al. (2001). "Induction of dendritic cell differentiation by IFN-alpha in systemic lupus erythematosus." Science **294**(5546): 1540-1543.
- Bonilla, F. A. and H. C. Oettgen (2010). "Adaptive immunity." The Journal of allergy and clinical immunology **125**(2 Suppl 2): S33-40.
- Bouvier, N. M. and P. Palese (2008). "THE BIOLOGY OF INFLUENZA VIRUSES." Vaccine **26**(Suppl 4): D49-D53.
- Braun, D. (2003). "Type I Interferon controls the onset and severity of autoimmune manifestations in *lpr* mice." Journal of autoimmunity **20**(1): 15-25.
- Broz, P. and V. M. Dixit (2016). "Inflammasomes: mechanism of assembly, regulation and signalling." Nature reviews. Immunology **16**(7): 407-420.
- Burdette, D. L., K. M. Monroe, et al. (2011). "STING is a direct innate immune sensor of cyclic di-GMP." Nature **478**(7370): 515-518.

- Cai, X., J. Chen, et al. (2014). "Prion-like polymerization underlies signal transduction in antiviral immune defense and inflammasome activation." Cell **156**(6): 1207-1222.
- Cai, X., Y. H. Chiu, et al. (2014). "The cGAS-cGAMP-STING pathway of cytosolic DNA sensing and signaling." Molecular cell **54**(2): 289-296.
- Chandra Mohan, E. A., Laurence Morel, Ping Yang, Edward K. Wakeland (1998). "Genetic Dissection of SLE Pathogenesis: Sle1 on Murine Chromosome 1 Leads to a Selective Loss of Tolerance to H2A/H2B/DNA Subnucleosomes." J. Clin. Invest. **101**: 1362-1372.
- Chen, Y., C. Cuda, et al. (2005). "Genetic Determination of T Cell Help in Loss of Tolerance to Nuclear Antigens." The Journal of Immunology **174**(12): 7692-7702.
- Christensen, S. R., M. Kashgarian, et al. (2005). "Toll-like receptor 9 controls anti-DNA autoantibody production in murine lupus." The Journal of Experimental Medicine **202**(2): 321-331.
- Christensen, S. R., J. Shupe, et al. (2006). "Toll-like receptor 7 and TLR9 dictate autoantibody specificity and have opposing inflammatory and regulatory roles in a murine model of lupus." Immunity **25**(3): 417-428.
- Civril, F., T. Deimling, et al. (2013). "Structural mechanism of cytosolic DNA sensing by cGAS." Nature **498**(7454): 332-337.
- Collins, A. C., H. Cai, et al. (2015). "Cyclic GMP-AMP Synthase Is an Innate Immune DNA Sensor for Mycobacterium tuberculosis." Cell host & microbe **17**(6): 820-828.
- Comoy EE, C. A., Thyphronitis G. (1997). "In vivo induction of type 1 and 2 immune responses against protein antigens." Int Immunol. **9**: 523-531.
- Cotter R., R. C. A., and Bender, B.S. (2001). "Animal Models For Infectious Diseases." Current Protocols in Immunology: 19.11.11-19.11.32.
- Crispin, J. C., S. N. Liou, et al. (2010). "Pathogenesis of human systemic lupus erythematosus: recent advances." Trends in molecular medicine **16**(2): 47-57.
- Crispín JC, O. M., Bayliss G, Cohen RA, Van Beek CA, Stillman IE, Kyttaris VC, Juang YT, Tsokos GC. (2008). "Expanded double negative T cells in patients with systemic lupus erythematosus produce IL-17 and infiltrate the kidneys." J Immunol. **181**(12): 8761-8766.
- Crow, M. K. (2014). "Type I interferon in the pathogenesis of lupus." Journal of immunology **192**(12): 5459-5468.
- Crow, Y. J., B. E. Hayward, et al. (2006). "Mutations in the gene encoding the 3'-5' DNA exonuclease TREX1 cause Aicardi-Goutieres syndrome at the AGS1 locus." Nature Genetics **38**(8): 917-920.
- Cunningham, A. F., K. Serre, et al. (2004). "Pinpointing IL-4-independent acquisition and IL-4-influenced maintenance of Th2 activity by CD4 T cells." European journal of immunology **34**(3): 686-694.
- Dempsey, P. W., S. A. Vaidya, et al. (2003). "The art of war: Innate and adaptive immune responses." Cellular and molecular life sciences : CMLS **60**(12): 2604-2621.

- Deng, G.-M. and G. C. Tsokos (2008). "Cholera toxin B accelerates disease progression in lupus-prone mice by promoting lipid raft aggregation." Journal of immunology (Baltimore, Md. : 1950) **181**(6): 4019-4026.
- Dillon, S. R., C. Sprecher, et al. (2004). "Interleukin 31, a cytokine produced by activated T cells, induces dermatitis in mice." Nature immunology **5**(7): 752-760.
- Dinarello, C. A. (2009). "Immunological and inflammatory functions of the interleukin-1 family." Annual review of immunology **27**: 519-550.
- Dozmorov, I. and I. Lefkovits (2009). "Internal standard-based analysis of microarray data. Part 1: analysis of differential gene expressions." Nucleic acids research **37**(19): 6323-6339.
- Dozmorov, I. M., J. Jarvis, et al. (2011). "Internal standard-based analysis of microarray data2--analysis of functional associations between HVE-genes." Nucleic acids research **39**(18): 7881-7899.
- Eggleton, P. (2001). Hypersensitivity: Immune Complex Mediated (Type III). eLS, John Wiley & Sons, Ltd.
- Ehlers M, F. H., McGaha TL, Aderem A, Ravetch JV. (2006). "TLR9/MyD88 signaling is required for class switching to pathogenic IgG2a and 2b autoantibodies in SLE." J Exp Med. **203**(3): 553-561.
- Eloranta, M. L. and L. Ronnblom (2016). "Cause and consequences of the activated type I interferon system in SLE." Journal of molecular medicine **94**(10): 1103-1110.
- Fairhurst, A. M., S. H. Hwang, et al. (2008). "Yaa autoimmune phenotypes are conferred by overexpression of TLR7." European journal of immunology **38**(7): 1971-1978.
- Fairhurst, A. M., A. E. Wandstrat, et al. (2006). "Systemic Lupus Erythematosus: Multiple Immunological Phenotypes in a Complex Genetic Disease." **92**: 1-69.
- Farkas, L., K. Beiske, et al. (2001). "Plasmacytoid Dendritic Cells (Natural Interferon- α/β -Producing Cells) Accumulate in Cutaneous Lupus Erythematosus Lesions." The American Journal of Pathology **159**(1): 237-243.
- Fecho K, B. S., Cohen PL (1998). "Mice deficient in fas ligand (gld) or fas (lpr) show few alterations in granulopoiesis." Cell Immunol. **188**(1): 19-32.
- Fernandes-Alnemri, T., J. W. Yu, et al. (2009). "AIM2 activates the inflammasome and cell death in response to cytoplasmic DNA." Nature **458**(7237): 509-513.
- Fields, B. N., D. M. Knipe, et al. (2007). Fields virology. Philadelphia, Wolters Kluwer Health/Lippincott Williams & Wilkins.
- Frank, M. M. (2010). "Complement disorders and hereditary angioedema." The Journal of allergy and clinical immunology **125**(2 Suppl 2): S262-271.
- Fridlender ZG, S. J., Kim S, Kapoor V, Cheng G, Ling L, Worthen GS, Albelda SM. (2009). "Polarization of tumor-associated neutrophil phenotype by TGF-beta: "N1" versus "N2" TAN." Cancer Cell. **16**(3): 183-194.
- Gall, A., P. Treuting, et al. (2012). "Autoimmunity Initiates in Nonhematopoietic Cells and Progresses via Lymphocytes in an Interferon-Dependent Autoimmune Disease." Immunity **36**(1): 120-131.
- Gao, D., T. Li, et al. (2015). "Activation of cyclic GMP-AMP synthase by self-DNA causes autoimmune diseases." Proceedings of the National Academy of Sciences of the United States of America.

- Gao, D., J. Wu, et al. (2013). "Cyclic GMP-AMP synthase is an innate immune sensor of HIV and other retroviruses." Science **341**(6148): 903-906.
- Gao, P., M. Ascano, et al. (2013). "Cyclic [G(2',5')pA(3',5')p] is the metazoan second messenger produced by DNA-activated cyclic GMP-AMP synthase." Cell **153**(5): 1094-1107.
- Gao, P., M. Ascano, et al. (2013). "Structure-function analysis of STING activation by c[G(2',5')pA(3',5')p] and targeting by antiviral DMXAA." Cell **154**(4): 748-762.
- Germann, T., M. Bongartz, et al. (1995). "Interleukin-12 profoundly up-regulates the synthesis of antigen-specific complement-fixing IgG2a, IgG2b and IgG3 antibody subclasses in vivo." European journal of immunology **25**(3): 823-829.
- Goubau, D., S. Deddouche, et al. (2013). "Cytosolic sensing of viruses." Immunity **38**(5): 855-869.
- Grove, J. and M. Marsh (2011). "The cell biology of receptor-mediated virus entry." The Journal of cell biology **195**(7): 1071-1082.
- Guo, H., J. B. Callaway, et al. (2015). "Inflammasomes: mechanism of action, role in disease, and therapeutics." Nature medicine **21**(7): 677-687.
- Gurunathan, S., Klinman, D. M. & Seder, R. A. (2000). "DNA vaccines: immunology, application, and optimization." Annu. Rev. Immunol. **18**: 927-974.
- Hale, B. G., R. E. Randall, et al. (2008). "The multifunctional NS1 protein of influenza A viruses." The Journal of general virology **89**(Pt 10): 2359-2376.
- Hanson MC, C. M., Abraham W, Moynihan KD, Szeto GL, Chen SH, Melo MB, Mueller S, Irvine DJ (2015). "Nanoparticulate STING agonists are potent lymph node-targeted vaccine adjuvants." J Clin Invest. **125**(6): 2532-2546.
- Hayden, Frederick G. and Andrew T. Pavia (2006). "Antiviral Management of Seasonal and Pandemic Influenza." The Journal of infectious diseases **194**(Supplement_2): S119-S126.
- He, J., R. Hao, et al. (2016). "Inhibition of hepatitis B virus replication by activation of the cGAS-STING pathway." The Journal of general virology **97**(12): 3368-3378.
- Hespel, C. and M. Moser (2012). "Role of inflammatory dendritic cells in innate and adaptive immunity." European journal of immunology **42**(10): 2535-2543.
- Hewicker, M., E. Kromschroder, et al. (1990). "Detection of circulating immune complexes in MRL mice with different forms of glomerulonephritis." Z Versuchstierkd **33**(4): 149-156.
- Holm, C. K., S. B. Jensen, et al. (2012). "Virus-cell fusion as a trigger of innate immunity dependent on the adaptor STING." Nature immunology **13**(8): 737-743.
- Holm, C. K., S. H. Rahbek, et al. (2016). "Influenza A virus targets a cGAS-independent STING pathway that controls enveloped RNA viruses." Nature communications **7**: 10680.
- Hornung, V., A. Ablasser, et al. (2009). "AIM2 recognizes cytosolic dsDNA and forms a caspase-1-activating inflammasome with ASC." Nature **458**(7237): 514-518.
- Hron, J. D. and S. L. Peng (2004). "Type I IFN Protects Against Murine Lupus." The Journal of Immunology **173**(3): 2134-2142.

- Hwang, S. H., H. Lee, et al. (2012). "B cell TLR7 expression drives anti-RNA autoantibody production and exacerbates disease in systemic lupus erythematosus-prone mice." Journal of immunology **189**(12): 5786-5796.
- Ishii, K. J., C. Coban, et al. (2005). "A Toll-like receptor-independent antiviral response induced by double-stranded B-form DNA." Nature immunology **7**(1): 40-48.
- Ishii, K. J., T. Kawagoe, et al. (2008). "TANK-binding kinase-1 delineates innate and adaptive immune responses to DNA vaccines." Nature **451**(7179): 725-729.
- Ishikawa, H. and G. N. Barber (2008). "STING is an endoplasmic reticulum adaptor that facilitates innate immune signalling." Nature **455**(7213): 674-678.
- Ishikawa, H., Z. Ma, et al. (2009). "STING regulates intracellular DNA-mediated, type I interferon-dependent innate immunity." Nature **461**(7265): 788-792.
- Iwasaki, A. and R. Medzhitov (2015). "Control of adaptive immunity by the innate immune system." Nature immunology **16**(4): 343-353.
- Janeway CA Jr, T. P., Walport M, et al. (2001). Immunobiology: The Immune System in Health and Disease. New York, Garland Science.
- Janeway, C. A., Jr. and R. Medzhitov (2002). "Innate immune recognition." Annual review of immunology **20**: 197-216.
- Jankovic D, C. P., Zweig M, Garcia-Moll M, Showalter SD, Vogel FR, Sher A. (1997). "Adsorption to aluminum hydroxide promotes the activity of IL-12 as an adjuvant for antibody as well as type 1 cytokine responses to HIV-1 gp120." J Immunol. **159**: 2409-2417.
- Jego, G., A. K. Palucka, et al. (2003). "Plasmacytoid Dendritic Cells Induce Plasma Cell Differentiation through Type I Interferon and Interleukin 6." Immunity **19**(2): 225-234.
- Jin, L., K. K. Hill, et al. (2011). "MPYS is required for IFN response factor 3 activation and type I IFN production in the response of cultured phagocytes to bacterial second messengers cyclic-di-AMP and cyclic-di-GMP." Journal of immunology **187**(5): 2595-2601.
- Jonsson, K. L., A. Laustsen, et al. (2017). "IFI16 is required for DNA sensing in human macrophages by promoting production and function of cGAMP." Nature communications **8**: 14391.
- Kawai, T. and S. Akira (2011). "Toll-like receptors and their crosstalk with other innate receptors in infection and immunity." Immunity **34**(5): 637-650.
- Kawasaki, T. and T. Kawai (2014). "Toll-like receptor signaling pathways." Frontiers in immunology **5**: 461.
- Kelley, V. E. and J. B. Roths (1985). "Interaction of mutant *lpr* gene with background strain influences renal disease." Clin Immunol Immunopathol **37**(2): 220-229.
- Kerur, N., M. V. Veetil, et al. (2011). "IFI16 acts as a nuclear pathogen sensor to induce the inflammasome in response to Kaposi Sarcoma-associated herpesvirus infection." Cell host & microbe **9**(5): 363-375.
- Konig, N., C. Fiehn, et al. (2016). "Familial chilblain lupus due to a gain-of-function mutation in STING." Annals of the rheumatic diseases.
- Kramers C, H. M., van Bruggen MC, van de Lagemaat R, Dijkman HB, Assmann KJ, Smeenk RJ, Berden JH. (1994). "Anti-nucleosome antibodies complexed to

- nucleosomal antigens show anti-DNA reactivity and bind to rat glomerular basement membrane in vivo." J Clin Invest. **94**(2): 568-577.
- Kranzusch, P. J., A. S. Lee, et al. (2013). "Structure of human cGAS reveals a conserved family of second-messenger enzymes in innate immunity." Cell reports **3**(5): 1362-1368.
- Krishnan, S., Y. T. Juang, et al. (2008). "Differential Expression and Molecular Associations of Syk in Systemic Lupus Erythematosus T Cells." The Journal of Immunology **181**(11): 8145-8152.
- Kutzler, M. A. and D. B. Weiner (2008). "DNA vaccines: ready for prime time?" Nature reviews. Genetics **9**(10): 776-788.
- Lahaye, X., T. Satoh, et al. (2013). "The capsids of HIV-1 and HIV-2 determine immune detection of the viral cDNA by the innate sensor cGAS in dendritic cells." Immunity **39**(6): 1132-1142.
- Lam, E., S. Stein, et al. (2014). "Adenovirus detection by the cGAS/STING/TBK1 DNA sensing cascade." Journal of virology **88**(2): 974-981.
- Larche, M., C. A. Akdis, et al. (2006). "Immunological mechanisms of allergen-specific immunotherapy." Nature reviews. Immunology **6**(10): 761-771.
- Lartigue, A., P. Courville, et al. (2006). "Role of TLR9 in Anti-Nucleosome and Anti-DNA Antibody Production in lpr Mutation-Induced Murine Lupus." The Journal of Immunology **177**(2): 1349-1354.
- Latz, E., T. S. Xiao, et al. (2013). "Activation and regulation of the inflammasomes." Nature reviews. Immunology **13**(6): 397-411.
- Levinson, W. (2016). Hypersensitivity (Allergy). Review of Medical Microbiology and Immunology, 14e. New York, NY, McGraw-Hill Education.
- Li, L., Q. Yin, et al. (2014). "Hydrolysis of 2'3'-cGAMP by ENPP1 and design of nonhydrolyzable analogs." Nature chemical biology.
- Li QZ, X. C., Wu T, Mackay M, Aranow C, Putterman C, Mohan C. (2005). "Identification of autoantibody clusters that best predict lupus disease activity using glomerular proteome arrays." J Clin Invest. **115**(12): 3428-3439.
- Li, X., C. Shu, et al. (2013). "Cyclic GMP-AMP synthase is activated by double-stranded DNA-induced oligomerization." Immunity **39**(6): 1019-1031.
- Li, X. D., J. Wu, et al. (2013). "Pivotal roles of cGAS-cGAMP signaling in antiviral defense and immune adjuvant effects." Science **341**(6152): 1390-1394.
- Liu, Y., A. A. Jesus, et al. (2014). "Activated STING in a Vascular and Pulmonary Syndrome." The New England journal of medicine.
- Mathian, A., M. Gallegos, et al. (2011). "Interferon-alpha induces unabated production of short-lived plasma cells in pre-autoimmune lupus-prone (NZBxNZW)F1 mice but not in BALB/c mice." European journal of immunology **41**(3): 863-872.
- Medina, R. A. and A. Garcia-Sastre (2011). "Influenza A viruses: new research developments." Nature reviews. Microbiology **9**(8): 590-603.
- Medzhitov, R. and C. Janeway, Jr. (2000). "Innate immunity." The New England journal of medicine **343**(5): 338-344.
- Medzhitov, R. and C. A. Janeway, Jr. (2002). "Decoding the patterns of self and nonself by the innate immune system." Science **296**(5566): 298-300.

- Mohan, C., L. Morel, et al. (1997). "Genetic dissection of systemic lupus erythematosus pathogenesis: Sle2 on murine chromosome 4 leads to B cell hyperactivity." The Journal of Immunology **159**(1): 454.
- Mohan, C., Y. Yu, et al. (1999). "Genetic Dissection of Sle Pathogenesis: Sle3 on Murine Chromosome 7 Impacts T Cell Activation, Differentiation, and Cell Death." The Journal of Immunology **162**(11): 6492.
- Morel, L., B. P. Croker, et al. (2000). "Genetic reconstitution of systemic lupus erythematosus immunopathology with polycongenic murine strains." Proceedings of the National Academy of Sciences of the United States of America **97**(12): 6670-6675.
- Morel, L., C. Mohan, et al. (1997). "Functional dissection of systemic lupus erythematosus using congenic mouse strains." Journal of immunology **158**(12): 6019-6028.
- Morita, M., G. Stamp, et al. (2004). "Gene-targeted mice lacking the Trex1 (DNase III) 3'→5' DNA exonuclease develop inflammatory myocarditis." Molecular and cellular biology **24**(15): 6719-6727.
- Morse HC 3rd, D. W., Yetter RA, Murphy ED, Roths JB, Coffman RL (1982). "Abnormalities induced by the mutant gene lpr: expansion of a unique lymphocyte subset." J Immunol. **129**(6): 2612-2615.
- Mueller, D. L. (2010). "Mechanisms maintaining peripheral tolerance." Nature immunology **11**(1): 21-27.
- Murira, A. and A. Lamarre (2016). "Type-I Interferon Responses: From Friend to Foe in the Battle against Chronic Viral Infection." Frontiers in immunology **7**: 609.
- Murphy, T. L., M. G. Cleveland, et al. (1995). "Regulation of interleukin 12 p40 expression through an NF-kappa B half-site." Molecular and cellular biology **15**(10): 5258-5267.
- Nickerson, K. M., S. R. Christensen, et al. (2010). "TLR9 regulates TLR7- and MyD88-dependent autoantibody production and disease in a murine model of lupus." Journal of immunology **184**(4): 1840-1848.
- O'Neill, L. A. J. (2013). "Sensing the Dark Side of DNA." Science **339**(6121): 763-764.
- Orzalli, M. H., N. M. Broekema, et al. (2015). "cGAS-mediated stabilization of IFI16 promotes innate signaling during herpes simplex virus infection." Proceedings of the National Academy of Sciences of the United States of America **112**(14): E1773-1781.
- Orzalli, M. H., N. A. DeLuca, et al. (2012). "Nuclear IFI16 induction of IRF-3 signaling during herpesviral infection and degradation of IFI16 by the viral ICP0 protein." Proceedings of the National Academy of Sciences of the United States of America **109**(44): E3008-3017.
- Paijo, J., M. Doring, et al. (2016). "cGAS Senses Human Cytomegalovirus and Induces Type I Interferon Responses in Human Monocyte-Derived Cells." PLoS pathogens **12**(4): e1005546.
- Pandey S, K. T., Akira S. (2014). "Microbial sensing by Toll-like receptors and intracellular nucleic acid sensors." Cold Spring Harb Perspect Biol. **7**(1): a016246.

- Pascual, V., L. Farkas, et al. (2006). "Systemic lupus erythematosus: all roads lead to type I interferons." Current opinion in immunology **18**(6): 676-682.
- Peihong Dai, W. W., Hua Cao, Francesca Avogadri, Lianpan Dai, Ingo Drexler, Johanna A. Joyce, Xiao-Dong Li, Zhijian Chen, Taha Merghoub, Stewart Shuman, Liang Deng (2014). "Modified Vaccinia Virus Ankara Triggers Type I IFN Production in Murine Conventional Dendritic Cells via a cGAS/STING-Mediated Cytosolic DNA-Sensing Pathway." PLoS pathogens **10**(4).
- Perdiguero, B. and M. Esteban (2009). "The interferon system and vaccinia virus evasion mechanisms." Journal of interferon & cytokine research : the official journal of the International Society for Interferon and Cytokine Research **29**(9): 581-598.
- Platanias, L. C. (2005). "Mechanisms of type-I- and type-II-interferon-mediated signalling." Nature reviews. Immunology **5**(5): 375-386.
- Rahman, M. A. and D. A. Isenberg (1994). "Autoantibodies in systemic lupus erythematosus." Curr Opin Rheumatol **6**(5): 468-473.
- Rathinam, V. A., Z. Jiang, et al. (2010). "The AIM2 inflammasome is essential for host defense against cytosolic bacteria and DNA viruses." Nature immunology **11**(5): 395-402.
- Ratsimandresy, R. A., A. Dorfleutner, et al. (2013). "An Update on PYRIN Domain-Containing Pattern Recognition Receptors: From Immunity to Pathology." Frontiers in immunology **4**: 440.
- Reinert, L. S., K. Lopusna, et al. (2016). "Sensing of HSV-1 by the cGAS-STING pathway in microglia orchestrates antiviral defence in the CNS." Nature communications **7**: 13348.
- Rönblom, L. and G. V. Alm (2003). "Systemic lupus erythematosus and the type I interferon system." Arthritis research & therapy **5**(2): 68-75.
- Sanders, C. J., B. Johnson, et al. (2013). "Intranasal influenza infection of mice and methods to evaluate progression and outcome." Methods in molecular biology **1031**: 177-188.
- Schroeder, H. W., Jr. and L. Cavacini (2010). "Structure and function of immunoglobulins." The Journal of allergy and clinical immunology **125**(2 Suppl 2): S41-52.
- Schwarting, A., K. Paul, et al. (2005). "Interferon-beta: a therapeutic for autoimmune lupus in MRL-Fas^{pr} mice." Journal of the American Society of Nephrology : JASN **16**(11): 3264-3272.
- Sharma, S., A. M. Campbell, et al. (2015). "Suppression of systemic autoimmunity by the innate immune adaptor STING." Proceedings of the National Academy of Sciences of the United States of America.
- Shi, X., C. Xie, et al. (2002). "Genetic Dissection of SLE: SLE1 and FAS Impact Alternate Pathways Leading to Lymphoproliferative Autoimmunity." The Journal of Experimental Medicine **196**(3): 281-292.
- Shirota, H., L. Petrenko, et al. (2009). "Contribution of IRF-3 mediated IFN β production to DNA vaccine dependent cellular immune responses." Vaccine **27**(15): 2144-2149.

- Shortman, K. and Y. J. Liu (2002). "Mouse and human dendritic cell subtypes." Nature reviews. Immunology **2**(3): 151-161.
- Skrnjug I., G. C. A., Ruecker C. (2014). "cGAMP displays mucosal adjuvant activity in mice." PLoS One **9**(10).
- Smith-Bouvier, D. L., A. A. Divekar, et al. (2008). "A role for sex chromosome complement in the female bias in autoimmune disease." The Journal of Experimental Medicine **205**(5): 1099-1108.
- Sokolovska, A., S. L. Hem, et al. (2007). "Activation of dendritic cells and induction of CD4(+) T cell differentiation by aluminum-containing adjuvants." Vaccine **25**(23): 4575-4585.
- Solovjov, D. A., E. Pluskota, et al. (2005). "Distinct roles for the alpha and beta subunits in the functions of integrin alphaMbeta2." The Journal of biological chemistry **280**(2): 1336-1345.
- Spies, B., H. Hochrein, et al. (2003). "Vaccination with Plasmid DNA Activates Dendritic Cells via Toll-Like Receptor 9 (TLR9) but Functions in TLR9-Deficient Mice." The Journal of Immunology **171**(11): 5908-5912.
- Stetson, D. B. and R. Medzhitov (2006). "Recognition of Cytosolic DNA Activates an IRF3-Dependent Innate Immune Response." Immunity **24**(1): 93-103.
- Stevens, T. L., A. Bossie, et al. (1988). "Regulation of antibody isotype secretion by subsets of antigen-specific helper T cells." Nature **334**(6179): 255-258.
- Summers, S. A., A. Hoi, et al. (2010). "TLR9 and TLR4 are required for the development of autoimmunity and lupus nephritis in pristane nephropathy." Journal of autoimmunity **35**(4): 291-298.
- Sun, L., J. Wu, et al. (2012). "Cyclic GMP-AMP Synthase Is a Cytosolic DNA Sensor That Activates the Type I Interferon Pathway." Science.
- Suschak, J. J., S. Wang, et al. (2015). "A cGAS-Independent STING/IRF7 Pathway Mediates the Immunogenicity of DNA Vaccines." Journal of immunology.
- Suschak, J. J., S. Wang, et al. (2015). "Identification of Aim2 as a sensor for DNA vaccines." Journal of immunology **194**(2): 630-636.
- Tada, Y., S. Kondo, et al. (2011). "Interferon regulatory factor 5 is critical for the development of lupus in MRL/lpr mice." Arthritis and rheumatism **63**(3): 738-748.
- Takahashi, T., M. Tanaka, et al. (1994). "Generalized lymphoproliferative disease in mice, caused by a point mutation in the Fas ligand." Cell **76**(6): 969-976.
- Takaoka, A., Z. Wang, et al. (2007). "DAI (DLM-1/ZBP1) is a cytosolic DNA sensor and an activator of innate immune response." Nature **448**(7152): 501-505.
- Takeda, K. and S. Akira (2005). "Toll-like receptors in innate immunity." International immunology **17**(1): 1-14.
- Tanaka, Y. and Z. J. Chen (2012). "STING specifies IRF3 phosphorylation by TBK1 in the cytosolic DNA signaling pathway." Sci Signal **5**(214): ra20.
- Taubenberger, J. K. and J. C. Kash (2010). "Influenza Virus Evolution, Host Adaptation, and Pandemic Formation." Cell host & microbe **7**(6): 440-451.
- Taubenberger, J. K. and D. M. Morens (2008). "The pathology of influenza virus infections." Annual review of pathology **3**: 499-522.

- Temizoz, B., E. Kuroda, et al. (2015). "TLR9 and STING agonists synergistically induce innate and adaptive type-II IFN." European journal of immunology **45**(4): 1159-1169.
- Theofilopoulos, A. N. and F. J. Dixon (1985). "Murine models of systemic lupus erythematosus." Adv Immunol **37**: 269-390.
- Thibault, D. L., K. L. Graham, et al. (2009). "Type I interferon receptor controls B-cell expression of nucleic acid-sensing Toll-like receptors and autoantibody production in a murine model of lupus." Arthritis research & therapy **11**(4): R112.
- Topham, D. J., R. A. Tripp, et al. (1997). "CD8+ T cells clear influenza virus by perforin or Fas-dependent processes." Journal of immunology **159**(11): 5197-5200.
- Trinchieri, G. (1995). "Interleukin-12: a proinflammatory cytokine with immunoregulatory functions that bridge innate resistance and antigen-specific adaptive immunity." Annual review of immunology **13**: 251-276.
- Trinchieri, G. (2010). "Type I interferon: friend or foe?" The Journal of Experimental Medicine **207**(10): 2053-2063.
- Tsokos, G. C. (2011). "Mechanisms of Disease: Systemic Lupus Erythematosus." The New England Journal of Medicine **365**: 2110-2121.
- Tudor, D., S. Riffault, et al. (2001). "Type I IFN modulates the immune response induced by DNA vaccination to pseudorabies virus glycoprotein C." Virology **286**(1): 197-205.
- Turvey, S. E. and D. H. Broide (2010). "Innate immunity." The Journal of allergy and clinical immunology **125**(2 Suppl 2): S24-32.
- Ulmer, J. B., T.-M. Fu, et al. (1998). "Protective CD4(+) and CD8(+) T Cells against Influenza Virus Induced by Vaccination with Nucleoprotein DNA." Journal of virology **72**(7): 5648-5653.
- Unterholzner, L., S. E. Keating, et al. (2010). "IFI16 is an innate immune sensor for intracellular DNA." Nature immunology **11**(11): 997-1004.
- Urbanaviciute, V., C. Starke, et al. (2013). "Toll-like receptor 2 is required for autoantibody production and development of renal disease in pristane-induced lupus." Arthritis and rheumatism **65**(6): 1612-1623.
- van Bruggen MC, W. B., Rijke TP, Tamboer W, Kramers K, Smeenk RJ, Monestier M, Fournie GJ, Berden JH. (1997). "Antigen specificity of anti-nuclear antibodies complexed to nucleosomes determines glomerular basement membrane binding in vivo." Eur J Immunol. **27**(6): 1564-1569.
- Walport, M. J., C. M. Black, et al. (1982). "The immunogenetics of SLE." Clin Rheum Dis **8**(1): 3-21.
- Wang, J., P. Li, et al. (2016). "Natural STING agonist as an "ideal" adjuvant for cutaneous vaccination." The Journal of investigative dermatology.
- Wang, R., J. Epstein, et al. (2001). "Induction of CD4(+) T cell-dependent CD8(+) type 1 responses in humans by a malaria DNA vaccine." Proceedings of the National Academy of Sciences of the United States of America **98**(19): 10817-10822.
- Wang, Y., K. Zhou, et al. (2014). "A nanoparticle-based strategy for the imaging of a broad range of tumours by nonlinear amplification of microenvironment signals." Nat Mater **13**(2): 204-212.

- Waring, P. and A. Mullbacher (1999). "Cell death induced by the Fas/Fas ligand pathway and its role in pathology." Immunology and cell biology **77**(4): 312-317.
- Warrington, R., W. Watson, et al. (2011). "An introduction to immunology and immunopathology." Allergy, Asthma & Clinical Immunology **7**(1): S1.
- Watanabe-Fukunaga, R., C. I. Brannan, et al. (1992). "Lymphoproliferation disorder in mice explained by defects in Fas antigen that mediates apoptosis." Nature **356**(6367): 314-317.
- Watson, R. O., S. L. Bell, et al. (2015). "The Cytosolic Sensor cGAS Detects Mycobacterium tuberculosis DNA to Induce Type I Interferons and Activate Autophagy." Cell host & microbe **17**(6): 811-819.
- Wong, S. S. and R. J. Webby (2013). "Traditional and new influenza vaccines." Clinical microbiology reviews **26**(3): 476-492.
- Wu, J. and Z. J. Chen (2014). "Innate Immune Sensing and Signaling of Cytosolic Nucleic Acids." Annual review of immunology **32**(1): 461-488.
- Wu, J., L. Sun, et al. (2012). "Cyclic GMP-AMP Is an Endogenous Second Messenger in Innate Immune Signaling by Cytosolic DNA." Science.
- Y TOKANO, S. M., H KANEKO, H AMANO, K NOZAWA, Y TAKASAKI, and H HASHIMOTO (1999). "Levels of IL-12 in the sera of patients with systemic lupus erythematosus (SLE)—relation to Th1- and Th2-derived cytokines." Clin Exp Immunol. **116**(1): 169–173.
- Yang, Z. Y. e. a. (2004). "A DNA vaccine induces SARS coronavirus neutralization and protective immunity in mice." Nature **428**: 561-564.
- Yildiz, S., E. Alpdundar, et al. (2015). "Enhanced immunostimulatory activity of cyclic dinucleotides on mouse cells when complexed with a cell-penetrating peptide or combined with CpG." European journal of immunology **45**(4): 1170-1179.
- Zhang, X., H. Shi, et al. (2013). "Cyclic GMP-AMP Containing Mixed Phosphodiester Linkages Is An Endogenous High-Affinity Ligand for STING." Molecular cell **51**(2): 226-235.
- Zhang, X., J. Wu, et al. (2014). "The Cytosolic DNA Sensor cGAS Forms an Oligomeric Complex with DNA and Undergoes Switch-like Conformational Changes in the Activation Loop." Cell reports.
- Zhang, Z., B. Yuan, et al. (2011). "The helicase DDX41 senses intracellular DNA mediated by the adaptor STING in dendritic cells." Nature immunology **12**(10): 959-965.
- Zhong, B., Y. Yang, et al. (2008). "The adaptor protein MITA links virus-sensing receptors to IRF3 transcription factor activation." Immunity **29**(4): 538-550.
- Zhou, K., H. Liu, et al. (2012). "Multicolored pH-tunable and activatable fluorescence nanoplatfrom responsive to physiologic pH stimuli." Journal of the American Chemical Society **134**(18): 7803-7811.
- Zhu, J., H. Yamane, et al. (2010). "Differentiation of effector CD4 T cell populations (*)." Annual review of immunology **28**: 445-489.
- Zhuang, H., C. Szeto, et al. (2015). "Animal Models of Interferon Signature Positive Lupus." Frontiers in immunology **6**: 291.